KFKI–2002–03/G
REPORT

Z. HÓZER
P. WINDBERGER
I. NAGY
L. MARÓTI
L. MATUS
M. HORVÁTH
A. PINTÉR
Á. GRIGER
M. BALASKÓ
B. ALFÖLDY

CODEX-AIT-2 EXPERIMENT: CORE DEGRADATION TEST WITH STEAM OXIDATION AND AIR INGRESS

Hungarian Academy of Sciences
CENTRAL
RESEARCH
INSTITUTE FOR
PHYSICS
BUDAPEST

CODEX-AIT-2 EXPERIMENT: CORE DEGRADATION TEST WITH STEAM OXIDATION AND AIR INGRESS

Z. Hózer, P. Windberg, I. Nagy, L. Maróti, L. Matus,
M. Horváth, A. Pintér, Á. Griger, M. Balaskó, B. Alföldy
KFKI Atomic Energy Research Institute
H-1525 Budapest, P.O.Box.49, Hungary

A. Czitrovszky, P. Jani
Research Institute for Solid State Physics and Optics
H-1525 Budapest, P.O.Box.49, Hungary

Abstract

Z. Hózer, P. Windberg, I. Nagy, L. Maróti, L. Matus,
M. Horváth, A. Pintér, Á. Griger, M. Balaskó, B. Alföldy, A. Czitrovszky, P. Jani:
CODEX-AIT-2 EXPERIMENT: CORE DEGRADATION TEST WITH STEAM OXIDATION AND AIR INGRESS

The CODEX-AIT-2 test was performed in the CODEX facility in order to study the fuel rod degradation in the pre-oxidised bundle under air ingress conditions. The fuel rod cladding was oxidised in steam atmosphere in two steps: at 820^{o}C and 950^{o}C to give an oxide layer thickness of 20-25 microns. After the air injection temperature excursion was observed on the fuel rods to a maximum indicated temperature of 1900 ^{o}C. In the AIT-2 test the damage of the bundle was more severe than in the first test, for the high temperature conditions were kept for longer time in AIT-2 than in AIT-1. The rod-like structure was lost in the upper part of the bundle. The formation of higher uranium oxides was not observed.

Kivonat

Hózer Z., Windberg P., Nagy I., Maróti L., Matus L.,
Horváth M., Pintér A., Griger Á., Balaskó M., Alföldy B., Czitrovszky A., Jani P.:
A CODEX-AIT-2 KÍSÉRLET: ZÓNASÉRÜLÉSES MÉRÉS VÍZGŐZÖS OXIDÁCIÓVAL ÉS LÉGBETÖRÉSSEL

A CODEX-AIT-2 kísérlet célja az előzetesen oxidált fűtőelemrudak sérülésének vizsgálata volt légbetöréses körülmények között, a mérést a CODEX berendezésen hajtottuk végre. A fűtőelem burkolat oxidációja két lépésben történt: 820 ^{o}C és 950 ^{o}C-on, ami 20-25 mikronos oxidréteg képződéséhez vezetett. A levegő beáramoltatás után hőmérséklet megszaladást tapasztaltunk a rudakon 1900 ^{o}C hőmérsékletig. Az AIT-2 mérésben a köteg súlyosabb sérülést szenvedett, mint a korábbi AIT-1 kísérletben. Ennek az az oka, hogy az AIT-2 mérésben a magas hőmérsékletű degradációs periódus hosszabb volt. A köteg felső részén a rúdgeometria megsérült, magasabb urán-oxidok kialakulását nem tapasztaltuk.

Contents

1. INTRODUCTION **7**

2. THE CODEX FACILITY **8**

3. THE CODEX EXPERIMENTAL PROGRAMME **10**

4. COMMISSIONING TEST **11**

5. THE CODEX-AIT-2 EXPERIMENT **11**

6. BUNDLE POST-TEST EXAMINATION **13**

6.1 X-RAY RADIOGRAPHY INSPECTION OF THE BUNDLE 17
6.2 X-RAY POWDER DIFFRACTION (XRD) INVESTIGATIONS 18
6.3 LAYER THICKNESS MEASUREMENTS 19

7. AEROSOL MEASUREMENTS **21**

7.1 MORPHOLOGICAL STUDIES AND IMAGE ANALYSIS 22
7.2 ELECTRON BEAM MICROANALYSIS AND PARTICLE CLASSIFICATION 23
7.3 MASS SPECTROMETRY AND X-RAY FLUORESCENCE SPECTROSCOPY 25
7.4 MEASUREMENT OF AEROSOL MASS ON IMPACTORS AND COLLECTORS 27
7.5 MAIN RESULTS OF AEROSOL SAMPLE EXAMINATIONS 27

8. EXPERIMENTAL DATABASE **29**

9. SUMMARY AND CONCLUSIONS **32**

ACKNOWLEDGMENTS **32**

REFERENCES **33**

List of tables

TABLE 1 MAIN CHARACTERISTICS OF THE CODEX-AIT FACILITY 9
TABLE 2 POSITION AND MATERIAL OF THERMOCOUPLES IN THE TEST SECTION 10
TABLE 3 MAIN PARAMETERS OF CODEX TEST MATRIX 11
TABLE 4 THE IDENTIFIED COMPOUNDS AND THEIR ESTIMATED QUANTITIES 19
TABLE 5 ELEMENTAL COMPOSITION OF COLLECTED PARTICLES (SSMS RESULTS) 26
TABLE 6 PARAMETERS AVAILABLE IN THE CODEX-AIT-2 DATABASE 30
TABLE 7 PARAMETERS IN THE CODEX-AIT-2 COMMISSIONING TEST DATABASE 31

List of figures

FIG. 1 SCHEME OF THE CODEX-AIT-1 FACILITY 34
FIG. 2 HORIZONTAL CROSS SECTION OF THE CODEX-AIT-1 9 ROD PWR BUNDLE 35
FIG. 3 AEROSOL SAMPLING IN THE CODEX-AIT-1 TEST 35
FIG. 4 VERTICAL CROSS SECTION OF HEATED AND UNHEATED RODS 36
FIG. 5 ELECTRICAL POWER IN THE CODEX-AIT-2 COMMISSIONING TEST 37
FIG. 6 ARGON FLOWRATE IN THE CODEX-AIT-2 COMMISSIONING TEST 37
FIG. 7 HEATED ROD TEMPERATURES IN THE CODEX-AIT-2 COMMISSIONING TEST 38
FIG. 8 STEEL TEMPERATURES IN THE HEAT SHIELD IN THE COMMISSIONING TEST 38
FIG. 9 UH50: UNHEATED ROD TEMPERATURE AT 50 MM 39
FIG. 10 UH150: UNHEATED ROD TEMPERATURE AT 150 MM 39
FIG. 11 UH300: UNHEATED ROD TEMPERATURE AT 300 MM 40
FIG. 12 UH375: UNHEATED ROD TEMPERATURE AT 375 MM 40
FIG. 13 UH450: UNHEATED ROD TEMPERATURE AT 450 MM 41
FIG. 14 UH535: UNHEATED ROD TEMPERATURE AT 535 MM 41
FIG. 15 UH570: UNHEATED ROD TEMPERATURE AT 570 MM 42
FIG. 16 H50: HEATED ROD TEMPERATURE AT 50 MM 42
FIG. 17 H150: HEATED ROD TEMPERATURE AT 150 MM 43
FIG. 18 H450: HEATED ROD TEMPERATURE AT 450 MM 43
FIG. 19 H535: HEATED ROD TEMPERATURE AT 535 MM 44
FIG. 20 H570: HEATED ROD TEMPERATURE AT 570 MM 44
FIG. 21 SH50: SHROUD TEMPERATURE AT 50 MM 45
FIG. 22 SH150: SHROUD TEMPERATURE AT 150 MM 45
FIG. 23 SH300: SHROUD TEMPERATURE AT 300 MM 46
FIG. 24 SH450: SHROUD TEMPERATURE AT 450 MM 46
FIG. 25 SH570: SHROUD TEMPERATURE AT 570 MM 47
FIG. 26 HS50: STEEL HEAT SHIELD TEMPERATURE AT 50 MM 47
FIG. 27 HS150: STEEL HEAT SHIELD TEMPERATURE AT 150 MM 48
FIG. 28 HS300: STEEL HEAT SHIELD TEMPERATURE AT 300 MM 48
FIG. 29 HS450: STEEL HEAT SHIELD TEMPERATURE AT 450 MM 49
FIG. 30 HS535: STEEL HEAT SHIELD TEMPERATURE AT 535 MM 49
FIG. 31 OS50: OUTSIDE SHIELD TEMPERATURE AT 50 MM 50
FIG. 32 OS150: OUTSIDE SHIELD TEMPERATURE AT 150 MM 50
FIG. 33 OS300: OUTSIDE SHIELD TEMPERATURE AT 300 MM 51

FIG. 34 OS450: OUTSIDE SHIELD TEMPERATURE AT 450 MM 51
FIG. 35 OS535: OUTSIDE SHIELD TEMPERATURE AT 535 MM 52
FIG. 36 TLOCH: LOWER CHAMBER TEMPERATURE 52
FIG. 37 TUPCH: UPPER CHAMBER TEMPERATURE 53
FIG. 38 TMELT: BUNDLE TEMPERATURE AT -20 MM 53
FIG. 39 PYR450: PYROMETER TEMPERATURE AT 450 MM 54
FIG. 40 PYR535: PYROMETER TEMPERATURE AT 535 MM 54
FIG. 41 TWATER: WATER TEMPERATURE IN THE STEAMGENERATOR 55
FIG. 42 TSTEAM: STEAMGENERATOR OUTLET TEMPERATURE 55
FIG. 43 TIN1: GAS TEMPERATURE AT THE SUPERHEATER OUTLET 56
FIG. 44 TIN2: GAS TEMPERATURE IN THE INLET JUNCTION 56
FIG. 45 TCOUT: GAS TEMPERATURE IN THE OUTLET JUNCTION 57
FIG. 46 TCOOL: GAS TEMPERATURE AT THE COOLER INLET 57
FIG. 47 TOUTC: GAS TEMPERATURE AT THE COOLER OUTLET 58
FIG. 48 PSYS: SYSTEM PRESSURE 58
FIG. 49 STEAM: STEAM FLOWRATE 59
FIG. 50 ARGON: ARGON FLOWRATE 59
FIG. 51 AIR: AIR FLOWRATE 60
FIG. 52 POWER: ELECTRIC POWER 60
FIG. 53 API1 AND APE1: CONCENTRATION OF 0,3-0,5 μM AEROSOLS 61
FIG. 54 API2 AND APE2: CONCENTRATION OF 0,5-1,0 μM AEROSOLS 61
FIG. 55 API3 AND APE3: CONCENTRATION OF 1-3 μM AEROSOLS 62
FIG. 56 API4 AND APE4: CONCENTRATION OF 3-5 μM AEROSOLS 62
FIG. 57 API5 AND APE5: CONCENTRATION OF 5-10 μM AEROSOLS 63
FIG. 58 API6 AND APE6: CONCENTRATION OF >10 μM AEROSOLS 63
FIG. 59 X-RAY RADIOGRAPHY OF THE OF CODEX-AIT-2 BUNDLE 64
FIG. 60 X-RAY RADIOGRAPHY OF THE OF CODEX-AIT-2 BUNDLE 65
FIG. 61 X-RAY RADIOGRAPHY OF THE OF CODEX-AIT-2 BUNDLE 66
FIG. 62 VIEW OF TUNGSTEN HEATER ROD 67
FIG. 63 CLADDING AND PELLET 67
FIG. 64 BROKEN UP CLADDING AT 280 MM ELEVATION 67
FIG. 65 OXIDE AND α-PHASE ON ROD NO.1 AT 375 MM ELEVATION 68
FIG. 66 CLADDING OF ROD NO. 9 AT 375 MM ELEVATION 68
FIG. 67 TUNGSTEN-UO_2 INTERACTION ON ROD NO. 7 AT 375 MM ELEVATION 68
FIG. 68 INTACT RODS AT 450 MM ELEVATION, A) NO.1, B) NO.9 69
FIG. 69 OXIDISED AND SWELLED UO_2 ON ROD NO.5 AT 450 MM ELEVATION 69
FIG. 70 PEELED OFF TUBE NEAR TO HEATER ROD 69
FIG. 71 CROSS SECTION OF ROD NO. 1 AT 535 MM ELEVATION 69
FIG. 72 BREAK ON CLAD AND PELLET OF ROD NO. 6 AT 535 MM ELEVATION 69
FIG. 73 SPACER AT 555 MM ELEVATION 70
FIG. 74 EARLIER β-PHASE OF CLADDING OF ROD NO. 2 AT 555 MM ELEVATION 70
FIG. 75 PELLET CLAD INTERACTION IN ROD NO. 3 AT 555 MM ELEVATION 70
FIG. 76 DETAILS OF FRAGMENTED PARTICLES 71
FIG. 77 DIFFUSION LAYER ON THE BOUNDARY 71
FIG. 78 THE SITE OF U,ZR GLOBULE, THE MOLTEN ALLOY ESCAPED 71
FIG. 79 ADVANCING OF ZR METAL α-PHASE ON GRAIN BOUNDARY OF UO_2 71
FIG. 80 CHARACTERISTIC CLADDING DETAIL OF A FALLEN DOWN FRAGMENT 71

FIG. 81 SELECTED GRAINS COLLECTED FROM THE BOTTOM OF THE SYSTEM 72
FIG. 82 DIGITAL BEI IMAGE AND X-RAY MAPS OF ZR, U AND SI 72
FIG. 83 ARRANGEMENT OF THE DYNAMIC RADIOGRAPHY STATION 73
FIG. 84 X-RAY DIFFRACTOGRAMS OF DIFFERENT FUEL ROD SAMPLES 74
FIG. 85 β-PHASE THICKNESS ON THE RODS 75
FIG. 86 α-PHASE THICKNESS ON THE RODS 76
FIG. 87 OXIDE LAYER THICKNESS ON THE RODS 77
FIG. 88 NITRIDE LAYER THICKNESS ON THE RODS 78
FIG. 89 PELLET-CLADDING INTERACTION LAYER THICKNESS ON THE RODS 79
FIG. 90 OXIDE AND α-PHASE LAYER THICKNESS ON THE SHROUD 80
FIG. 91 SCHEME OF IMPACTOR SAMPLER 81
FIG. 92 SEM IMAGE AND ED SPECTRA OF U-RICH PARTICLES 82
FIG. 93 WEIGHT INCREASE OF IMPACTOR SAMPLES IN THE AIT-2 TEST 83
FIG. 94 SSMS RESULTS GAINED ON QUARTZ FIBRE FILTER 83

1. INTRODUCTION

The investigation of the degraded core at TMI-2 revealed that the most extensive damage took place initially along the centreline of the reactor core while the peripheral regions remained intact although they were heavily oxidised. In the late phase of core degradation the core debris can slump to the lower plenum and cause rupture of the vessel. As a result of the chimney effect air can be sucked into the vessel from the reactor cavity and interact with the core materials. The ingress of air into the vessel will result in an extremely high oxidation rate of the remaining zirconium and oxidation of the fuel can be followed by the release of different kinds of fission products [1].

For the analysis of air ingress scenarios it is necessary to perform small-scale and integral tests. Their results can provide the basic information for code development and validation. In the framework of the OPSA (Oxidation Phenomena in Severe Accident) project decision has been made to carry out two air ingress tests in the CODEX facility at the Atomic Energy Research Institute in Budapest for clarification of the most important problems arising when air enters the reactor core during a severe accident.

The first air ingress test CODEX-AIT-1 was performed in May 1998 [2]. The scenario for the second test was selected on the basis of learnings from the first test. This report presents the description of the CODEX facility and the results of the CODEX-AIT-2 test.

2. THE CODEX FACILITY

The CODEX facility was built in 1995 for the investigation of the behaviour of small fuel bundles under severe accident conditions. The first test series was devoted to the experimental study of VVER type fuel assemblies. Escalation in steam and quenching at high temperatures were analysed in 7-rod hexagonal bundles made of VVER materials.

The main components of the facility are shown in Fig.1 and the most important parameters are summarised in Table 1. The details of aerosol sampling are given in the picture of the upper part of the bundle and of the cooler (Fig. 3). Fig. 4 presents the vertical view of the heated and unheated (central) rods and Fig. 2. the horizontal cross section of the bundle.

In the Air Ingress Tests (AIT) 9-rod PWR type bundles were used. The rods were arranged on a square lattice, 8 peripheral rods were electrically heated with tungsten bars (Fig. 2). The central rod was not heated, it was used for instrumentation. Two spacer grids were applied to fix the bundle. The heated length of the bundle was 600 mm (Fig. 4). The cladding material was Zircaloy, the shroud part was made of a 2 mm thick Zr2%Nb alloy. Inside of the fuel rods annular UO_2 pellets were placed between the heater bars and the cladding. Around the shroud ZrO_2 thermal insulation was added.

The test section was connected to the preheater and to the cooler sections as coolant inlet and outlet respectively (Fig. 1). An additional junction was connected to the bottom part of the bundle to inject cold (room temperature) air. The preheater unit was able to supply either hot gases or steam to the test section. The off-gas streaming out of the test section was cooled down by the cooler/condenser unit and before releasing it into the atmosphere it was conducted through an aerosol trap and filtered by a special system. For the investigation of the aerosol release a cascade impactor system was connected to the upper plenum of the cooler (Fig. 3) and two pipelines allowed the continuous measurement of aerosols by means of laser particle counters.

The instrumentation of the facility consisted of the measurements of the operational parameters as heating power, flowrates, temperatures, levels and pressures. Thermocouples were placed in several positions in the heat insulation material, on the heat shield, on the external surface of the shroud, on the fuel rods and inside of the central (unheated) rod (Table 2). Two pyrometers were located at 450 and 535 mm elevations. Flowmeters, pressure transducers and analog multiplayer using shunt current and total voltage were applied.

The on-line aerosol measurements were made with two Laser Airborne Particle Counters (APC-03-2 and PAPC-03-2). The measuring principle of these airborne particle counters is based on laser light scattering. The data evaluation system comprises opto-electronic detecting and filtering, multichannel signal analysing interface and lap-top PC. The velocity of the gas stream was about 1 l/s. The APC method resulted in particle concentrations directly, dividing the light scattering signals into 6 ranges, 0.3-0.5, 0.5-1, 1-3, 3-5, 5-10 and >10 μm interval. The particle concentrations could be detected up to $5x10^6$ particles/l values.

In the CODEX-AIT experiments the sampling head of the PAPC-03-2 counter was mounted on the top of the cooler using a ~20 cm long copper tube. The APC-03-2 counter was placed out of the container and coupled with a 2 m long cable to the cooler head.

Bundle type:	PWR
Bundle size:	9 rods
Number of heated rods:	8
Number of unheated rods:	1
Pitch:	14.3 mm
Rod outside diameter:	10.75 mm
Cladding thickness:	0.725 mm
Cladding material:	Zircaloy-4
Heater material:	Tungsten (W)
Heater length:	600 mm
Heater diameter:	6 mm
Fuel pellets - heated rods:	UO_2 annular pellets
Fuel pellets - unheated rod:	UO_2 annular pellets
Pellet outer diameter:	9.1 mm
U-235 enrichment:	0.2%
Pellet stack:	600 mm
Grid spacer material:	Zircaloy-4
Grid spacer location:	lower: -15 mm, upper: 535 mm
Shroud material:	Zr2%Nb
Shroud wall thickness:	2 mm
Shroud inside dimensions:	48 x 48 mm
Shroud insulation material:	ZrO_2 fibre
Shroud insulation thickness:	19 mm
Shroud insulation elevation:	-50 - 620 mm
Max. inlet argon, steam and air temperature	800 ºC
Max. inlet argon flow:	10 g/s
Max. argon + 25%O_2 flow:	10 g/s
Max. air flow:	5 g/s
Max. system pressure	3.5 bar
Max. power of tungsten heaters	5 kW
Max power of steam generator	9 kW
Max. power of superheater	3 kW

Table 1 Main characteristics of the CODEX-AIT facility

The following parameters were measured and recorded during the experiments:

- central (unheated) rod temperatures
- heated rod temperatures, shroud temperatures
- heat insulation temperatures, heat shield temperatures
- steam, air, argon flowrates
- gas inlet/outlet temperatures at the test section, cooler inlet/outlet temperatures

- water temperature in steamgenerator, pyrometer temperature measurements
- electric power, system pressure, argon, air and impactor valve positions.

Elevation, mm	Heat insulation outside R=130mm	Heat shield R=80mm	Shroud outside	Heated rod cladding	Unheated (central) rod
760					NiCr-Ni
570				W- WRe	W- WRe
535	NiCr-Ni	NiCr-Ni	W- WRe	W- WRe	W- WRe
450	NiCr-Ni	NiCr-Ni	W- WRe		W- WRe
300	NiCr-Ni	NiCr-Ni	Pt-PtRh	Pt-PtRh	W- WRe
150	NiCr-Ni	NiCr-Ni	NiCr-Ni	NiCr-Ni	NiCr-Ni
50	NiCr-Ni	NiCr-Ni	NiCr-Ni	NiCr-Ni	NiCr-Ni
0					NiCr-Ni
-20					NiCr-Ni
-350					NiCr-Ni

Table 2 Position and material of thermocouples in the test section

3. THE CODEX EXPERIMENTAL PROGRAMME

In AEKI an experimental programme was initiated focusing on the high temperature behaviour of VVER fuel and core materials. The interactions of Zr1%Nb cladding with UO_2 pellet, stainless steel spacer and boron steel absorber were studied in small scale separate effect tests [3]. On the basis of the experience gained in these tests the CODEX integral test facility was constructed to continue this work under more prototypic conditions.

First the capabilities of the facility were demonstrated carrying out the CODEX-1 experiment with Al_2O_3 pellets. The test section was heated up with argon, then the electric power was increased. When the rod bundle degradation was indicated by temperature measurements, the power was switched off and the section was cooled down by argon. The post-test examination showed that the rod bundle partially damaged, the further melting was stopped in time. So the facility proved to be applicable to the experimental analysis of controlled core degradation processes.

In the second experiment similar procedures were taken, but the Al_2O_3 pellets were replaced with UO_2 [4,5]. The CODEX-3/1 and CODEX-3/2 experiments were performed with quick water cooling [6,7]. Air ingress conditions were simulated in the AIT-1 and AIT-2 tests with PWR fuel rods [2]. The B4C test was devoted to the examination of control rod degrdadation and gas production during a severe reactor accident. The main parameters of the test matrix are given in Table 3.

Test	Bundle type	Pellet	Year	Test type
CODEX-1	7-rod VVER	Al_2O_3	1995	scoping test
CODEX-2	7-rod VVER	UO_2	1995	escalation and slow cooling down
CODEX-3/1	7-rod VVER	UO_2	1996	water quench at 1150 ^oC
CODEX-3/2	7-rod VVER	UO_2	1997	water quench at 1500 ^oC
CODEX-AIT-1	9-rod PWR	UO_2	1998	air ingress
CODEX-AIT-2	9-rod PWR	UO_2	1999	steam oxidation and air ingress
CODEX-B4C	7-rod VVER	UO_2,B_4C	2001	control rod degradation

Table 3 Main parameters of CODEX test matrix

4. COMMISSIONING TEST

The test preparation started with a systematic checking of the different components of the facility. In order to show the operability of the system a commissioning type test was perfomed with stabilisation at different power levels in argon atmosphere.

The most important results of the commissioning test are the temperature histories at the different points of the test section. The time variation of the measurement data is illustrated in Figs. 5-8. The commissioning test was carried out with the CODEX-AIT-2 bundle. The available measurement data make possible the tuning of heat loss simulation and the checking of the system thermal response.

5. THE CODEX-AIT-2 EXPERIMENT

The test conditions achieved in CODEX-AIT-1 test were not favourable to U-bearing aerosol formation, little UO_2 was believed to be exposed to oxygen. For this reason the AIT-2 test was to be allowed to proceed to more severely degraded state. Use of steam rather than Ar/O_2 for pre-oxidation can avoid an excursion and is more prototypic for a reactor accident.

The proposed test sequence consisted of :

- a thermal stabilisation phase at 600 ^oC,
- pre-oxidation in Ar/steam mixture in two stages at 820^oC and 950 ^oC,
- cooling to 820 ^oC and flushing with hot Ar,
- changing to cold air and ramping at 0.5 ^oC /s until the oxidation excursion starts.

The experiment was to be terminated on evidence of melt reaching the lower parts of the bundle, by turning off the power and replacing the air supply by cold Ar.

The second air ingress test in the CODEX facility was performed 27th January 1999 at the KFKI Atomic Energy Research Institute, Budapest. The AIT-2 test has been performed according to the proposed scenario:

- The test started with a preheating period using hot argon and electrical heating. The bundle temperature was stabilised at ~600^{o}C.

- The fuel rod cladding was oxidised in steam atmosphere in two steps: at 820^{o}C and 950^{o}C to give an oxide layer thickness of 20-25 microns. Both steps lasted for 30 minutes. The temperature stabilisation was reached with manual power control. Then the steam injection was stopped and the temperature decreased to ~800^{o}C. Due to a valve leak a small amount of air flow joined the steam/Ar mixture during the preoxidation period.

- The air ingress phase started with the injection of 2.5 g/s cold air and with a linear increase of electrical power of 2 W/s to give an initial heating rate of 0.5 K/s. Temperature excursion was observed on the fuel rods to a maximum indicated temperature of 1900 ^{o}C. Similar excursion took place on the shroud as well. The air injection was stopped when the temperature in the central elevation reached 1700 ^{o}C, indicating the melting process.

Aerosol samples were taken using impactors before the preoxidation, before the air ingress phase, during temperature excursion in the air ingress period and also in the cooling down phase.

Video recording was applied to the test through an observation window at the elevation of the upper spacer grid. The temperature increase and the relocation of the spacer grid and the rod melting are clearly seen on the video tape.

The particle counters were activated after the preoxidation phase. The indicated peak in the aerosol release was about three times higher than in the previous AIT-1 test.

The first conclusion on the AIT-2 test was that the damage of the bundle was more severe than in the first test. The high temperature conditions were kept for longer time in AIT-2 than in AIT-1.

The time variation of the most important parameters during the total test period is shown in Figs. 9-58.

6. BUNDLE POST-TEST EXAMINATION

The visual observation of the bundle showed strong oxidation and damage both of the shroud and fuel rods. The 600 mm long UO_2 pellet filled stage of experimental bundle was cut and polished and ground at the following elevations (in mm):

a.) –20
b.) 150
c.) 280
d.) 375
e.) 450
f.) 535
g.) 555

The -20 mm cut was made under the UO_2 pellet filled stage. It was prepared for getting view of debris fallen down as was established from the X-ray picture.

During the grinding process multiple embedding of the surface with epoxy resin was applied in order to avoid any breakout of the brittle materials.

The outlook of polished slices has been thoroughly investigated to identify the high temperature physical and chemical processes playing main role at change of bundle parameters.

For better identification the rods in the cross sections were numbered. Looking at the slice with outer thermocouple tube at the top, the upper right is the No. 1 and the numbering advances clockwise, the No. 9 is the rod in the middle.

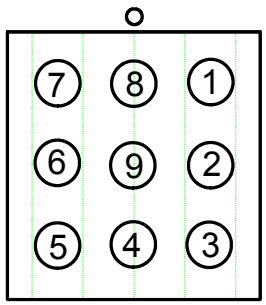

At and above the 280 mm elevations the degradations are strong. At many places only the naked W-rods indicate the positions of rods. The photos of the whole cross sections are shown in Fig. 59 for elevations -20, in Fig. 60 for elevations 150, 280 and 375, moreover in Fig. 61 for 450, 535 and 555 mm, together with the bundle X-ray radiography.

a.) -20 mm elevation

The cladding at this elevation is entirely intact. In the middle of the cladding tubes the Mo electrodes can be seen. Some remarkable views and conclusions regarding the fallen down particles are presented at point h.).

b.) 150 mm elevation

The cladding intact but each pellet is broken at some sites. The tungsten rods seem to be reacted with some kind of metal flowed down between the pellet and W heater. On Fig. 62 this spot at rod No. 5 is shown. Similar sites appeared at rods No. 2, 4 and 6, as well.

c.) 280 mm elevation

The rods are damaged on different extent. Rods 5 and 6 are entirely disappeared, only the W heaters indicate their positions. On the others the cladding and pellet remained back with the signs of strong chemical interactions between the oxidant gas and the pellet and cladding, moreover between the pellet and cladding (PCI). The cladding of central rod (No. 9) remained intact at this height, only the outer side is oxidised (Fig. 63). At the others the claddings are broken through at many sites. The time of formation of crack can be roughly assessed by looking at the pellet behind it. At some places the UO_2 was oxidised, at others not. Obviously the latter formed after the air inlet was stopped, may be late in the cooling down phase.

On Fig. 64/a a break on rod No. 8 is shown. Neither the pellet nor the cladding metal nearby is oxidised. On Fig. 64/b a break on rod No. 7 can be seen with oxidised pellet behind it. The thicker oxide scale on the outer side indicates a higher maximum temperature at the second case. The damage of rods and extent of oxidation were asymmetric on a degree, that on rod No. 1 even β-phase remained back on about 90° of clad circumference while in the opposite corner of bundle only the W heaters remained back.

d.) 375 mm elevation

The degradation and oxidation on claddings and pellets are more pronounced. Similar to elevation 280, the rods No. 1 and 9 (unheated) remained back on the heaters, with whole circumference, the 7 and 8 only partly. About 30% of clad thickness oxidised to zirconium-dioxide, the remaining converted to α-phase. On Fig. 65 characteristic view of cladding of rod No. 1 can be seen. The PCI typical (U,Zr) phase is less pronounced, may be because of slight contact. A part of cladding and pellet of unheated rod No. 9 - where the PCI originated (U,Zr) layer is stronger - can be seen on Fig. 66. The extent of oxidation is like at the rod No. 1.

At this elevation only the tungsten heater remained back of rod No. 7, but a piece of pellet was stuck to the rod. The rod seems to be damaged through the interaction between the W and UO_2, as shown on Fig. 67.

e.) 450 mm elevation

The claddings and pellets this elevation were fragmented and fallen dwon from rods 2, 3, 4, 7 and 8, while rods 1, 5, 6 and 9 the fuel structure was kept (see Fig 61, cross section at 450 mm). Comparing with the slice at 375 mm the main differences appeared at rods 5 and 6, because at that lower level these rods were also destroyed. Further down at 280 mm only the 5 and 6 have lost their integrity. Presumable the reason why at 450 mm these two rods suffered less damages, it that beside them the shroud was opened for the optical pyrometer.

The radiation loss of heat reduced the temperature to a level where they could keep their shape.

Both the rods 1 and 9 have intact claddings and pellets, with less PCI at the former (Fig. 68/a) and stronger at the latter ones (Fig. 68/b). The metal part of both rods are transferred entirely to α-phase. The highest temperature of central unheated rod (No. 9) was obviously above that of rod in the corner of shroud (No. 1). At rod No. 5 a part of cladding is lost together with a piece of pellet. Nearby the UO_2 is oxidised and swelled with forming cracks between the grains as shown in Fig. 69.

Around the heater of rod No. 8 a part of cladding remained at a peeled off position without any pellet. The view of its cross section indicates strong PCI effect and nitride even on its inner surface (Fig. 70). It indicates an early break of the cladding when the gas phase contained air. The wide (U,Zr) layer refers to high temperature before the cracking. On this slice the typical view of chemical interaction with the UO_2 appeared at many W heater rods can be observed.

f.) 535 mm elevation

The degradation of bundle at this elevation was substantially lower than at lower level. The clads and pellets surround the heater W at every rod. Even β-phase remained back in the middle of metal phase at many areas. However, the clad has broken through at some places. The pellet-clad interaction resulted also in thin layers and can be identified only at very few places.

The large amount of β-phase remained back in clad of rod No. 1 as it can be seen in Fig. 71. A break through of clad and pellet of rod No. 6 is shown on Fig. 72.

g.) 555 mm elevation

This elevation is in the middle of upper spacer. The temperature of low heat capacity spacer sheets raised above the temperature of cladding of fuel rods at that elevation. In Fig. 73 a section of spacer is shown at a stage, where a part of the metal phase melted and escaped leaving back the boundary oxide and α-phase. It is the sign that here the temperature was in the range of 1800-2100°C.

The extent of oxidation was limited by lack of oxidising agent and large part of zirconium alloys remained as β-phase. In Fig. 74 a stage of clad on rod No. 2 can be seen, consisting mainly earlier β-phase with thin oxygen stabilised α-layer. The contact with the pellet was certainly not good enough for PCI.

At a site of rod No. 3 strong PCI can be identified as it is shown in Fig. 75 with two different magnifications. The (U,Zr) alloy layer and globules can be identified with a stage of layer from where the alloy escaped. Between the alloy layer and UO_2 the characteristic α-oxide with higher oxygen content and (U,Zr) inclusions can be seen. Fig. 75/a shows a part of pellet with two different morphologies separated by a crack. The area beside the clad was in chemical contact with the Zry-4, the other behind the crack certainly not.

The general view of this slice suggests a conclusion that the temperatures at this elevation were higher than at the lower 535 mm.

The oxygen content of β-phase is certainly higher than at the as-received metal resulting more pronounced Widmanstetten-lines. At some sites the β-phase or part of it melted and flowed out from the oxide boundaries. From this effect the maximum temperature value can be estimated. It was certainly in the range of 1800-1900°C.

h.) Debris at -20 mm elevation

The aim of cut here was to get information about the broken fragments fallen down during deterioration of bundle. The view of the particles may give informations about processes forwarded. A large part of particles consists of pellet and clad stuck to each other, fragmented and fallen down without separation. A characteristic detail can be seen on Fig. 76/a including traces of some processes. At the boundary of pellet and cladding the strong interaction resulted in globule of (U,Zr) alloy. From the middle of clad the molten β-phase zirconium alloy escaped. The morphology of UO_2 near to the wall has been changed. The fragment detail in Fig. 76/b shows how the cracking process advanced in fuel materials. The clad and pellet has been stuck so strongly that the break line does not follow the boundary. This is not surprising if the diffusion layer formed at he interaction is taken into account. Fig. 77 shows an enlarged view of the layer where the two phases are diffused into each other. In Fig. 78 two holes are shown, which have been left back when the melted U,Zr alloy flowed out.

The advance of zirconium phase in grain boundary of UO_2 is shown in Fig. 79. In the α-phase holes can be seen again, indicating the low viscosity of (U,Zr) alloy that can escape from small holes like these.

Fig. 80 shows again a characteristic detail of a fallen down fragment. Two types of ZrO_2 phase on the outer side, strong oxidation and PCI. On the lower part of the picture the inner side of wall metal has been melted and escaped, certainly because of eutectic melting and chemical interactions.

Looking over the cross sections, some conclusions can be made at different elevations. The temperature in the bundle was certainly above 2000°C, especially if the short transient time is taken into account. The physical and chemical processes forwarded can be reasonably understood on the basis of our present knowledge. The exception is the low amount of nitride phase, especially if we compare the results of CODEX-AIT1 and CODEX-AIT2. At present the role of the oxide layers formed during pre-oxidation is thought to be the main influencing factor.

Material felt down or melted and solidified at the bottom of the experimental facility was collected and some fragments were selected under optical microscope. The selected pieces were embedded into vacuum resistant epoxy resin, ground and polished for the studies carried out by a Philips SEM 505 electron microscope equipped with a LINK AN 10 energy dispersive microanalyser. The surface of the sample was made conductive by evaporating a thin (about 20 nm) carbon layer to it.

Sample was scanned at TV mode and digital BEI and SEI images characteristic to the sample were recorded with a resolution of 512x512 pixel points. Fragmented UO_2 grains, layered Zircaloy cladding and interaction zones are the most typical features of the sample. Typical areas are shown in the digital images of Fig. 81. The first image exhibits an interface between UO_2 and Zr and it can be recognised that U penetrates into the Zircaloy tube. The second image shows an interaction zone at higher magnification. The third image shows relatively intact piece of the Zircaloy cladding connected to oxidised Zr (exhibits darker contrast). At the right hand side of the image two small sized UO_2 grains can be seen. All these statements are based on EDS analysis of the above mentioned parts of the sample. The fourth image shows UO_2 grains with various grain sizes: the smallest are only micrometer sized, while the largest has several hundreds of micrometer. The fragmentation of the core material is probably due to the thermal and mechanical stresses.

Digital X-ray maps of Zr, U, Si and Fe were collected from some typical region of the sample at a resolution of 128 x 128 pixel points at 100 times of magnification. X-ray photons of the four elements mentioned above were collected during 20 msec at each measuring point and the total frame was scanned 5 times, i.e. the total measuring time was 100 msec for each pixel point. Fig. 82 shows digital BEI image and X-ray maps of Zr, U and Si taken from an interaction zone.

At the interface Zr and U are mixed, in other parts they are enriched in distinct areas. Si was enriched together with Zr, corresponding to the findings of the EDS and SSMS studies of grains found in the “pockets” of the Ni impaction plate. The amount of Fe was very small (for this reason it is not worth to show the X-ray map of it), a few tenth of mass % and it was detected mostly in the Zircaloy and at the interface. Probably it is an impurity element of Zircaloy.

6.1 X-RAY RADIOGRAPHY INSPECTION OF THE BUNDLE

The core model of the CODEX AIT-2 facility suffered a serious damage during the test. In order to find the placement, extension and the characteristic features of the damage before cutting into slices radiographic imaging was performed [8].

The Dynamic Radiography Station (DRS) at the Budapest 10 MW research reactor was used for this purpose. The DRS is situated at the No 2 horizontal thermal channel of the reactor, the arrangement is shown in Fig. 83. It can be used for neutron-, gamma-, X-ray radiography work as required by the investigated problem. In this case an MXR-300 type industrial X-ray generator was used as radiation source. The dimension of the beam was optimised by an aperture of the generator. The investigated object was scanned by a remote control mechanism.

As a first step video imaging was used to localise the damaged part(s). The radiography image was converted into light by a ZnS scintillation converter sheet and detected by a low-light level tv camera. The video tapes were analysed by a QUANTEL Sapphire-type video processor and hard copies were produced by a video printer . Their quality was suitable to obtain a fast information. For these measurements the parameters of the X-ray generator were 300 keV and 5 mA. The imaging time of the camera was 40 msec, the number of integrated images was 800.

In the second step - in order to obtain better quality pictures – film imaging technique was used with Structurix D7 Pb-type X-ray films. In this case the X-ray power was 220 keV and 2 mA, the exposure time was 6 minutes. The quality of the pictures was good enough to analyse the details of the damage.

The inner structure of the core model is complex. The uranium oxide pellets are situated on tungsten heaters of 6 mm diameter, and positioned in a zirconium-niobium shroud cassette with 2 mm wall thickness. Zirconium oxide is used for insulation. The whole assembly is placed in a stainless steel tube. Its diameter is 160 mm and the wall thickness is 4 mm. Figures 4-6 show some examples of the X-ray radiography pictures. As a result of the X-ray radiography inspection the place and extension of the damage could be localised, and on the basis of these pictures the cutting of the bundle could be performed at the actual position(s).

The application of X-ray radiography provided a detailed vertical picture of the AIT-2 bundle. In Figs. 59-61 the structure and the distribution of materials can be seen. The upper spacer grid remained in its original position. Below the spacer grid severe fuel damage can be seen, the fuel rods were fragmented. Large part of the fuels fell down to the lower elevations. In the central part some pieces got stuck. The lower grid stopped most of the fragmented fuel and cladding pieces. Above the lower spacer grid a debris bed was formed, which included the intact lower fuel rods as well.

6.2 X-RAY POWDER DIFFRACTION (XRD) INVESTIGATIONS

X-ray powder diffraction measurements were performed to identify the compounds formed during the reactions caused by air ingress. Computer controlled Philips diffractometer (type 1730) equipped with graphite monochromator was used. For all measurements CuK_α radiation was applied.

The samples were collected from the fallen down pieces of the fuel rods from under the lower spacer grid, from the lower chamber of the test section. Three, different type samples (OXOUT, COLOUR, RED) were selected from the different parts of the fuel rods. The sample OXOUT was obtained from the outside part of the clad, the sample COLOUR was originated from an interfacial layer between the clad and the fuel material and the third sample RED was a reacted uranium-oxide with special colour and with special morphology from the middle part of the UO_2 ring.

The brittle polycrystalline samples, one by one were ground down to 30-50 μm powder size and were homogenised for the purpose of XRD measurement. The XRD results can be seen in the Table 4 and diffractogramms of different fuel samples are shown in Fig. 84.

Compounds	Name	Reference: N° of PDF	Estimated quantity [%] Sample name	Remarks

		card				
			OXOUT	COLOUR	RED	
UO_2	Uraninite	41-1422	35-40	~45	~80	
α -Zr	Zirconium	05-0665	-	~40	~10	isom. subs.
ZrO_2	Zirconium Oxide	27-0997	-	~10	~5	
ZrO_2	Baddeleyite	37-1484	~39	-	-	
$ZrSiO_4$	Zircon	06-0266	25-30	-	-	
ZrN	Zirconium nitride	35-0753	-	~5	~2	
$Zr_{0.85}Ca_{0.15}O_{1.85}$	Calc.-Zirc. Oxide	26-0341	1	-		

Table 4 The identified compounds and their estimated quantities

In the OXOUT sample the presence of the uraninite (UO_2) and the baddeleyite (ZrO_2) as well as the absence of metallic zirconium means the total oxidation of the cladding. The zircon ($ZrSiO_4$) compound formed also under the air oxidation paralelly reacting the silicon content of used insulator paint. (The main component of the insulator paint is some kind of Al-Ca-(Na)-silicate).

Similarly, the calcium content of the insulator could cause the forming of the mixed oxide $Zr_{0.85}Ca_{0.15}O_{1.85}$ beside the equilibrium form (ZrO_2), instead of the formation high temperature ZrO_2, as it can be seen in the case of two other samples.

In the COLOUR and the RED samples isomorphous substitution of some kind of alkaline earth metal atoms also originated from the insulator paint can be observed in the hexagonal lattice of α-Zr ("isom. subs." in the Remarks).

The samples from the interfacial layer (COLOUR) and from the middle part of the UO_2 ring (RED) show the common presence of the metallic zirconium and the UO_2 as well as the high temperature form of ZrO_2 and the reaction product (ZrN) of the high temperature interaction of the metallic zirconium and the nitrogen content of air.

There was no evidence at all any transformation of the UO_2 to higher oxides.

6.3 LAYER THICKNESS MEASUREMENTS

The detailed investigation of bundle cross sections were carried out with optical microscope. Using the image analytical features the different layers of the cross section structures were measured. Detailed measurement data in form of tables are attached to the Figs. 85-90, the thickness is given in μm units.

Due to the severe rod damage the exact measurement of different layers on each was not possible. The layer thickness measurement of fuel rods included the determination of α

and β phases, oxide and nitride layers, and also the pellet clad interaction layers. These layers were measured on the intact fuel rods or on the fuel fragments, which were unambiguosly belonging to a given rod.

The thickness of different layers on the rod circumference and on the fragmented pieces was not homogeneous, but in some cases had large variations. For this reason each layer on each rod was measured several times at different positions and the average value was defined for the given rod. These average values are given in the tables.

The α and β phase thicknesses gave a complementary to each other picture. In the lower part of the bundle the total cladding thickness remained in β-phase. The top of the bundle contained also thick β-phase layers. The α-phase was present mostly in the central part of the bundle. Some thin (up to 100 μm thickness) layers were measured in the upper part, close to the spacer grid. (Figs. 85-86)

The oxide layer thickness has an average 50-100 μm value in the upper part of the bundle (Fig. 87). The presented values were measured as the thickness of the external oxide layer. The maximum oxide layer thickness was measured in the central part of the bundle and its value was 120-160 μm.

Nitride formation was seen in the central and upper parts of the bundle. The measured value of nitride layer thickness was ~30 μm. There was much less nitride in the AIT-2 test then in the AIT-1, however the nitride formation was not limited to the upper elevations, but nitrides were observed at the central part as well (Fig. 88).

Pellet-clad interaction took place only in the hottest part of the bundle and was observed above 280 mm elevation (Fig. 89). The measured values of interaction layer thickness were between 50-170 μm. The pellet-clad interaction was observed on all of the 9 rods.

The shroud part of the cross sections was also analysed with the optical microscope. The oxide layer thickness on the outside and on the inside of the shroud, and the α layer thickness also on the two sides of the shroud were measured. The shroud suffered strong oxidation on both sides, the layer thicknesses on the two sides were comparable to each other. (Fig. 90) The oxide layer thickness reached 100 μm on both sides at the central part of the bundle, at the upper elevations the thickness was less: ~20-50 μm. Nitride layer was also observed on the external surface of the shroud, its thickness was ~10 μm.

7. AEROSOL MEASUREMENTS

In the AIT-2 test the on-line laser particle counters were activated after the pre-oxidation phase. The highest aerosol release was observed in the period of steepest rise of the temperature slope (Figs. 53-58). The number of particles was high in the cool down phase at lower temperatures as well, probably due to the further fragmentation and degradation of the bundle. This period was accompanied by a change of particle composition and size distribution, the relative number of large particles increased while the amount of small particles decreased. The peak of the particle counter concentration in the aerosol release was several times higher than in the previous AIT-1 test [9].

The impactor sampler construction was completely changed compared to the CODEX-AIT-1 test. At the second test only two small impactor plates were used: one was made of Si, while the other was of conductive carbon (Fig. 91). The surface area of each plate was approximately 2 mm^2. Behind the plates, quartz fibre filters with 14 mm (12 mm free) diameter were mounted. The same Ni impaction plate that was used in the first air ingress test has been applied also in the new test, and it was again located in the upper plenum of the cooler opposite to the outlet tube of the test section. Two pockets were mounted on the plate to collect larger size particles falling down after colliding into the surfaces above them. Both had 2 x 20 mm open upper inlet. Two special collectors were introduced into the top of the cooler tubes. They had inlet surfaces looking opposite to the gas stream and rectangular closed profile going down about 120 mm into vertical tubes of the cooler. Like the impaction plate and its pockets, these were also made of Ni sheets of 0,25 mm thickness. The profile was opened above the closed bottom end with venetian blind like outlet for leaving the gas streaming through. The upper inlet areas were about 0,5 cm^2.

The impactor sampling time in AIT-2 was decreased. It was 30 seconds for sampler units between No. 3 and 8, however for the first and last two units it was 60 seconds. In AIT-1 each unit was operated for 60 s. The gas flow through the impactors was the same as in the first test, i.e., it was approximately 1 litre/min.

The objective of the examination was the investigation of the size, shape and elemental composition of aerosol particles released during the air ingress test. Special interest was given to the uranium release and the size and shape of the U containing aerosol particles. The following samples were gained from the test:

a) 10 collector plates with Si and conductive carbon surfaces from the samplers
b) 10 quartz fibre filters from the samplers
c) particles collected in two pockets of the Ni impaction plate
d) particles collected in the cooler samplers
e) impaction plate sheet surfaces (4 different areas were chosen, 2 from the middle, 2 from the edge)
f) sheets from the cooler samplers top area.

Some remarks about the sequence of the investigations where it was important:

- weighting of the sampler units for comparison with the starting weight
- dismantling of the samplers
- X-ray fluorescence (XRF) - analysis of quartz fibre filters (QFF)
- cut out 1 / 4 of QFF areas for studies by scanning electron microscope (SEM)
- 3 / 4 of QFF for spark source mass spectrometry (SSMS)
- selecting some characteristic particles from one pocket of the impaction plate and cutting two small pieces from the cooler sampler for SEM + EDS (energy dispersive system for electron beam microanalysis) studies
- particles remained from the pockets and the ones collected by the cooler sampler were prepared for SSMS measurement.

7.1 MORPHOLOGICAL STUDIES AND IMAGE ANALYSIS

There were aerosol particles on each collector plate, but the number was much less than it was on the collector plates of CODEX AIT-1. Also it was found that the very fine particle fraction (below 0,5 micrometer) was missing from the collectors in the second test. It is very much different from the findings of the CODEX-AIT-1 test where there was a lot of very fine particles especially on the surface of impactor No. 1 taken at the high temperature escalation. At the present test the greatest number of particle was found to settle on impactor No. 4. It was working during the highest temperature region of the test. There is a second maximum in the aerosol particle number and mass, between collector samples No. 6 and 8. This corresponds to the second smaller maximum in the curve of the particle cumulative mass gained by the internal laser particle counter. Impactors No. 9. and 10 were working in the cooling down phase of the test. The coverage of their collectors corresponds to the last two maximums in the curve of the cumulative particle mass mentioned above. It must again be emphasised that very limited number of aerosol particles was settled on the collectors. There was a better situation in this respect on the Ni impaction plate, where the number of particles was high enough to do image analysis, too.

By scanning the surfaces of the quartz fibre filters by SEM even less number of particle was found than on the collectors. The fibre structure was prominent and a few particles could be seen on the surface of the.

On the surface of the collector plates both individual aerosol particles and aggregates of them could be distinguished. It was found that less aerosol particle settled on the Si wafer pieces than on the conductive carbon. The size of the single aerosol particles has started at about 0,8 - 1 μm and generally has not extended over 5-6 μm. The shape of the particles was mostly slightly elongated. Globular particles, long plates and rectangular grains were also found. Plate-like structures appeared in the pre-heating and pre-oxidation phases, i.e. on the collectors No. 1. and 2, however they could be found also in the air ingress phase of the test. The length of these platelets was several tens of μm (sometimes more than 100 μm), while the width of them was about 2-3 μm.

Relatively large number of particles on the impaction plates and in the impactors were silicates or other impurities coming from the system. Only the particles having bright contrast were originating from the structural materials such as the cladding, the spacer or the

heating wire etc. The degree of coverage by particles was different at the studied parts of the cooler sampler and that of the Ni impaction plate. The upper part of the cooler sampler was more densely covered than the lower part of it. Also the middle part of the Ni impaction plate was more densely covered than the edge part of it.

For quantification of the particle size, the mean Feret diameter was chosen. On the Ni impaction plate the greatest number of particles was found between 1 and 3 μm. Diameter intervals larger than about 5 μm correspond to aggregates of some individual aerosol particles. The number and also the area percentage of the aggregates larger than 30 μm is zero. The larger mean diameters corresponds to the platelets.

The most important difference in the size of the aerosol particles collected during the two CODEX-AIT experiments that in the second test the very fine particles were settled more on the Ni impaction plate and not on the collectors which were densely covered at the AIT-1 test. Contrary in the first experiment there were only very limited number of particles on the Ni impaction plate. In the second test there were particles and aggregates on the Ni impaction plate but the degree of coverage by particles was depending on the place on the plate - i.e. whether it was directly opposite to the outstreaming flow or it was at the edge of the plate as already mentioned.

The shape of the aerosol particles characterised by the ratio of the minimum and maximum Feret diameters seems to be similar in the two experiments, i.e. the average particle shape is slightly elongated.

7.2 ELECTRON BEAM MICROANALYSIS AND PARTICLE CLASSIFICATION

Due to the importance of the uranium release first the uranium bearing particles are discussed. The elemental composition performed by EDS showed that uranium was present in some particles and aggregates. U could very scarcely be found on the collector plates, while it could be detected at different places of the Ni impaction plate. The other techniques like SSMS and XFS have not been able to find the very small amount of U on the impactor samples. One U-rich aggregate was found on the Si wafer of collector No. 7. The mass of this aggregate was about 1×10^{-8} g. On the surface of the other collector samples only trace amount of uranium could be found (e.g. at collector No. 5. and 6.). It means that the mass must be less than about 10^{-11} g.

BEI image and ED spectra of U-rich particles (with 5 μm length and 2 μm width) settled on the Ni impaction plate are shown in Fig. 92. By considering the size of this particle, the mass of it could be estimated as about 2×10^{-10} g. The smallest U-rich particles found by Centaurus and analysed by EDS had about 1 - 1,5 μm size. At the cooler sampler lower part larger sized (between 5 and 10 μm) aggregates were also found. The mass of the smallest detected uranium rich particle was only a few times 10^{-11} gram, while the aggregates with 10 μm had about one order of magnitude larger mass. The single U bearing particles had generally rectangular shape, while the aggregates were elongated or they had irregular form. Aggregates did not contain only uranium, but some amount of Si, Al and other impurity elements, too. U-rich particles and aggregates were found for by studying different parts of the Ni impaction plate and that of the cooler sampler. It was found by EDS that U could be detected more frequently in the cooler sampler lower part than in the upper

part. Also on the middle lower part (above the pockets) of the Ni impaction plate more U-rich particle was found than on the middle upper part. A rough estimation could be made for the total amount of uranium deposited on the Ni impaction plate if we took into account the studied sample areas and the number of the uranium rich particles. On this basis about 10^{-6} gram uranium could be assessed for the Ni impaction plate. These data correspond to the findings of the SSMS.

Only trace amount of U could be estimated by studying some platelets selected from pocket 1. The remained part of particles collected by the two pockets was analysed by SSMS which found uranium.

In the followings the other elements of the samples are described in the sequence of the AIT-2 test.

In the pre-heating and pre-oxidation stages of the experiment where impactor samplers No. 1 and 2. were working, the following type of particles were found on the collectors:

1. Silicates and Ca-containing particles, which could be present as impurities.
2. Zr-rich platelets, sometimes with Y, too, from which it might be supposed that they were originating from the insulating zirconia surrounding the bundle.
3. Fe, Ni, Cr and other metallic components, which might be present from the steel components.

Following the high temperature region of the air ingress test (collectors No. 3 -8.), most of the individual particles contained metallic elements, such as Fe, Ni, Cr and Mn. They might be originated from the spacer. Ni and Cr were detected together in some particles settled on collector No. 3. Cu and Zn were found on collector plate No. 7. Zirconium and small amount of nickel were found on different collectors. Zr was detected as the main component of platelets coming probably from the insulating material, too. Tin was detected in a few particles settled on collector plates No. 5, 6, 7. and 8., but the amount of it was very small for collectors No. 5. and 6.

There were a few particles which have elements from the other structural materials, such as tungsten from the heating wire. Such particles were found on the collectors No. 3. and 4.

During the cooling down phase of the test when impactor samplers No. 9 and 10 were working, Zr, Fe, Ni, Zn, Cr, Ti, Mn and impurity elements like Si, Al, K, Ca, S and Cl were found by EDS. Zr was detected mostly in the platelets of the insulating zirconia. The metallic elements were coming probably from the spacer. The impurity elements were the same as for collector No. 1. and 2.

On the surface of the Ni impaction plate besides some U rich particles several Zr rich particles together with Sn were found. There were particles containing metallic elements of the steel part of the spacer. There were particles with W and the elements of the steel, further Sn-Pb-Cu containing particles, too. Of course silicates and other impurity elements were also found.

EDS studies of the large platelets selected from pocket 1 have shown a lot of Zr, further Si, Sn, Fe, Cu, Zn, Ni and some other elements (e.g. Au coming together with Zr, Sn

and Si). As mentioned earlier trace amount of U could be suspected. It was found that large aggregates were formed which contained Zr and Si rich particles mixed with each other. Large amounts of Si and Zr were also found by SSMS. Also on the surface of some large platelets Sn was detected together with Zr. The tin rich particles were deposited on the large Zr -rich platelets in form of small (between a few tenth of μm - 1 μm) particles. They were originated probably from the cladding. Sometimes Y was also detected together with Zr for some aggregates. Their origin might be the insulating material surrounding the bundle.

Particle classification by the ED spectra was done for about 200 aerosol particles settled on the Ni impaction plate. It is necessary to mention, that this type of classification procedure is able to find the chemical classes where the majority of the particles belongs to. Also peak overlapping might be a problem. The elements of some structural material, such as the tungsten heating wire could be found only in a few particles.

The most important chemical class was enriched in Zr. Zr was coming probably from the cladding, but some amount of it might originate also from the insulating zirconia material. The Zr rich particles had an average size of 2,14 μm and the abundance of them was 15 %. The other components characteristic for this class were Si and some impurity elements. One of the other classes had a lot of Si, about 6 % Zr and metallic elements like Mn, Fe and Cr. The other two chemical classes correspond to the impurities and probably to some components of heat shielding materials. The relatively high abundance of Si and other impurity elements corresponds to the results of the SSMS technique discussed in the following chapter.

7.3 MASS SPECTROMETRY AND X-RAY FLUORESCENCE SPECTROSCOPY

The results relating to some main metallic components found on quartz fibre filters showed high value of Zr at the start, which can be attributed to impurities in the bundle from ZrO_2 fibre insulator applied for thermal isolation directly around the shroud. Low start value and a first maximum were observed for Ni and Sn. During the main escalation period the samplers from 3 to 8 were used. Their active time covered the escalation time interval. Indeed the results have indicated larger collected amounts for these elements. Many other elements were also found but they showed no characteristic behaviour or appeared in very low quantity.

The gas flow rate in the CODEX facility was 720 litre/minute. The mass escaping rate of these elements at maximum were about 0.1 mg/min of tin, 3.6 mg/min of iron and 2.6 mg/min of zirconium. Of course the samplers collected particles with relatively small sizes (not more than some μm). The gas velocity to samplers were too low to lift up larger particles. This is not in contradiction to the SEM results, because it might be supposed that the larger aggregates seen in the SEI images of the collectors were formed during deposition.

No uranium content was found on the filters.

The XRF results could be evaluated for elements Fe, Ni, Cu and Zn only. They agree reasonable well with the SSMS results. Neither Zr nor U could be detected. The Zr measurement was disturbed by the scattered exciting Mo lines.

The particles collected in the pockets of the impaction plate and in the cooler samplers showed quite different character. They were larger sheets (with about 2-4 mm lateral dimensions and 3-10 μm thickness). They were bent to half circle and showed colours from white to deep brown. Some aggregated particles were also found. Their shape indicated that at first they were deposited somewhere on a surface and later escaped, probably because of thermal expansion differences.

Element	Pockets on impaction plate μg	Cooler sampler μg
Mg	100	150
Al	1200	850
Si	1800	2000
Ca	8	4
Cr	160	500
Mn	30	100
Fe	850	1400
Ni	60	60
Zn	3	5
Zr	1300	6000
Mo	1,4	3
Sn	36	90
Hf	20	30
Pb	2,5	1,5
W	2	15
U	1,5	0,65

Table 5 Elemental composition of collected particles (SSMS results)

In Table 5 the results of SSMS measurements are shown for the main components of the above samples. The values are the total content of the given elements. The summa's of these components were in both cases slightly higher than half of the total mass of the sample. The remaining part was the oxygen and some components not listed here or determined.

As it can be seen in Table 5 the uranium appeared in these samples, 1.5 μg in the pockets and 0.65 μg in the cooler samplers. Making a rough assessment we think that on this way about 50-100 μg uranium was released from the bundle.

Some Ni-plates opposite to the outstreaming hot gas from the bundle were also investigated by SSMS method. The high value of manganese is not very surprising, this element has large vapour pressure at high temperature but definitely low at the impacting plate temperature. The low Zr values could be explained by supposing that the Zr escaped in form of oxide particles and did not stick to the certainly oxidised Ni surface. Some uranium was also found on these plates. A rough surface ratio assessment could result about a few μg for the whole impaction plate.

Looking at the cooler sampler results some thermochromatographic effects could be suspected. The volatile Mn, Cu and U have higher surface concentration at the colder lower level. However, the similar effect of Zr has certainly some other basis.

7.4 MEASUREMENT OF AEROSOL MASS ON IMPACTORS AND COLLECTORS

Before and after the test the total mass of the impactor units (containing the quartz filter and the collector plates together) was measured by an analytical balance. The results are shown in Fig 93.

Mass of precipitate:
- in pockets of the impaction plate: 10.4 mg
- in cooler samplers: 21.3 mg.

Mass increase of a separate Ni-plate (4.8 cm^2) fixed to the impacting Ni-plate near to the pockets: 1.13 mg; which corresponds to 0.23 mg/cm^2 surface coverage.

The results relating to the pockets and cooler sampler have indicated that the pockets collected with low efficiency. The two cooler samplers with about 1 cm^2 inlet had more material, than the pockets having about 4 cm upper slit.

The two maximums of total mass increase of samplers activated in series (Fig. 93) and the Ni and Sn content of them (Fig. 94) are in good agreement with the Aerosol Particle Counter results.

7.5 MAIN RESULTS OF AEROSOL SAMPLE EXAMINATIONS

The most important findings of the examination of aerosol samples can be summarised as follows:

- Particles were found on both type of the collector plate (more on the carbon conductive tape, less on the Si wafer), but the number of them was much less than for collector plates of CODEX AIT -1 experiment. It is not in contradiction with the higher degree of bundle damage, because there were a lot of aerosol particles deposited on the Ni impaction plate, which was not the case for the first test. Also the two-stage cascade impactors with larger collector surfaces were changed in the second test for smaller Si and conductive carbon plates.
- The number and the mass of the particles were the largest at sample 4 and there was a second maximum between collector samplers No. 6 and 8. This corresponds to the findings of the internal laser particle counting.
- There were valuable number of particles on the Ni impaction plate, where the smallest particles (below 0,5 μm) were deposited, too.
- Uranium was found in form of single particles and also in some aggregates both on the Ni impaction plate and in the cooler sampler. The smallest U-bearing particles had about 1-1,5 μm size which could be analysed by EDS. On the collector plate No.7 uranium containing aggregate with about 15 μm appeared. Other U rich particles had probably very small sizes and masses to detect by the EDS.
- In the aerosol samples taken during the pre-oxidation phase those elements appeared which might be components of the aerosol of the air. Zr-rich long platelets were also frequently found. Some of them had Y content, too, from which it might be supposed that the origin of them is the insulating material surrounding the bundle. Fe, Cr, Ni might be components of the steel.

- EDS analysis of the particles settled on the collector plates has shown that the following components were coming from the structural materials:
- W from the heaters: collector plate No. 3. and 4.
- Ni and Fe + Cr + Ni + Mn: from the spacer : present on each collector plate
- Zr (+Ni): might come from the spacer material
- Zr + Y: insulating material: present on each collector
- Cu, Zn : probably from the components of the system: collector No. 7, Zn was present also in sample No. 1., 2., 8 and 9.
- Sn: from the cladding: collector plates No. 5., 6., 7., 8. On the collector plates No. 5. and 6. the amount of Sn is very small.
- By EDS analysis of the particles settled on the Ni impaction plate U rich particles were found, besides Zr rich particles and components of the spacer. By EDS analysis of the particles collected by special pockets the following components were found: Zr, Sn (originating from the cladding), Fe, Cr, Mn, Ni (probably components of the spacer) and silicates from the heat shielding ceramics.
- The mass increase of the samplers at maximum values were about 0,8 mg for 30 s sampling times and 0,5 litre gas. On the basis of the fractions collected on the quartz fibre filters, the total aerosol particle flow rate could be estimated to be 0,6 g/min.
- Lamella like particles were collected by the cooler samplers and by the pockets placed on the Ni impaction plate opposite to the outstreaming gas. Their total escaped mass can be extrapolated to be about a few grams.
- SSMS analysis of quartz fibre filters indicated no uranium content (detection limit was about $5x10^{-9}$ g). The main collected metallic elements were Zr and Fe with about 1-7 approximately 1 μg/min total escaping rate and Ni and Sn with about one order of magnitude lower values.
- The larger particles collected by the pockets and by the cooler samplers were formed mainly from oxides of Zr, Si, Al, Fe and Cr with decreasing concentration in this series. Uranium has also been found in an amount of 1,5 and 0,7 μg, respectively. As a rough estimation 50-100 μg uranium was released from the bundle.
- The Ni impaction plate and the Ni sheets of the cooler sampler had mainly Mn, less Fe, Zn, Zr, Sn and W stacked to the surfaces. The quantities extended from 1 to 200 microgram/cm^2. Uranium was also detected in the following concentration per unit surface area: 0,003 - 0,012 μg/cm^2. On the basis of the results gained by the two techniques: EDS and SSMS, maximum a few μg uranium could be assessed to be deposited on the Ni impaction plate.

Approximately two orders of magnitude more uranium was detected in the aerosol released in AIT-2, than in AIT-1. In the aerosol samples taken in AIT-2 uranium could be found both in single particles (1-3 μm, Fig. 16.) and in aggregates (10 - 15 μm). The shape of the particles was mostly rectangular. The aggregates had elongated or irregular forms. Their composition contained other elements such as Si, Al, Fe etc. beside uranium. More uranium was found on the Ni impaction plate than on the collectors. SSMS analysis of the quartz fibre filters indicated no uranium content. On the impaction plate 0,07 μg/cm^2 uranium was determined by SSMS. In the particles collected in pockets of the impaction plate 1,5 μg, while in the cooler sampler 0,65 μg uranium was detected by SSMS. The total uranium release from the bundle of AIT-2 could be estimated as 50-100 μg.

8. EXPERIMENTAL DATABASE

The experimental data were collected for code validation purposes into a database, which cover 14056 s time period with 1 s frequency. The frequency of particle counter recording was different and for this reason the database has the appropriate values in the recorded points only. The parameters are listed in Table 6 and plotted in Fig. 9-58 for the period of 0-15000 s.

The database is presented in a large ASCII type file. The first column of the matrix contains the time. The "0" experimental time was set to real time 17:56:06, 28th January 1999. Each variable listed in Table 6 is given in a separate column in the file. The order of variables is the same as listed in the table. The commissioning test database has a similar structure, but the number of recorded variables was less (Table 7).

Name	Unit	Definition
Time	s	Time
UH50	°C	Unheated rod temperature at 50mm
UH150	°C	Unheated rod temperature at 150mm
UH300	°C	Unheated rod temperature at 300mm
UH375	°C	Unheated rod temperature at 375mm
UH450	°C	Unheated rod temperature at 450mm
UH535	°C	Unheated rod temperature at 535mm
UH570	°C	Unheated rod temperature at 570mm
H150	°C	Heated rod temperature at 150mm
H300	°C	Heated rod temperature at 300mm
H450	°C	Heated rod temperature at 450mm
H535	°C	Heated rod temperature at 535mm
H570	°C	Heated rod temperature at 570mm
SH50	°C	Shroud temperature at 50mm
SH150	°C	Shroud temperature at 150mm
SH300	°C	Shroud temperature at 300mm
SH450	°C	Shroud temperature at 450mm
SH570	°C	Shroud temperature at 570mm
HS50	°C	Steel heat shield temperature at 50mm
HS150	°C	Steel heat shield temperature at 150mm
HS300	°C	Steel heat shield temperature at 300mm
HS450	°C	Steel heat shield temperature at 450mm
HS535	°C	Steel heat shield temperature at 535mm
OS50	°C	Outside shield temperature at 50mm
OS150	°C	Outside shield temperature at 150mm
OS300	°C	Outside shield temperature at 300mm
OS450	°C	Outside shield temperature at 450mm
OS535	°C	Outside shield temperature at 535mm
TLOCH	°C	Lower Chamber temperature

TUPCH	°C	Upper Chamber temperature
TMELT	°C	Thermocouple with opened end at 0mm
PYR450	°C	Pyrometer temperature at 450mm
PYR535	°C	Pyrometer temperature at 535mm
TWATER	°C	Water temperature in steam generator
TSTEAM	°C	Steam generator outlet temperature
TIN1	°C	Gas inlet temperature at the superheater outlet
TIN2	°C	Gas inlet temperature in the inlet junction
TCOUT	°C	Gas outlet temperature in the outlet junction
TCOOL	°C	Gas temperature at the cooler inlet
TOUTC	°C	Gas temperature at the cooler outlet
PSYS	bar	System pressure
STEAM	g/s	Steam Flow
ARGON	g/s	Argon Flow
AIR	g/s	Air flow
POWER	W	Electric power
API1	particle/l	Concentration of 0,3-0,5 μm aerosols, internal counter
API2	particle/l	Concentration of 0,5-1,0 μm aerosols, internal counter
API3	particle/l	Concentration of 1-3 μm aerosols, internal counter
API4	particle/l	Concentration of 3-5 μm aerosols, internal counter
API5	particle/l	Concentration of 5-10 μm aerosols, internal counter
API6	particle/l	Concentration of >10 μm aerosols, internal counter
APE1	particle/l	Concentration of 0,3-0,5 μm aerosols, external counter
APE2	particle/l	Concentration of 0,5-1,0 μm aerosols, external counter
APE3	particle/l	Concentration of 1-3 μm aerosols, external counter
APE4	particle/l	Concentration of 3-5 μm aerosols, external counter
APE5	particle/l	Concentration of 5-10 μm aerosols, external counter
APE6	particle/l	Concentration of >10 μm aerosols, external counter

Table 6 Parameters available in the CODEX-AIT-2 database

Name	Unit	Definition
Time	s	Time
UH50	°C	Unheated rod temperature at 50mm
UH150	°C	Unheated rod temperature at 150mm
UH300	°C	Unheated rod temperature at 300mm
UH375	°C	Unheated rod temperature at 375mm
UH450	°C	Unheated rod temperature at 450mm
UH535	°C	Unheated rod temperature at 535mm
UH570	°C	Unheated rod temperature at 570mm
H150	°C	Heated rod temperature at 150mm
H300	°C	Heated rod temperature at 300mm
H450	°C	Heated rod temperature at 450mm

H535	°C	Heated rod temperature at 535mm
H570	°C	Heated rod temperature at 570mm
SH50	°C	Shroud temperature at 50mm
SH150	°C	Shroud temperature at 150mm
SH300	°C	Shroud temperature at 300mm
SH450	°C	Shroud temperature at 450mm
SH570	°C	Shroud temperature at 570mm
HS50	°C	Steel heat shield temperature at 50mm
HS150	°C	Steel heat shield temperature at 150mm
HS300	°C	Steel heat shield temperature at 300mm
HS450	°C	Steel heat shield temperature at 450mm
HS535	°C	Steel heat shield temperature at 535mm
OS50	°C	Outside shield temperature at 50mm
OS150	°C	Outside shield temperature at 150mm
OS300	°C	Outside shield temperature at 300mm
OS450	°C	Outside shield temperature at 450mm
OS535	°C	Outside shield temperature at 535mm
TLOCH	°C	Lower Chamber temperature
TUPCH	°C	Upper Chamber temperature
TMELT	°C	Thermocouple with opened end at 0mm
PYR450	°C	Pyrometer temperature at 450mm
PYR535	°C	Pyrometer temperature at 535mm
TWATER	°C	Water temperature in steam generator
TSTEAM	°C	Steam generator outlet temperature
TIN1	°C	Gas inlet temperature at the superheater outlet
TIN2	°C	Gas inlet temperature in the inlet junction
TCOUT	°C	Gas outlet temperature in the outlet junction
TCOOL	°C	Gas temperature at the cooler inlet
TOUTC	°C	Gas temperature at the cooler outlet
PSYS	bar	System pressure
STEAM	g/s	Steam Flow
ARGON	g/s	Argon Flow
AIR	g/s	Air flow
POWER	W	Electric power

Table 7 Parameters in the CODEX-AIT-2 commissioning test database

9. SUMMARY AND CONCLUSIONS

The second air ingress test in the CODEX facility was performed on 27th January, 1999 at the KFKI Atomic Energy Research Institute, Budapest in the framework of the OPSA project [2]. The test included a 9-rod PWR type rod bundle with UO_2 pellets. The aim of the experiment was to study the rod degradation in the pre-oxidised bundle under air ingress conditions [10].

The test started with a preheating period using hot argon and electrical heating. The bundle temperature was stabilised at ~600^{o}C. The fuel rod cladding was oxidised in steam atmosphere in two steps: at 820^{o}C and 950^{o}C to give an oxide layer thickness of 20-25 microns. Due to a valve leak a small amount of air flow joined the steam/Ar mixture during the pre-oxidation period. The air ingress phase was initiated with the injection of 2.5 g/s cold air and with a linear increase of electrical power of 2 W/s to give an initial heating rate of 0.5 K/s. Temperature excursion was observed on the fuel rods to a maximum indicated temperature of 1900 ^{o}C. Similar excursion took place on the shroud as well. The air injection was stopped when the temperature in the central elevation reached 1700 ^{o}C, indicating the melting process. Aerosol samples were taken using impactors before the pre-oxidation, before the air ingress phase, during temperature excursion in the air ingress period and also in the cooling down phase. Aerosol particle counters and video recording were also applied to the test.

In the AIT-2 test the damage of the bundle was more severe than in the first test, for the high temperature conditions were kept for longer time in AIT-2 than in AIT-1. The bundle suffered severe damage, the rod-like structure was lost in the upper part. The fallen down pieces of the fuel rods formed blockage on the lower spacer grid. The analysis of the cross sections at different elevations indicated that the temperature in the bundle was certainly above 2000°C. The nitride phase formation was observed in the AIT-2, but the thickness of nitride layers was much less than in the AIT-1 test. Intense pellet-cladding interaction took place in the rods. The cladding in the central and upper parts of the bundle was heavily oxidised. Strong oxidation occurred on the spacer grid and on the shroud surfaces as well. The structure of the UO_2 pellets changed at some places: there were cracks between the fuel grains and the fuel pulverized, probably due to the oxidation. The XRD investigation of the fuel did not indicate the formation of any higher uranium oxides. The total uranium release could be estimated as 50-100 μg.

ACKNOWLEDGMENTS

The CODEX-AIT-2 test was performed in the OPSA (Oxidation Phenomena in Severe Accidents) project of the Fourth Framework Programme with the financial support of the European Commission (contract number FI4S-CT96-0031).

REFERENCES

[1] D.A. Powers, L.N. Kmetyk, R.C. Schmidt, A review of the technical issues of air ingression during severe reactor accidents, Sandia National Laboratories operated by Sandia Corporation, NUREG/CR-6218 SAND94- 0731 (1994)

[2] Sheperd I, B. Adroguer B, Buchmann M, Gleisberg O, Haste T, Hofmann P, Hózer Z, Hummel R, Kaltofen R, Knorr J, Kourti N, Leonardi M, Oriolo F, Schneider R, Maróti L, Matus L, Schanz G, Windberg P. Oxidation Phenomena in Severe Accidents, Proceedings of FISA-99, Luxemburg 29 November - 1 December 1999, pp. 193-201

[3] L. Maróti, "Chemical Interaction between VVER Core Components under Accidental Conditions", Nucl. Eng. and Design vol. 172, 1997, pp. 73-81

[4] Z. Hózer, L. Maróti, B. Tóth, P. Windberg,"VVER-440 Core Degradation Experiment" Proceedings of NURETH-8, Vol. 2, Kyoto, 1997, pp. 605-611.

[5] Hózer Z, Maróti L, Nagy I, Windberg P: CODEX-2 Experiment: Integral VVER-440 Core Degradation Test, KFKI-2000-02/G

[6] Z. Hózer , L. Maróti ,P. Windberg, "Quenching of High Temperature VVER Bundle", Proceedings of NURETH-9 on CD, San Francisco, 1999, ISBN 0-89448-650-0

[7] Hózer Z, Maróti L, Nagy I, Windberg P: CODEX-3/1 and CODEX 3/2 Experiments: Quenching of High Temperature VVER Bundles, KFKI-2000-03/G

[8] Balaskó M, Hózer Z, Maróti L, Windberg P: X-ray radiography inspection of core model of the CODEX AIT-2 facility, Proc. International Conference Nuclear Enery in Central Europe'99, Portoroz, Slovenia, pp.763-770

[9] Pintér Csordás A, Matus L, Czitrovszky A, Jani P, Maróti L, Hózer Z, Windberg P, Hummel R: Investigation of aerosols released at high temperature from nuclear core models, J. Nucl. Materials, vol 282, Iss 2-3, pp. 205-215

[10] Trambauer K, Haste T J, Adroguer B, Hózer Z, Magallon D, Zurita A: In-Vessel Core Degradation Code Validation Matrix, Update 1996-1999, NEA/CSNI/R(2000)21

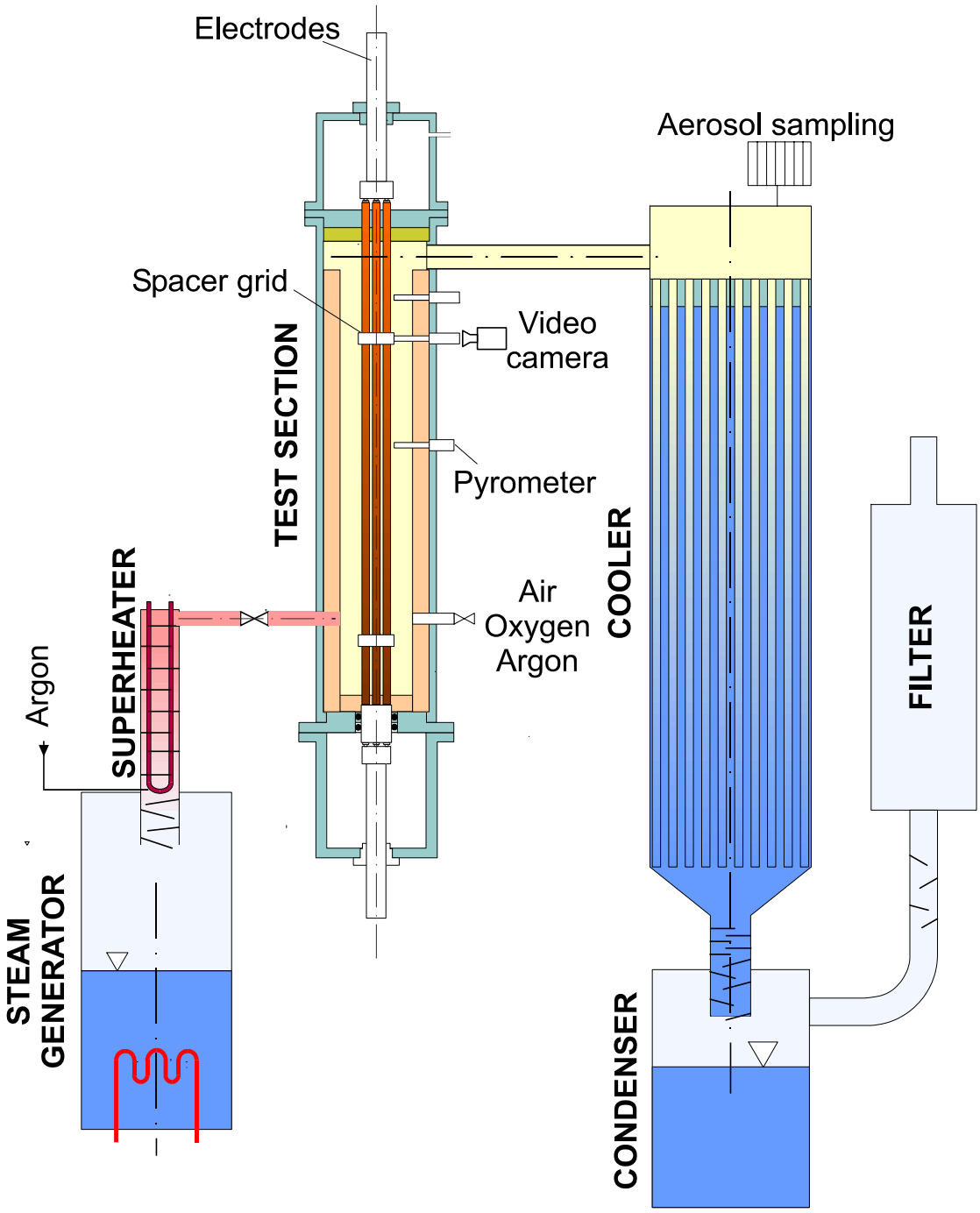

Fig. 1 Scheme of the CODEX-AIT-1 facility

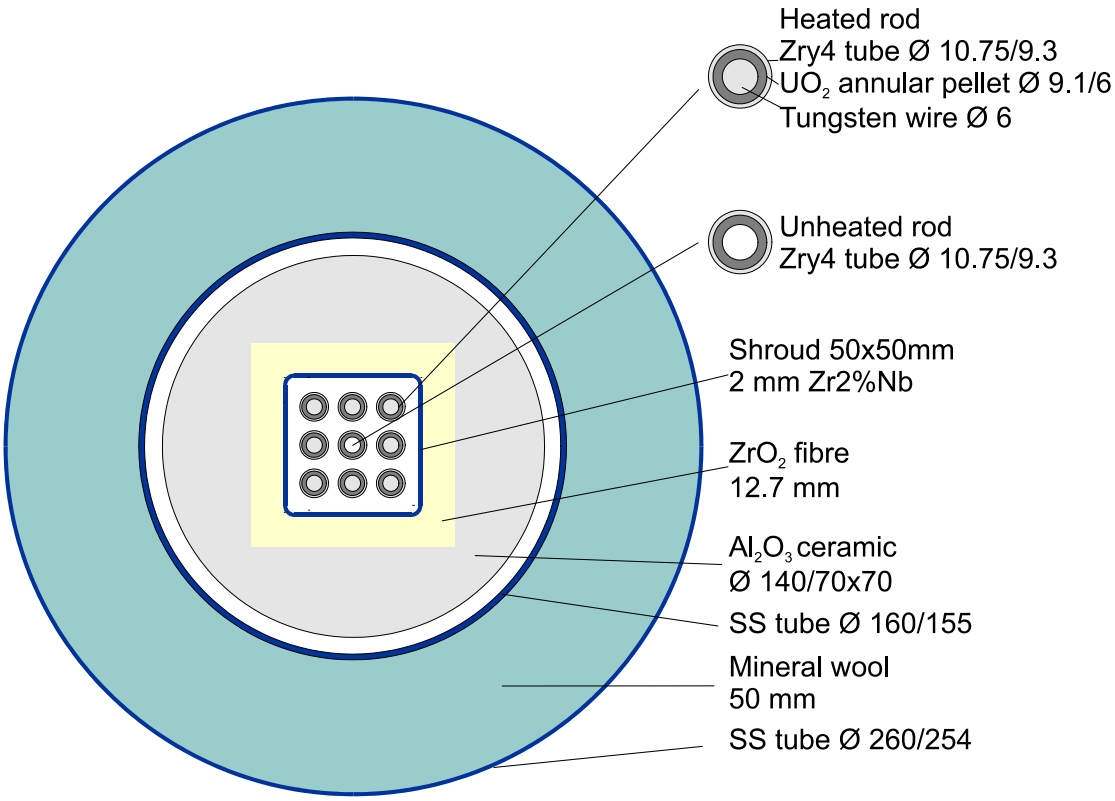

Fig. 2 Horizontal cross section of the CODEX-AIT-1 9 rod PWR bundle

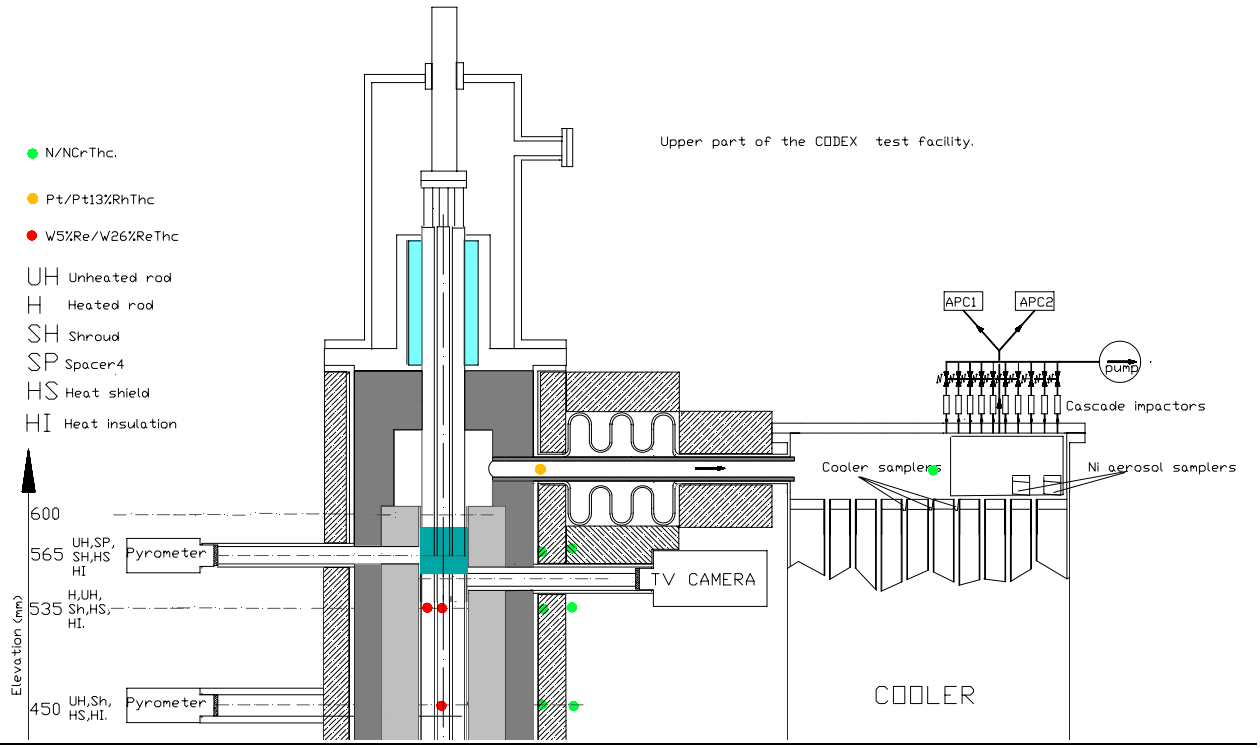

Fig. 3 Aerosol sampling in the CODEX-AIT-1 test

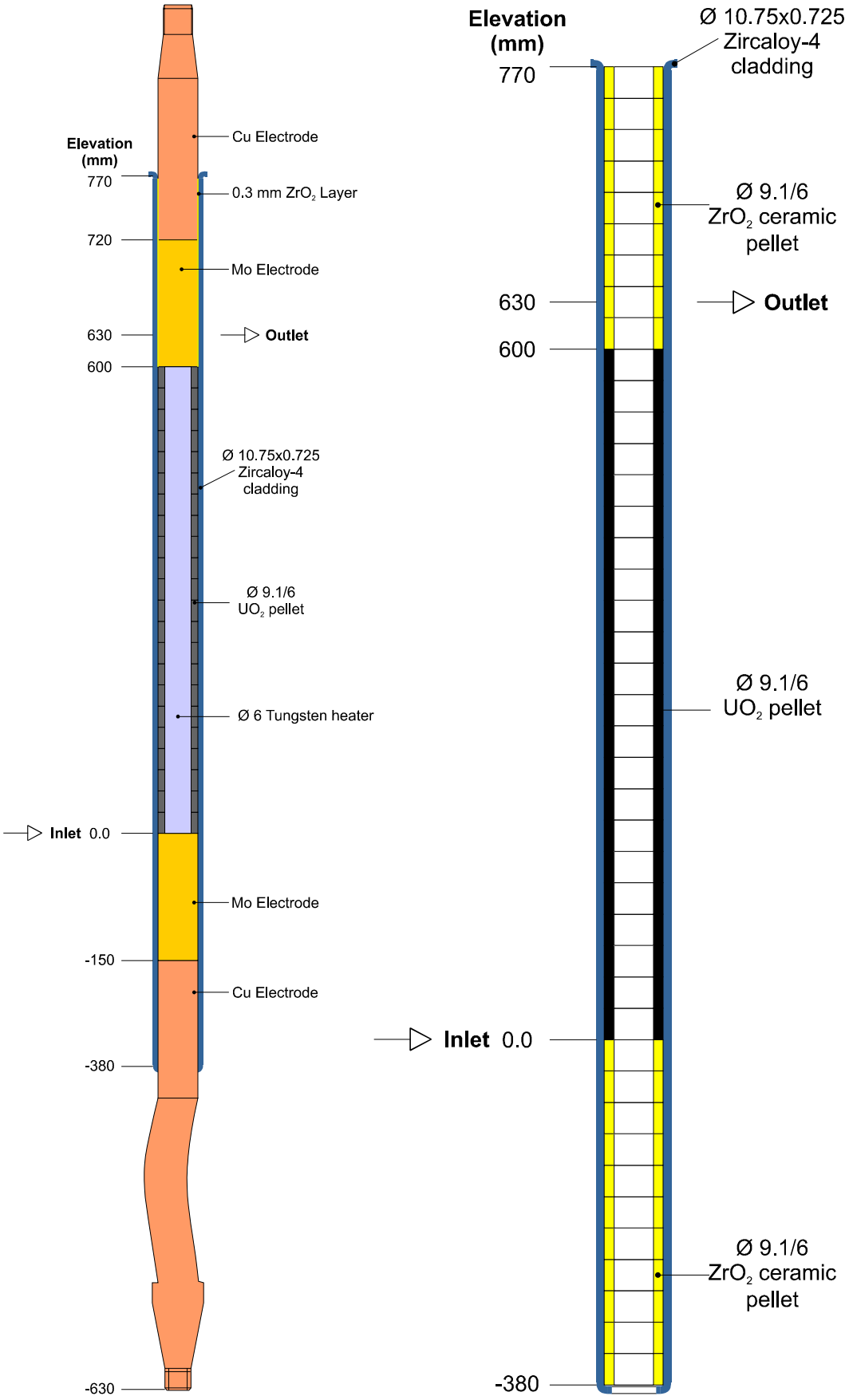

Fig. 4 Vertical cross section of heated and unheated rods

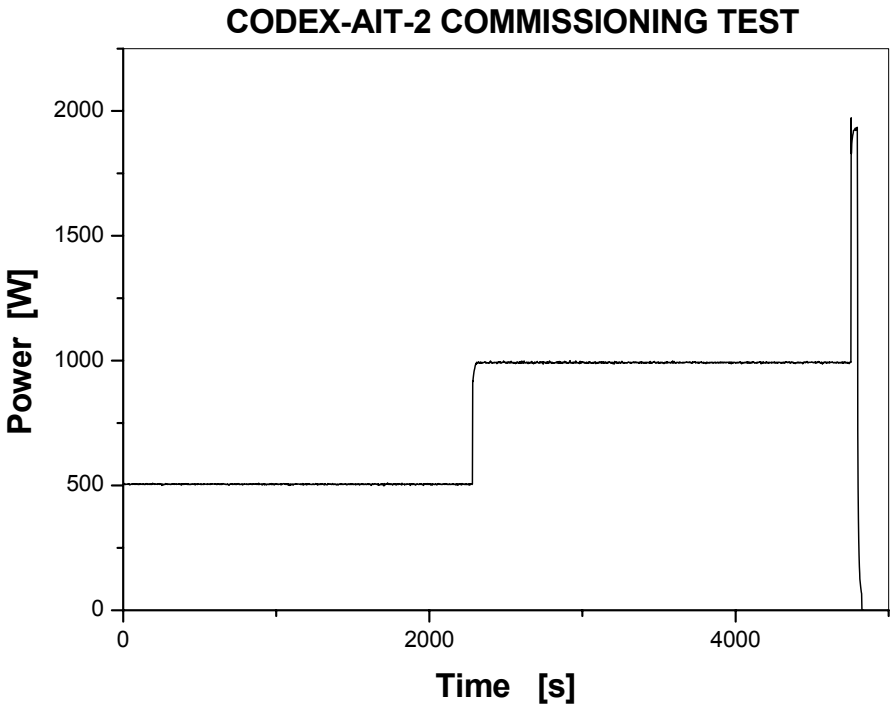

Fig. 5 Electrical power in the CODEX-AIT-2 commissioning test

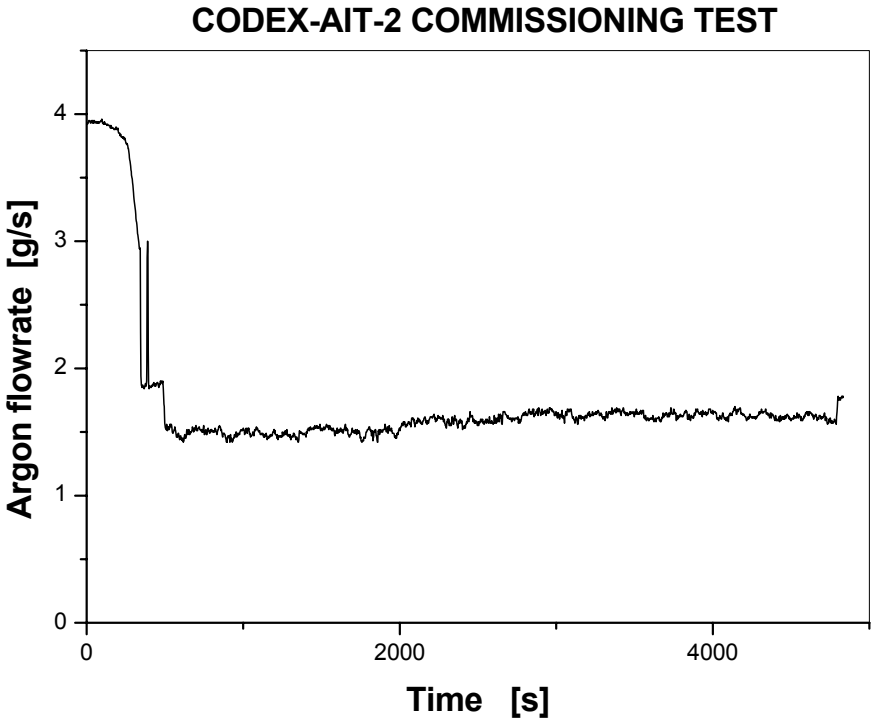

Fig. 6 Argon flowrate in the CODEX-AIT-2 commissioning test

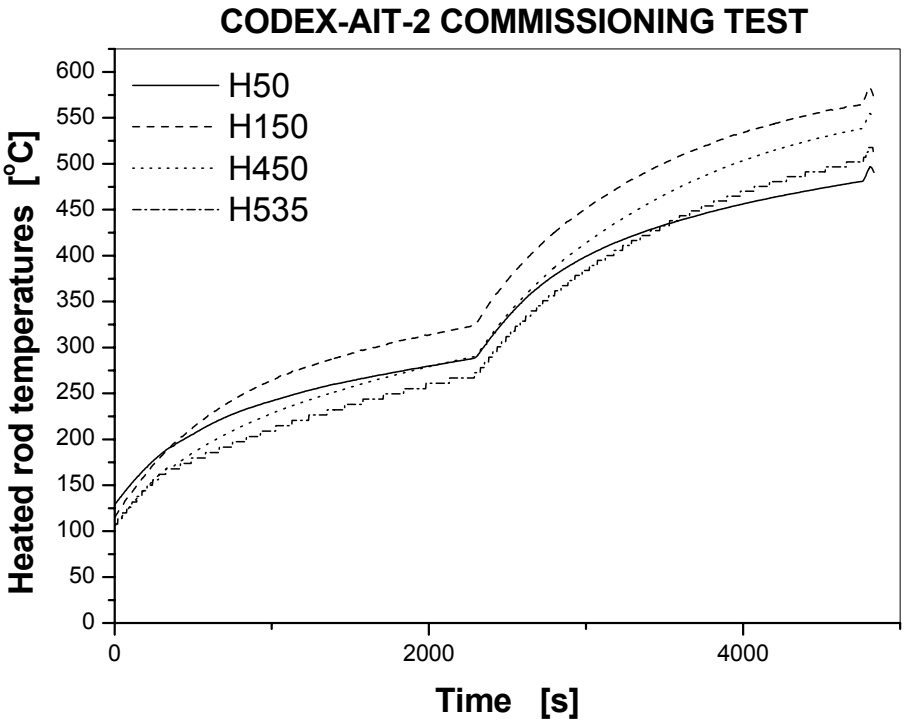

Fig. 7 Heated rod temperatures in the CODEX-AIT-2 commissioning test

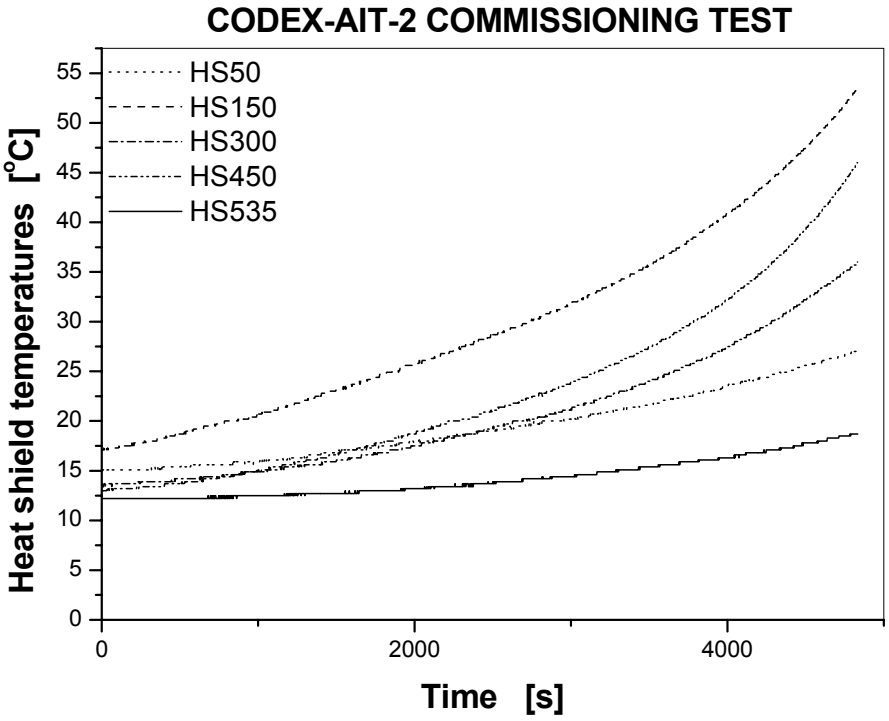

Fig. 8 Steel temperatures in the heat shield in the commissioning test

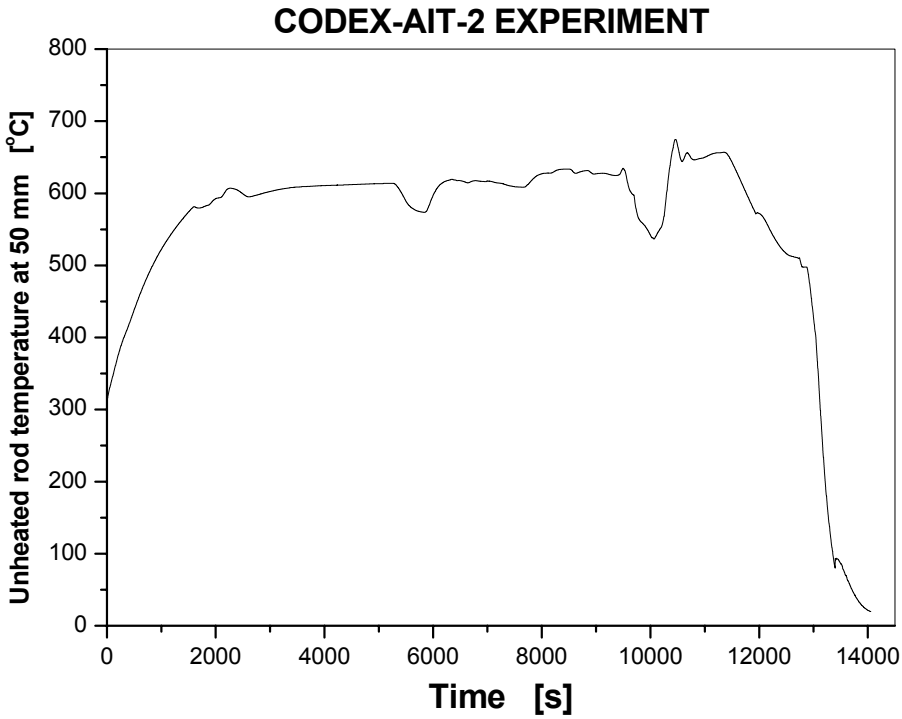

Fig. 9 UH50: Unheated rod temperature at 50 mm

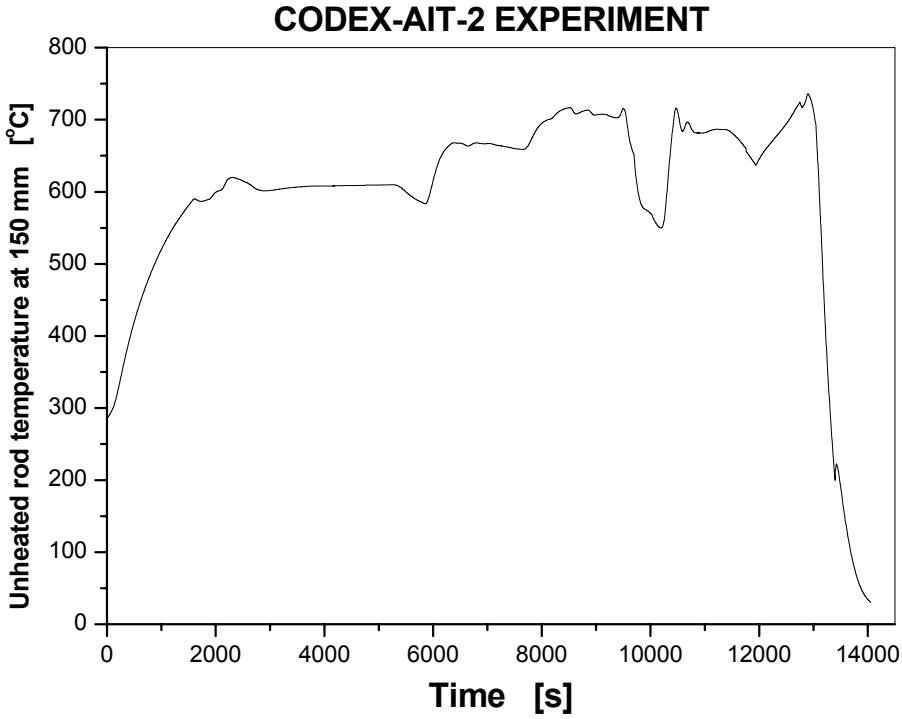

Fig. 10 UH150: Unheated rod temperature at 150 mm

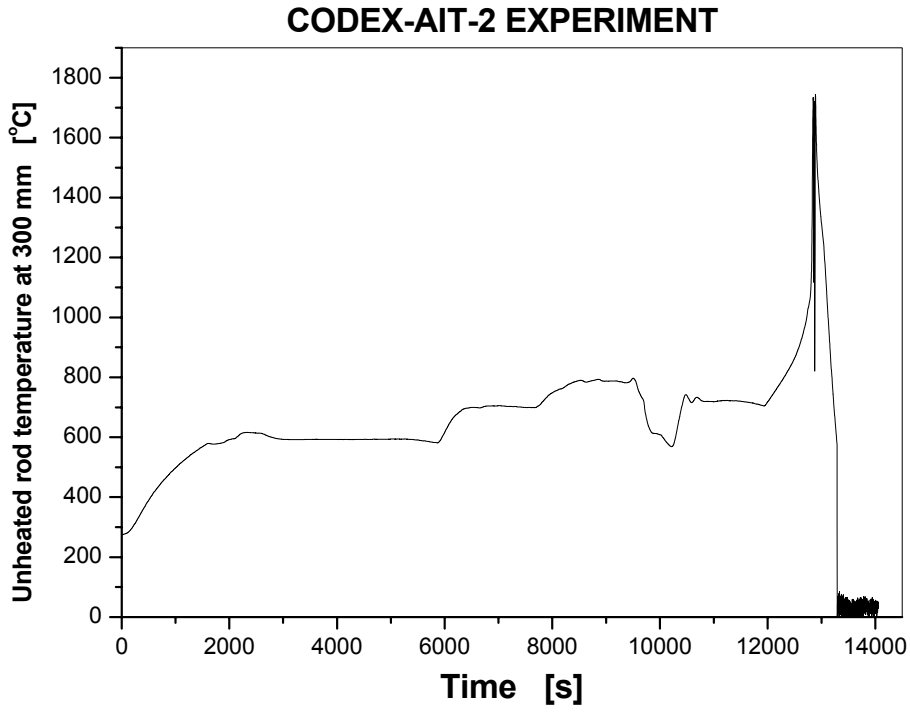

Fig. 11 UH300: Unheated rod temperature at 300 mm

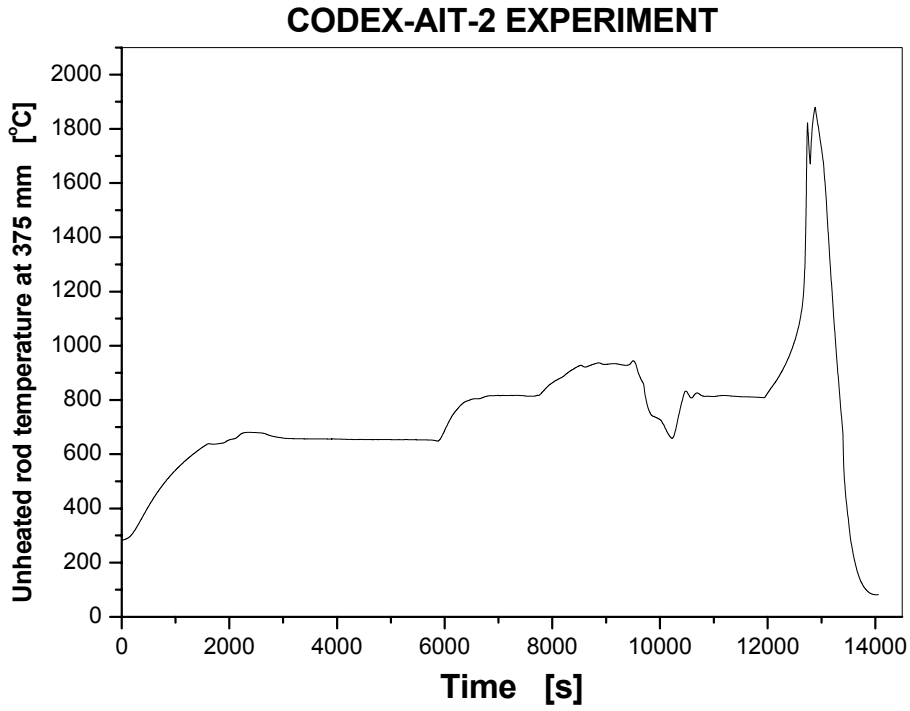

Fig. 12 UH375: Unheated rod temperature at 375 mm

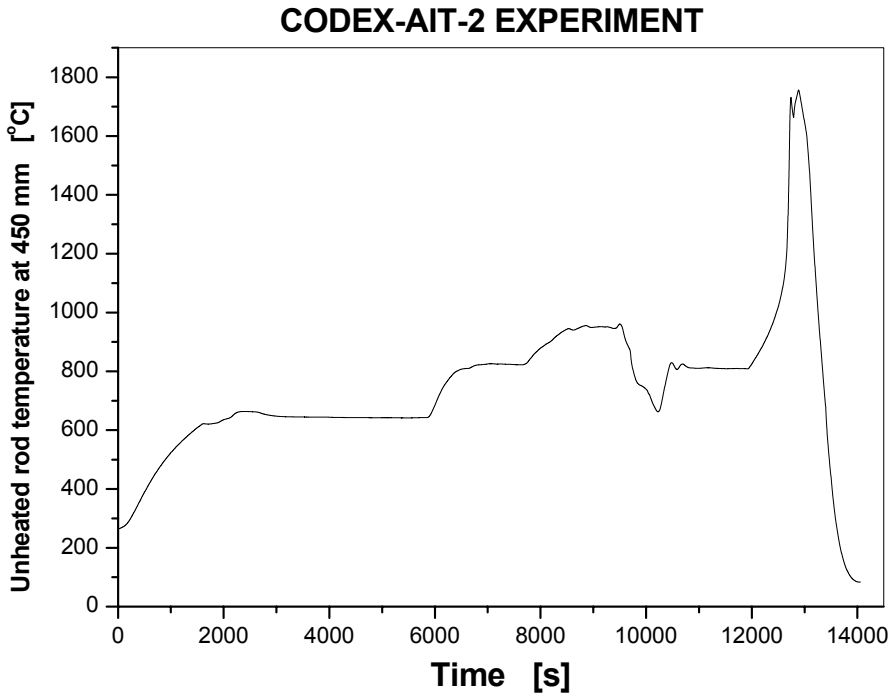

Fig. 13 UH450: Unheated rod temperature at 450 mm

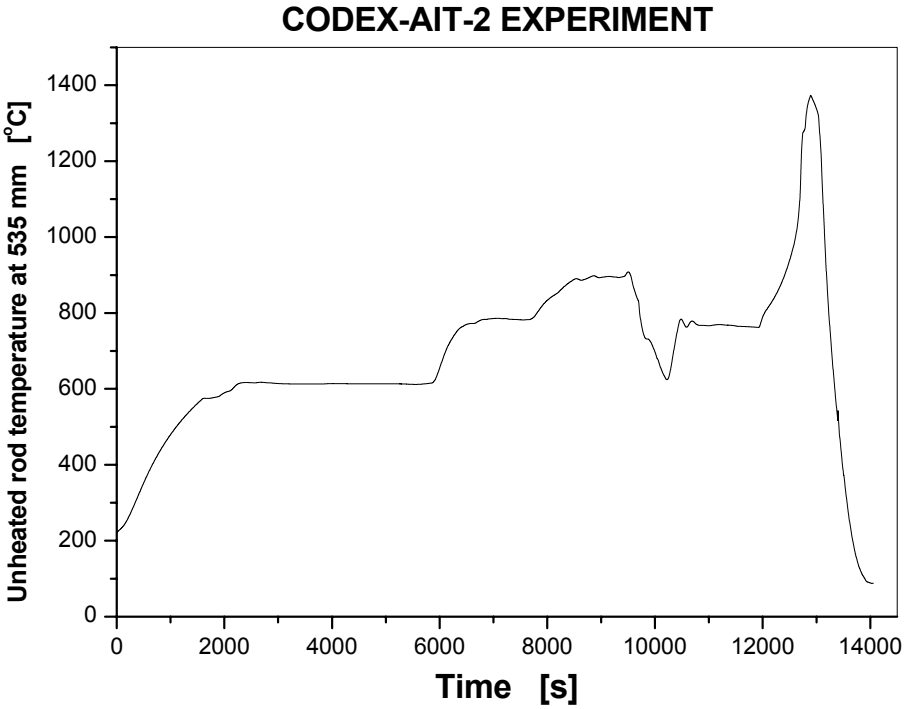

Fig. 14 UH535: Unheated rod temperature at 535 mm

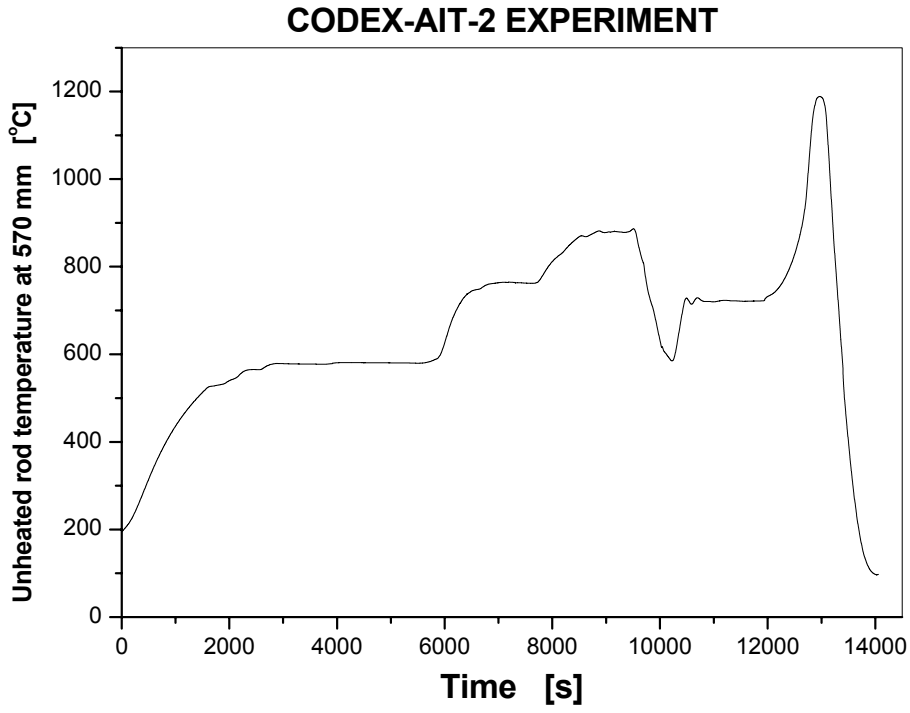

Fig. 15 UH570: Unheated rod temperature at 570 mm

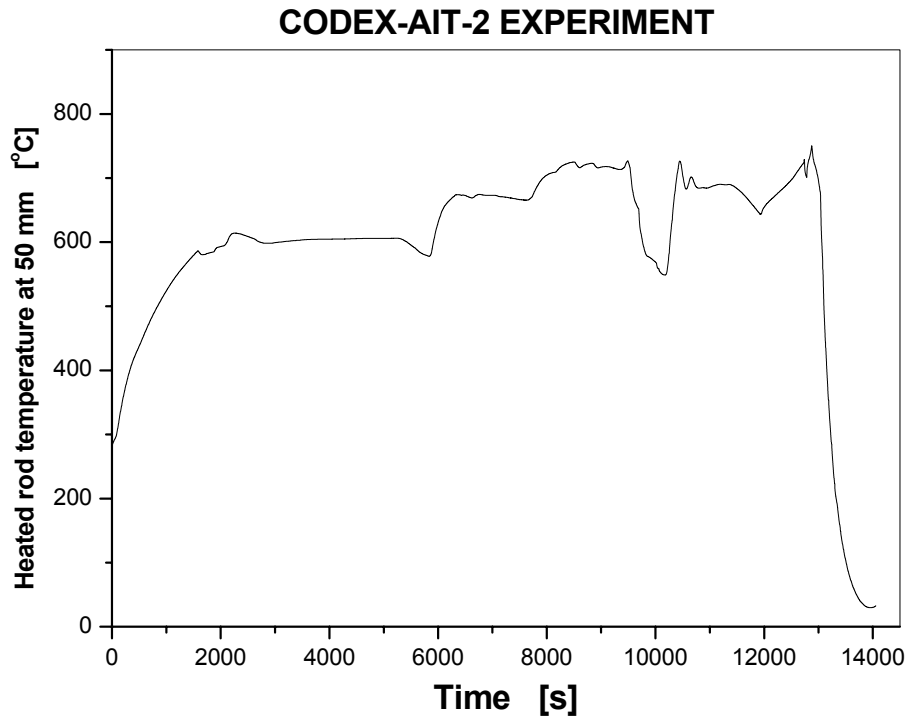

Fig. 16 H50: Heated rod temperature at 50 mm

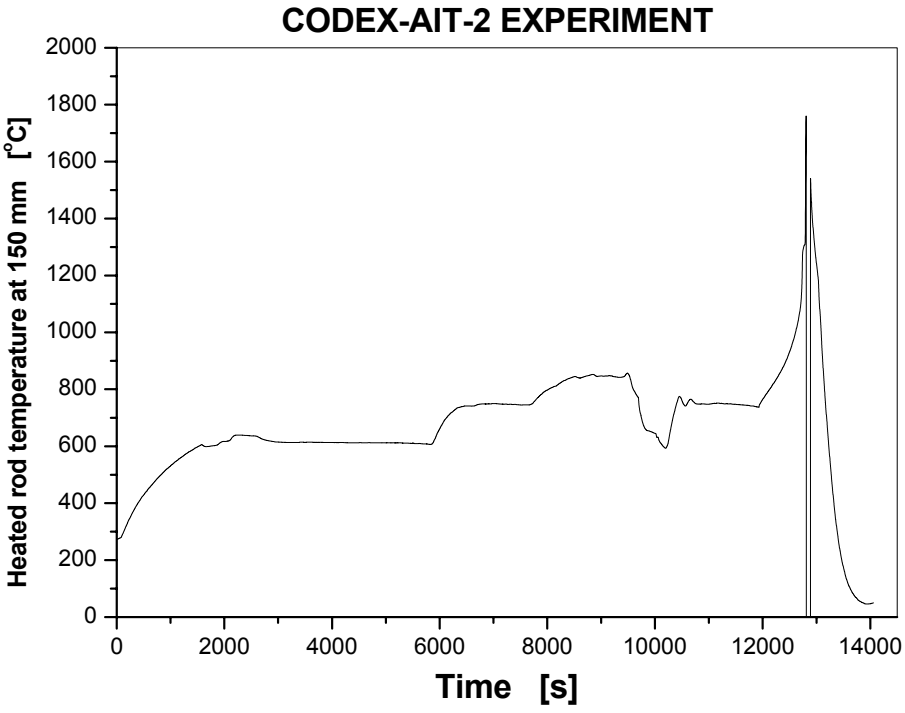

Fig. 17 H150: Heated rod temperature at 150 mm

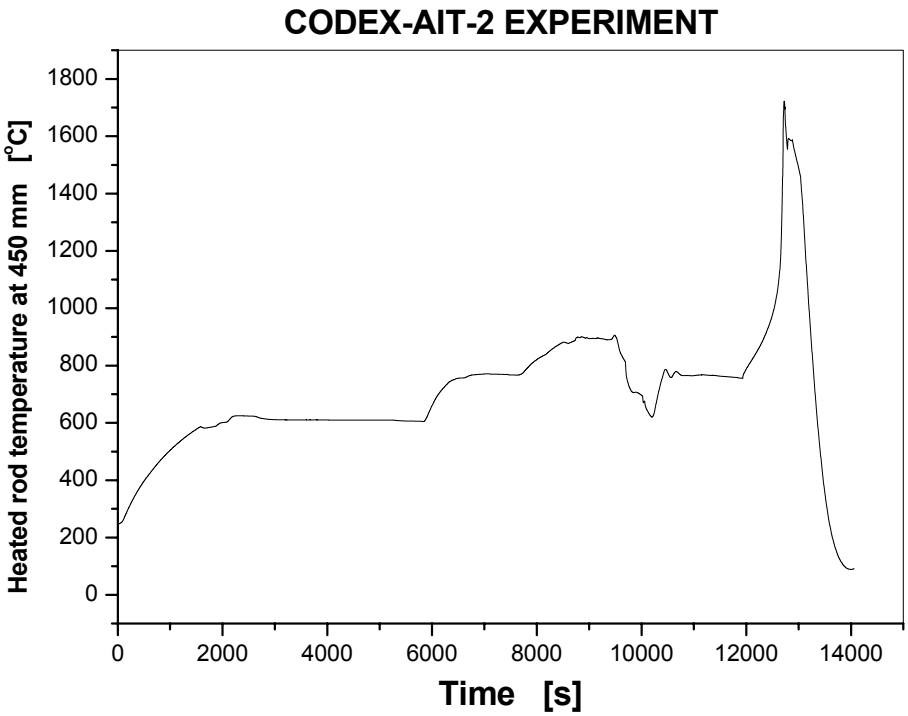

Fig. 18 H450: Heated rod temperature at 450 mm

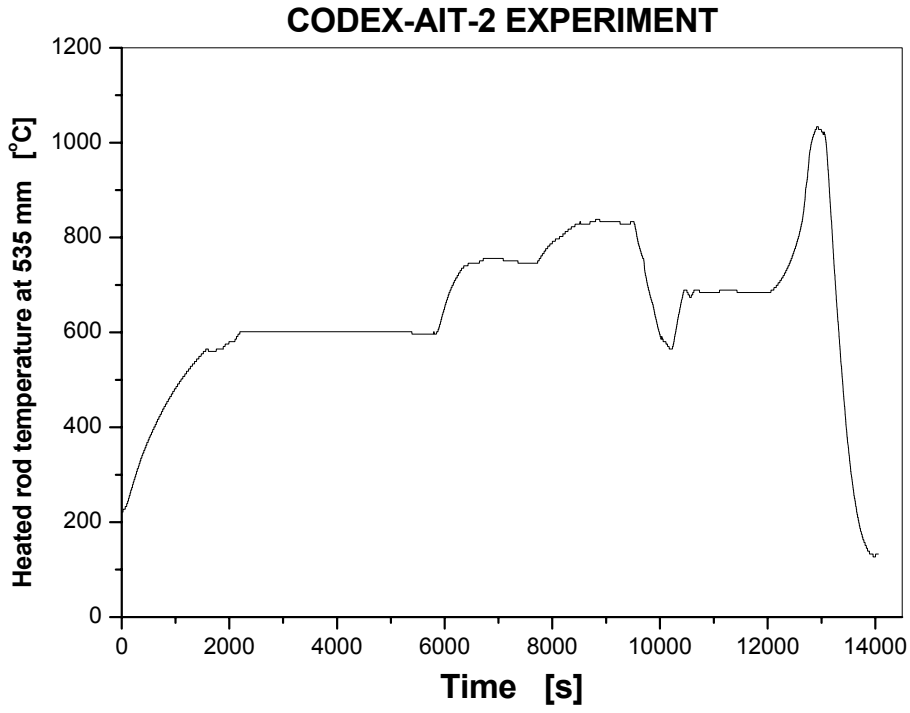

Fig. 19 H535: Heated rod temperature at 535 mm

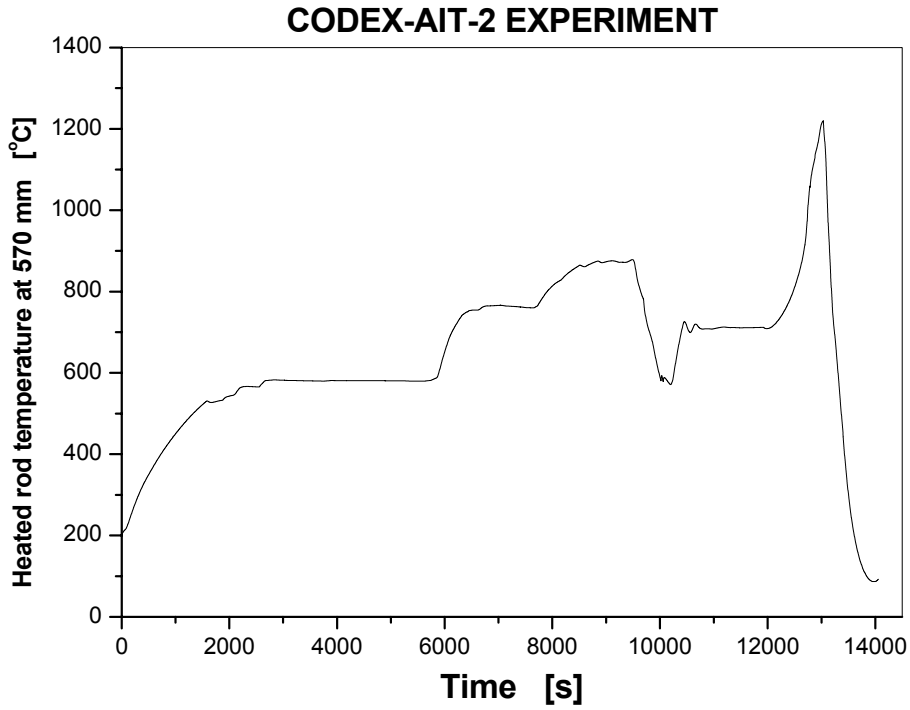

Fig. 20 H570: Heated rod temperature at 570 mm

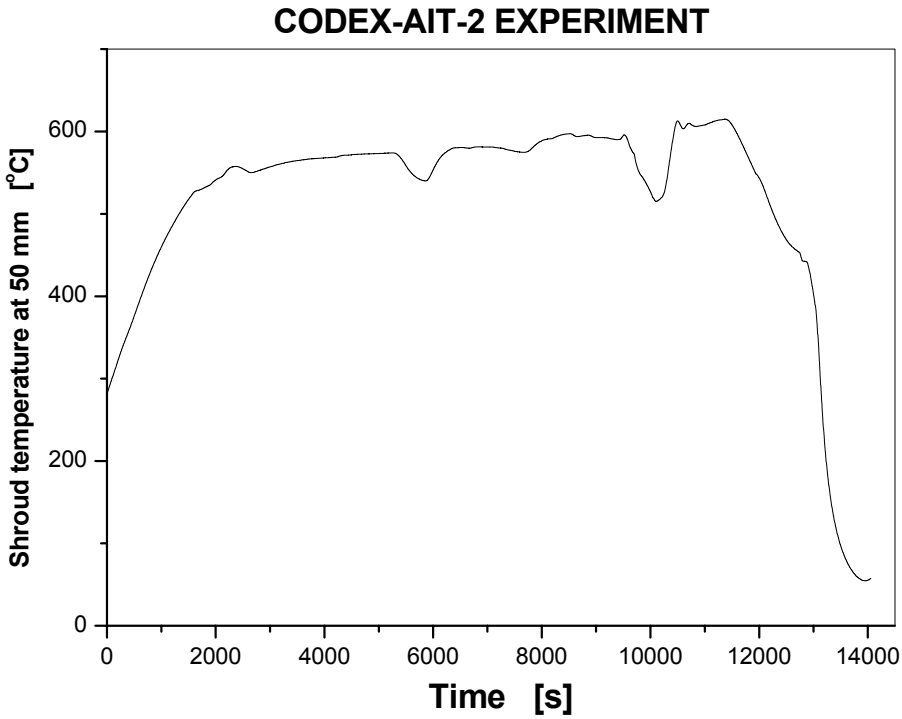

Fig. 21 SH50: Shroud temperature at 50 mm

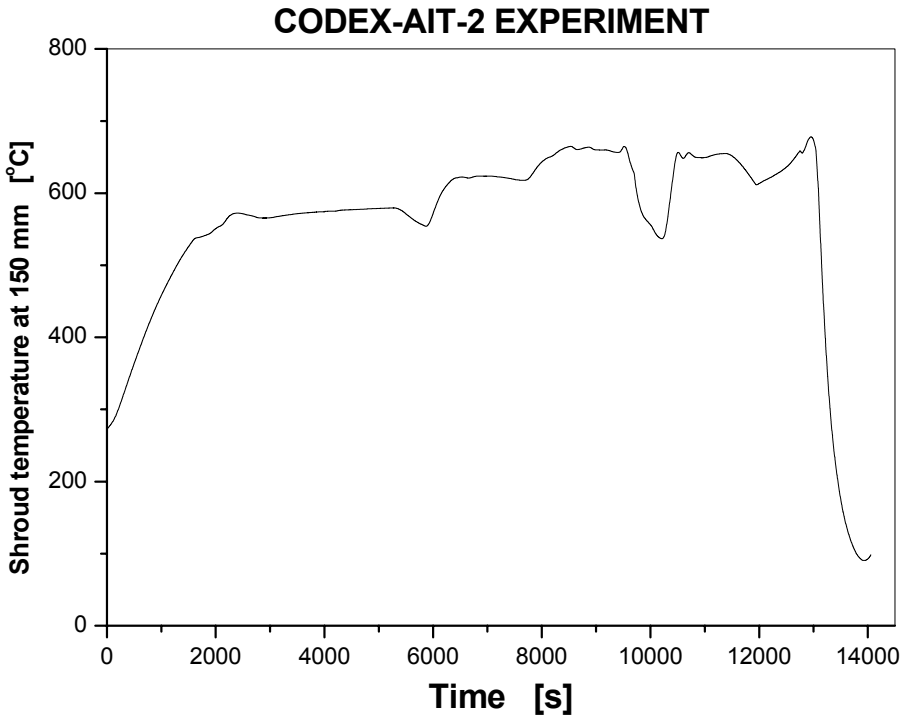

Fig. 22 SH150: Shroud temperature at 150 mm

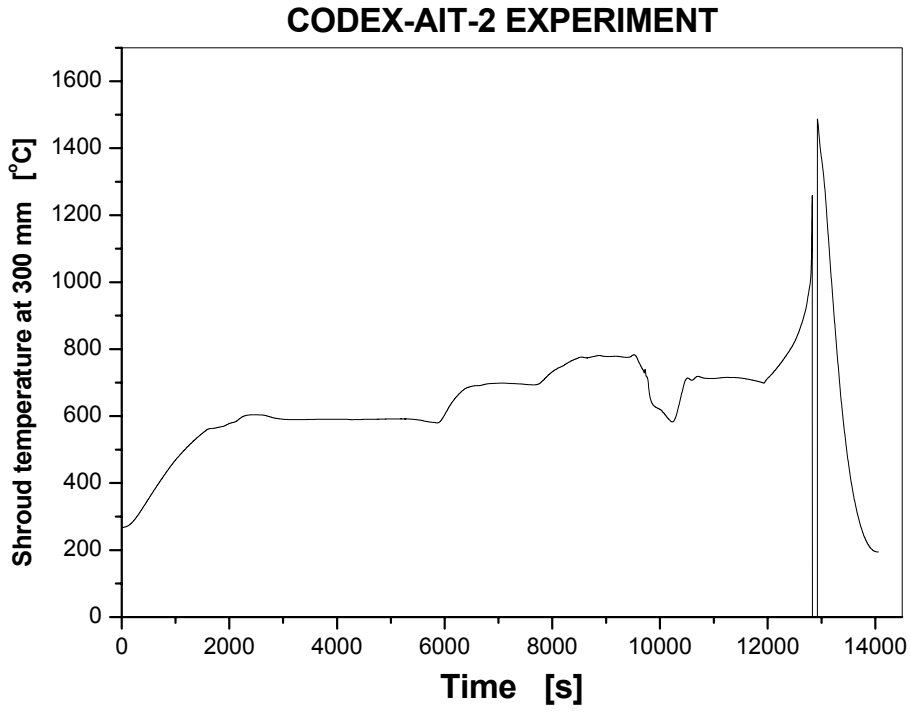

Fig. 23 SH300: Shroud temperature at 300 mm

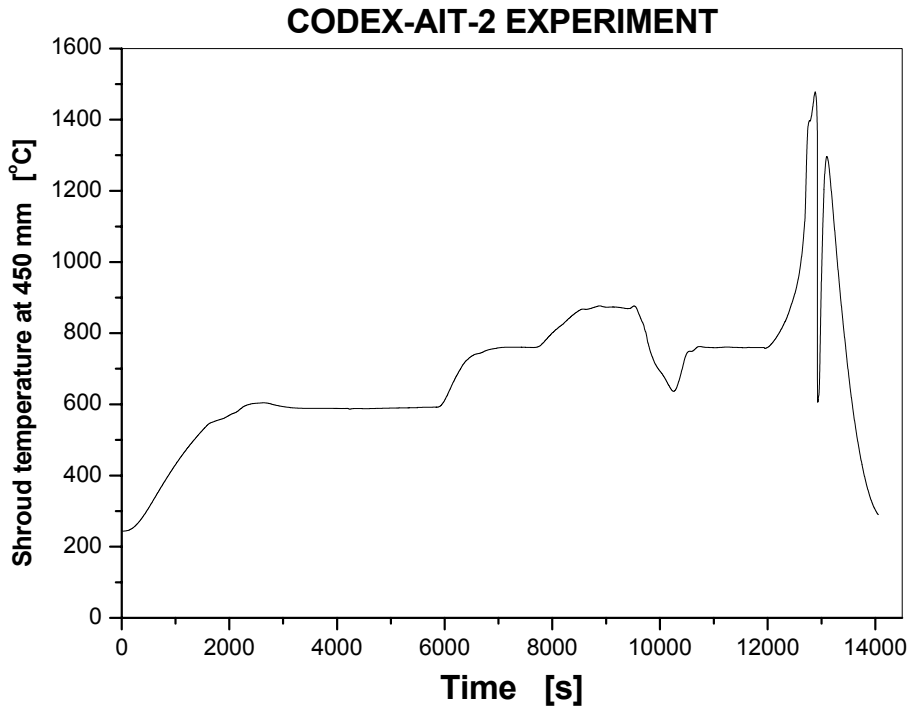

Fig. 24 SH450: Shroud temperature at 450 mm

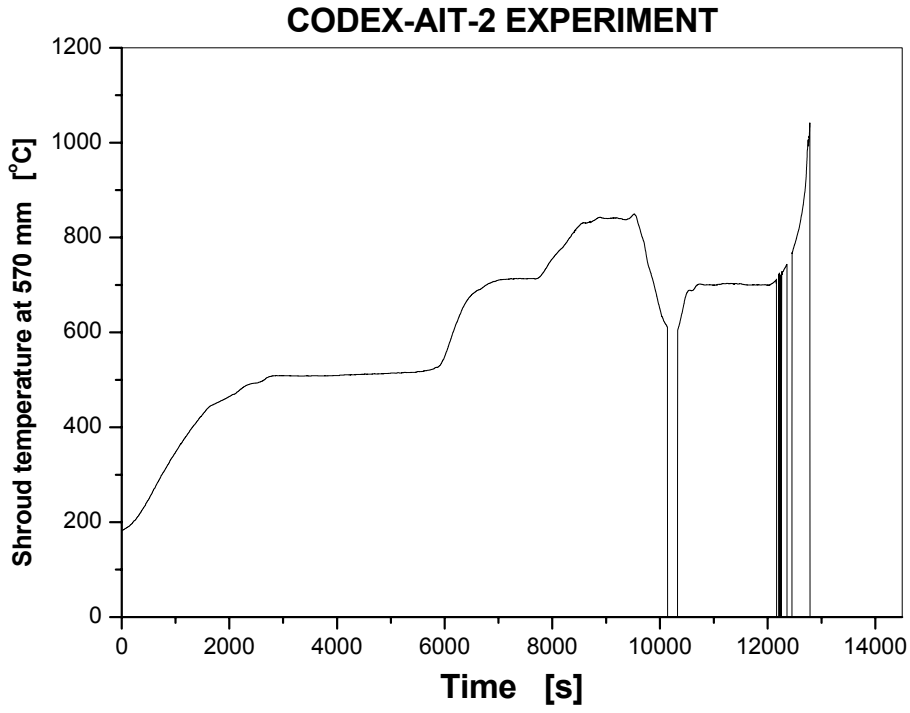

Fig. 25 SH570: Shroud temperature at 570 mm

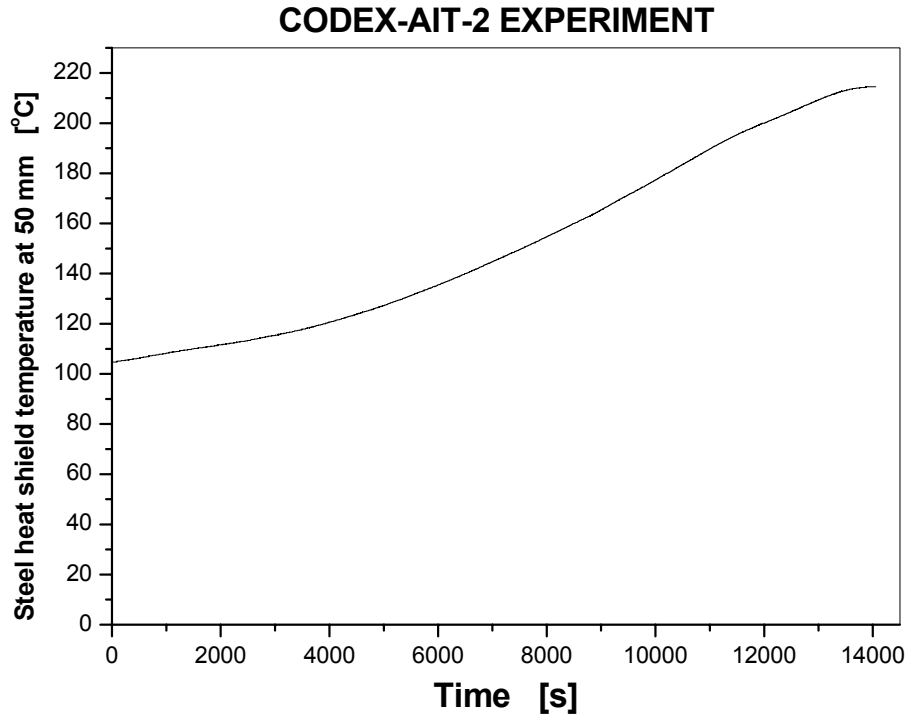

Fig. 26 HS50: Steel heat shield temperature at 50 mm

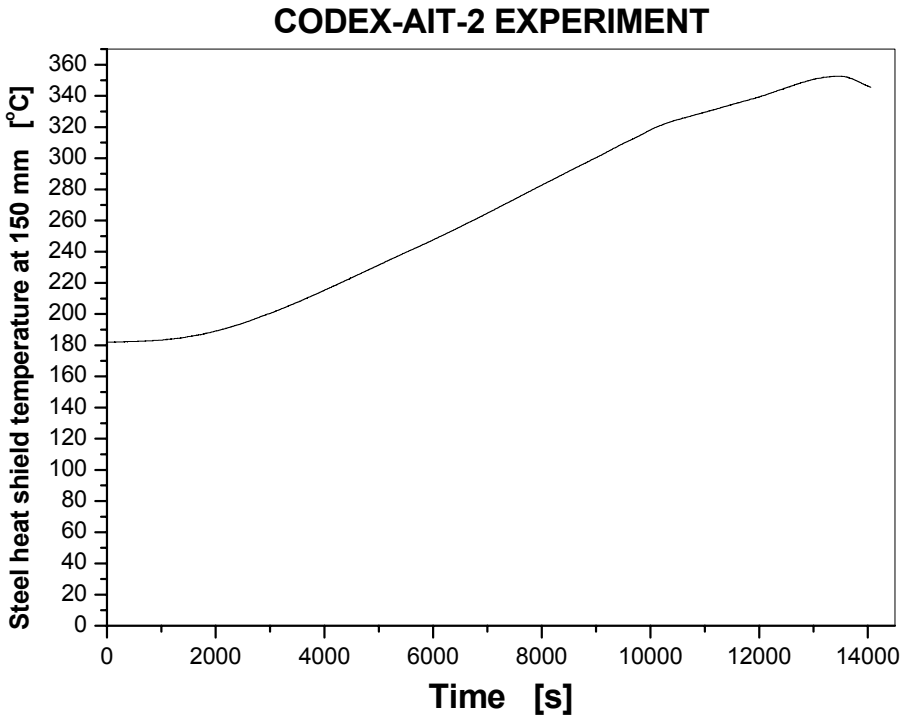

Fig. 27 HS150: Steel heat shield temperature at 150 mm

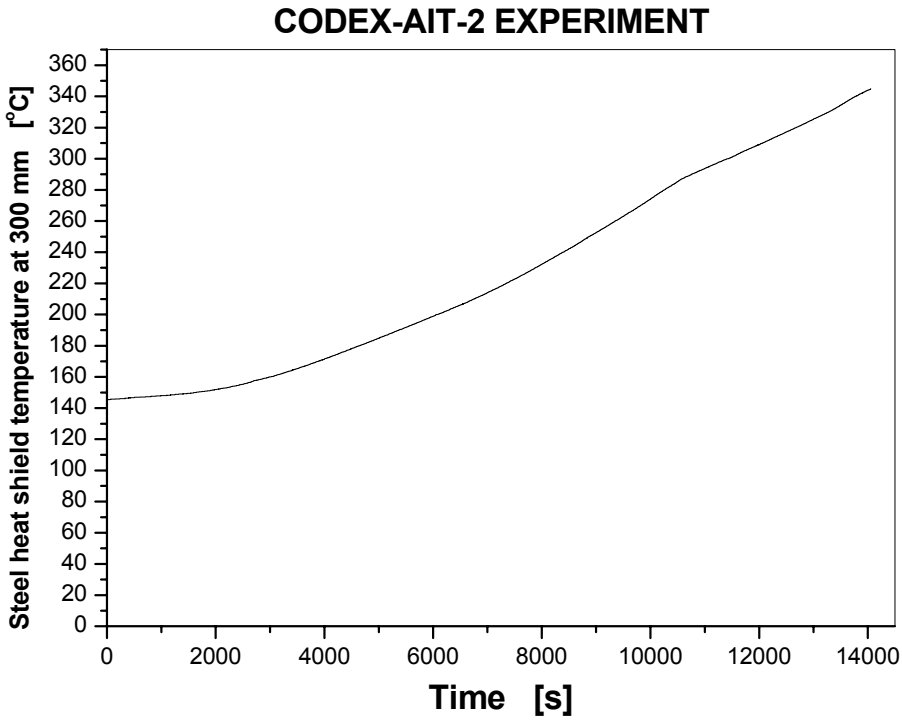

Fig. 28 HS300: Steel heat shield temperature at 300 mm

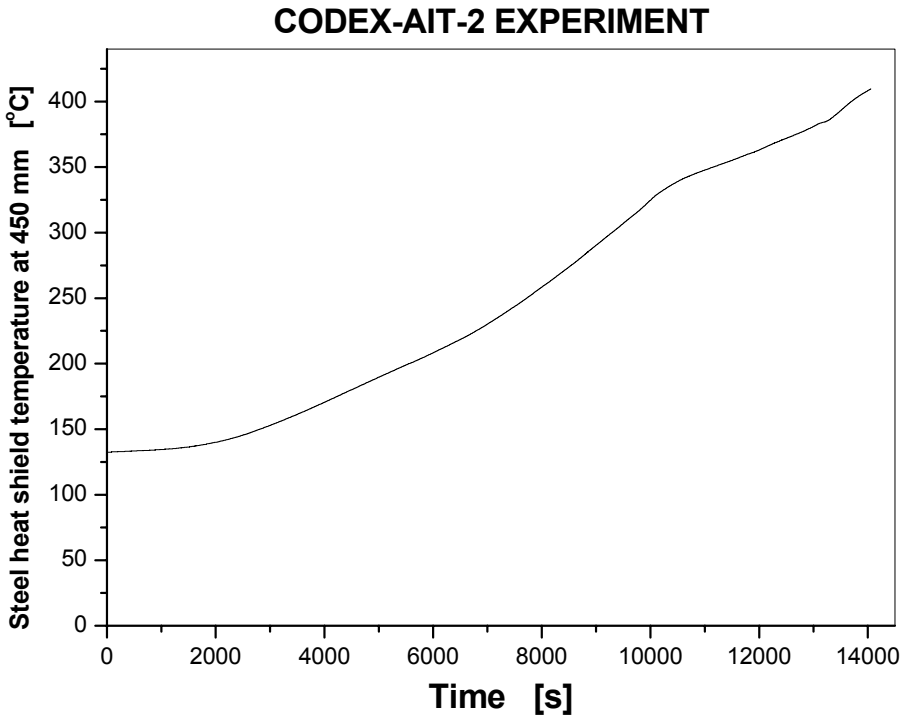

Fig. 29 HS450: Steel heat shield temperature at 450 mm

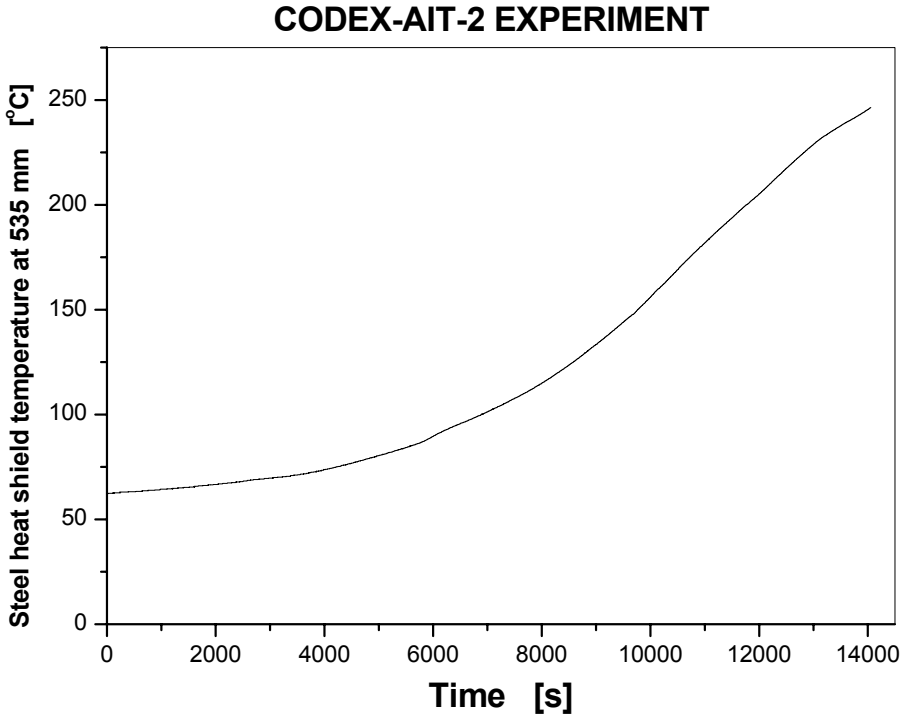

Fig. 30 HS535: Steel heat shield temperature at 535 mm

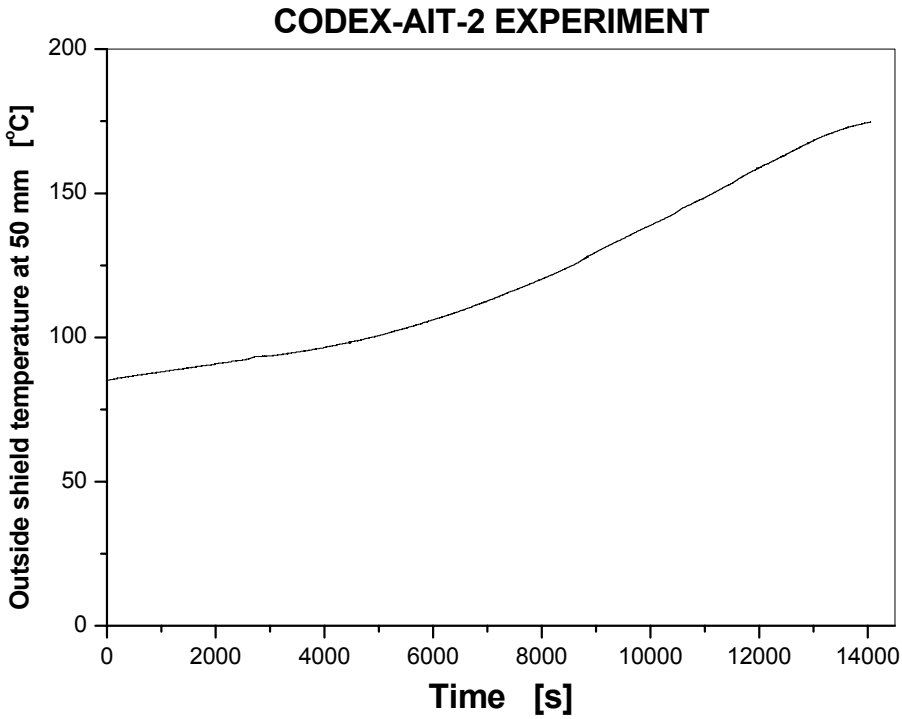

Fig. 31 OS50: Outside shield temperature at 50 mm

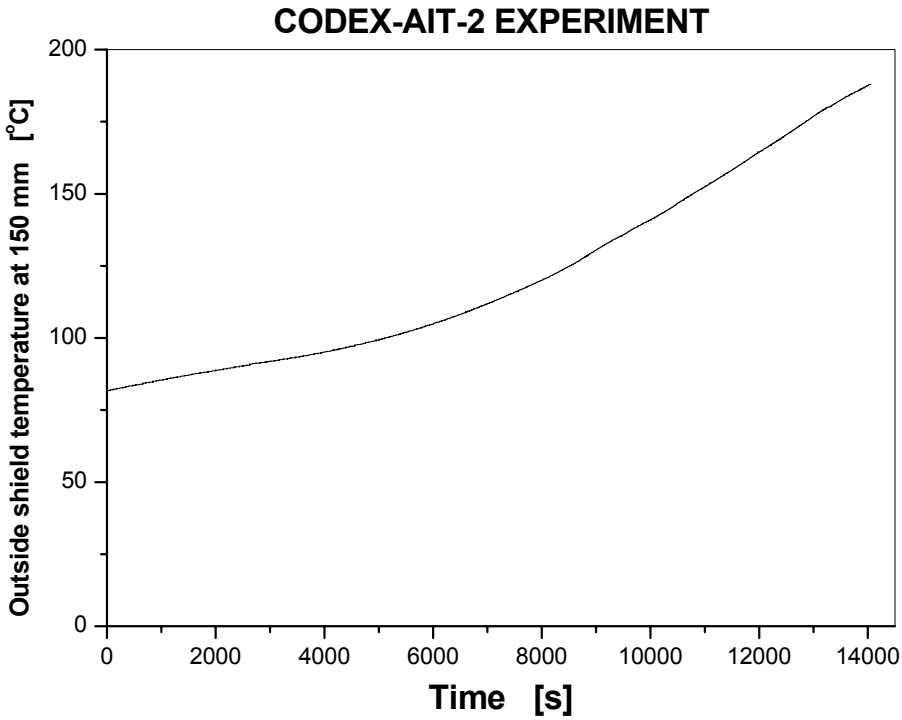

Fig. 32 OS150: Outside shield temperature at 150 mm

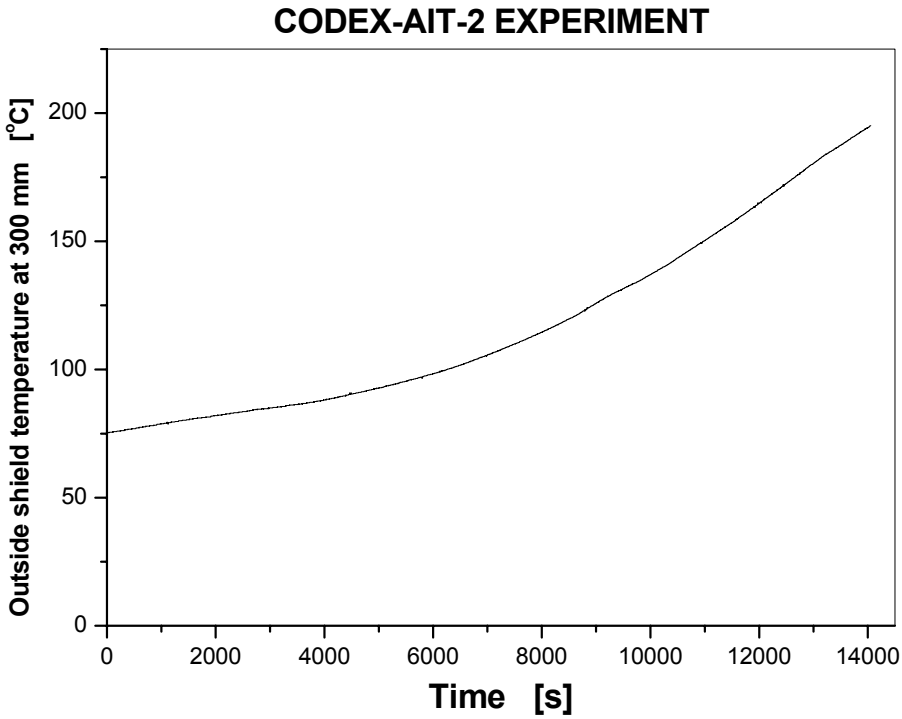

Fig. 33 OS300: Outside shield temperature at 300 mm

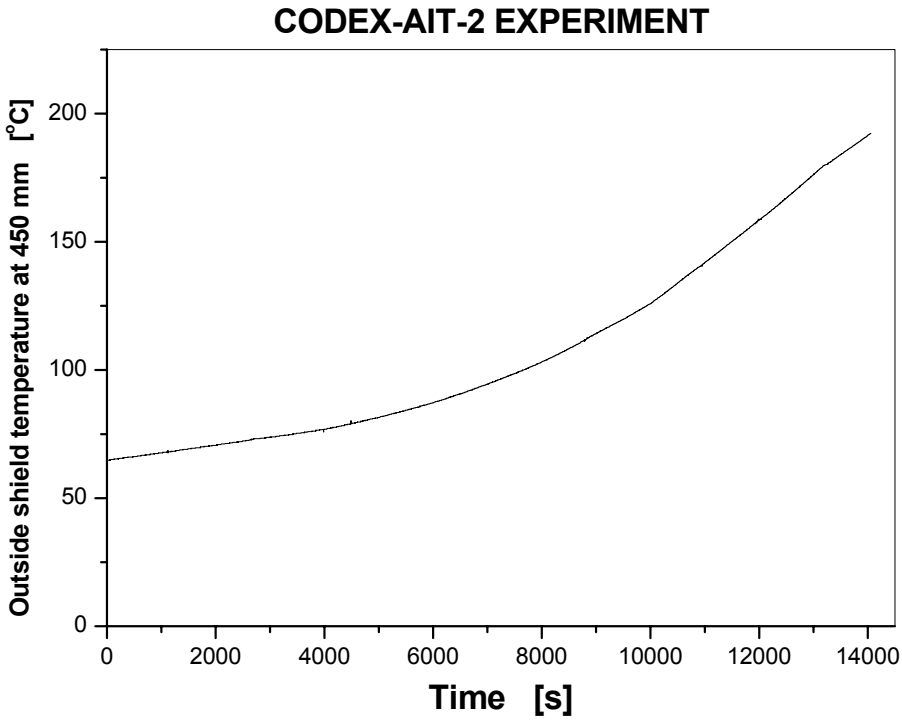

Fig. 34 OS450: Outside shield temperature at 450 mm

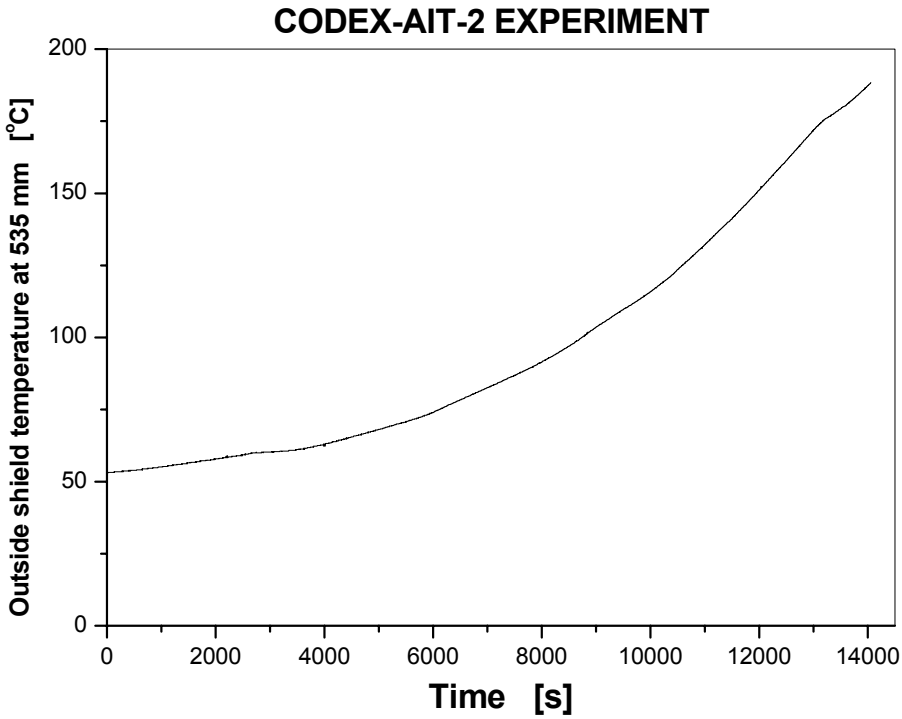

Fig. 35 OS535: Outside shield temperature at 535 mm

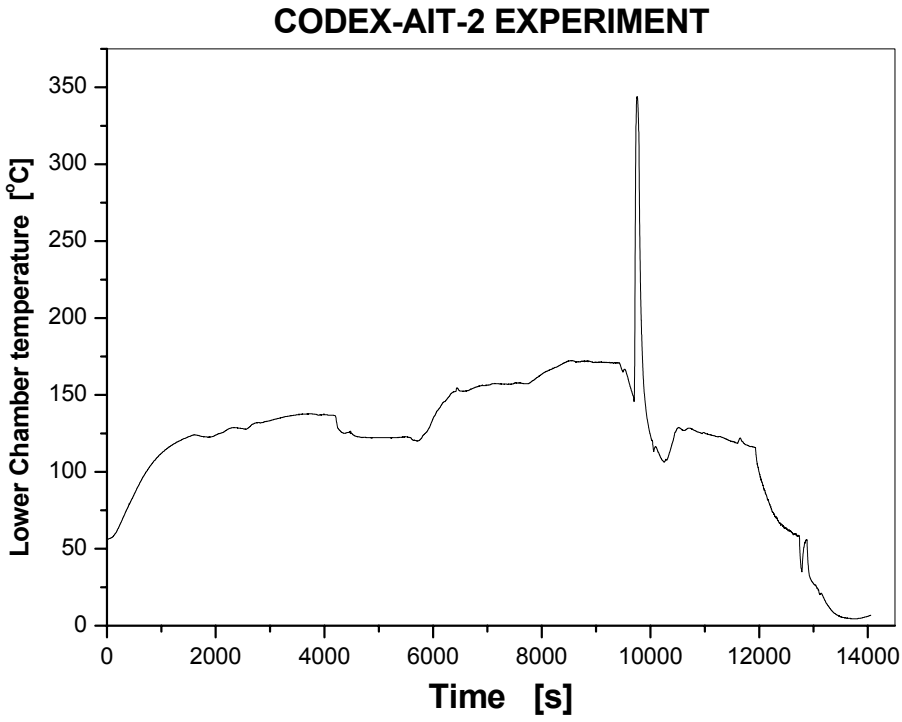

Fig. 36 TLOCH: Lower chamber temperature

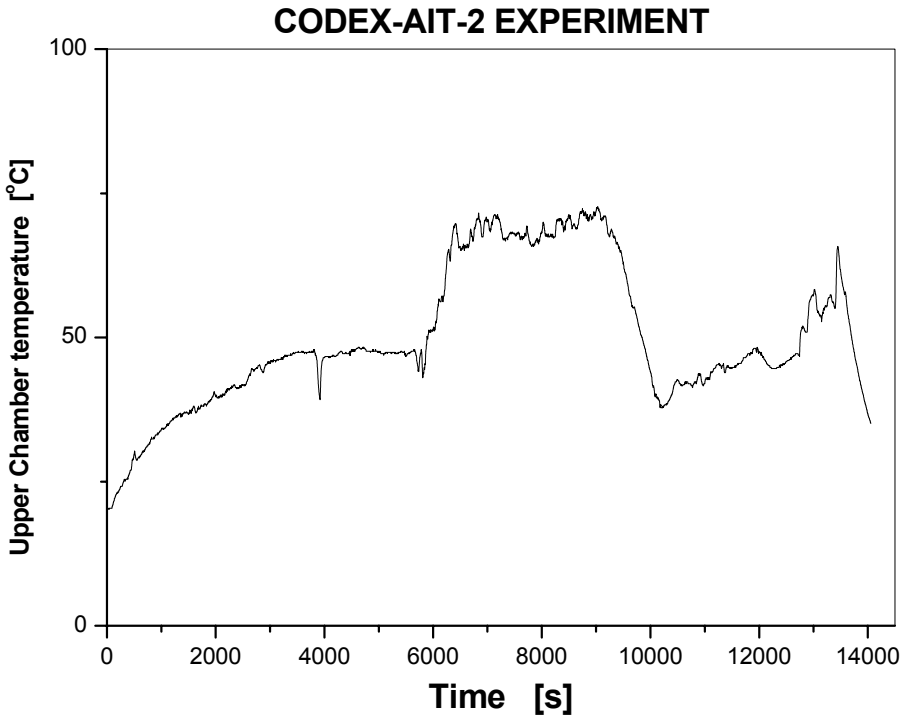

Fig. 37 TUPCH: Upper chamber temperature

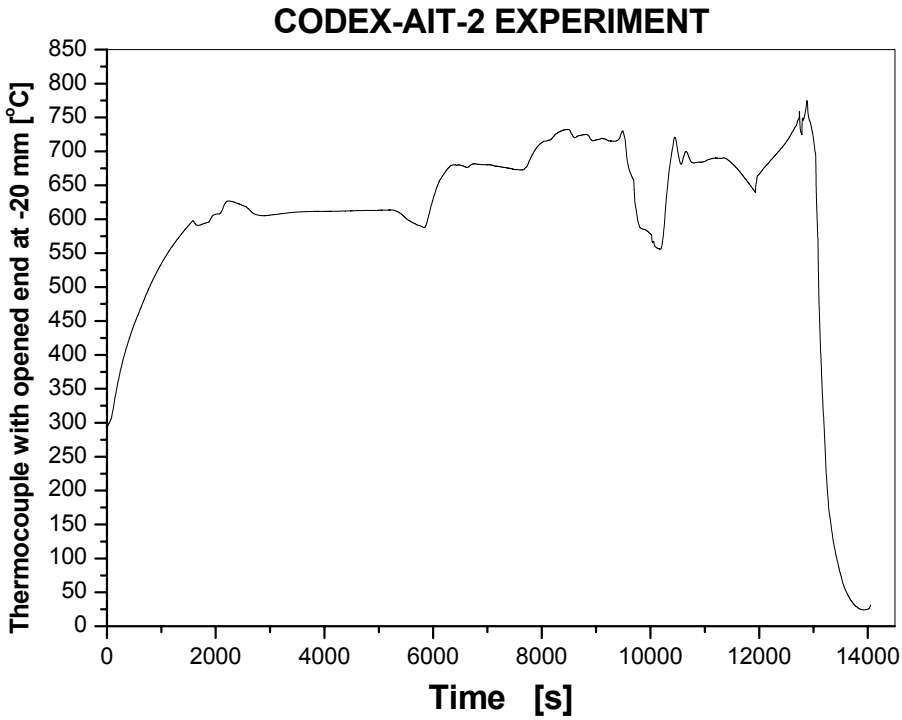

Fig. 38 TMELT: Bundle temperature at -20 mm

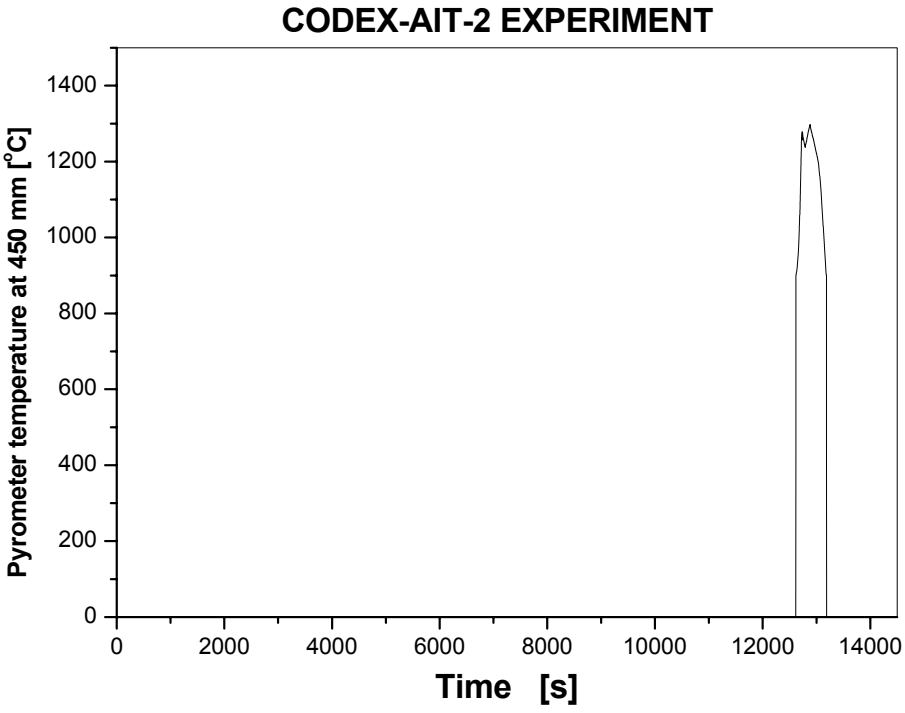

Fig. 39 PYR450: Pyrometer temperature at 450 mm

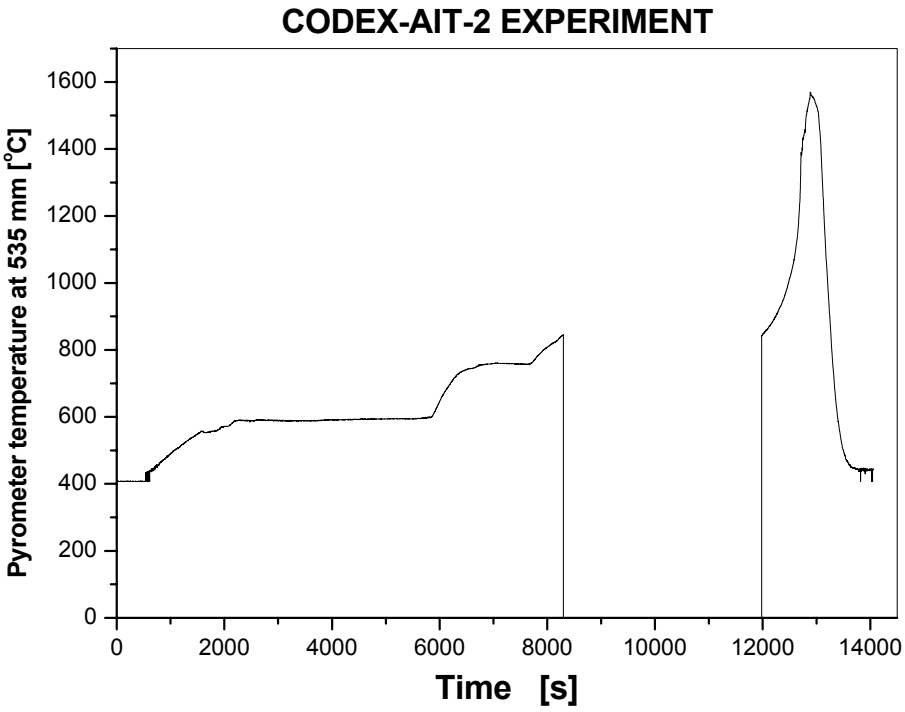

Fig. 40 PYR535: Pyrometer temperature at 535 mm

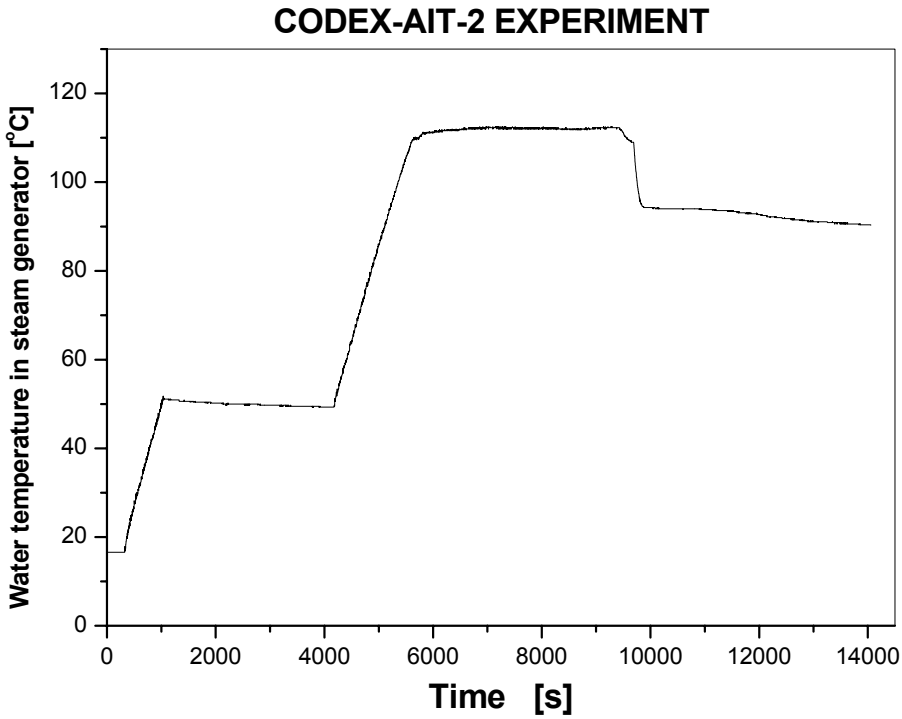

Fig. 41 TWATER: Water temperature in the steamgenerator

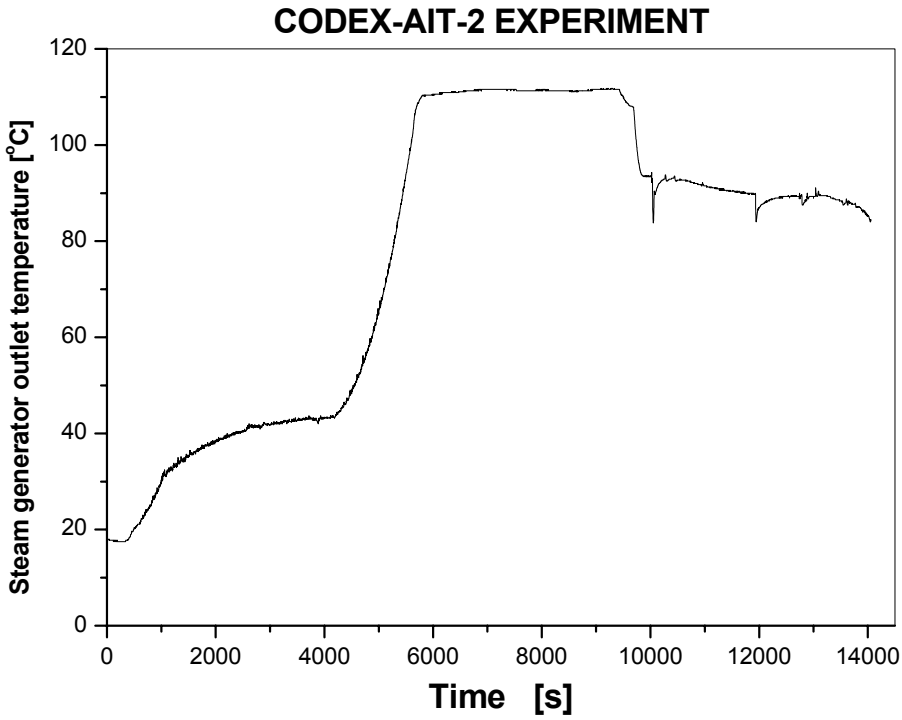

Fig. 42 TSTEAM: Steamgenerator outlet temperature

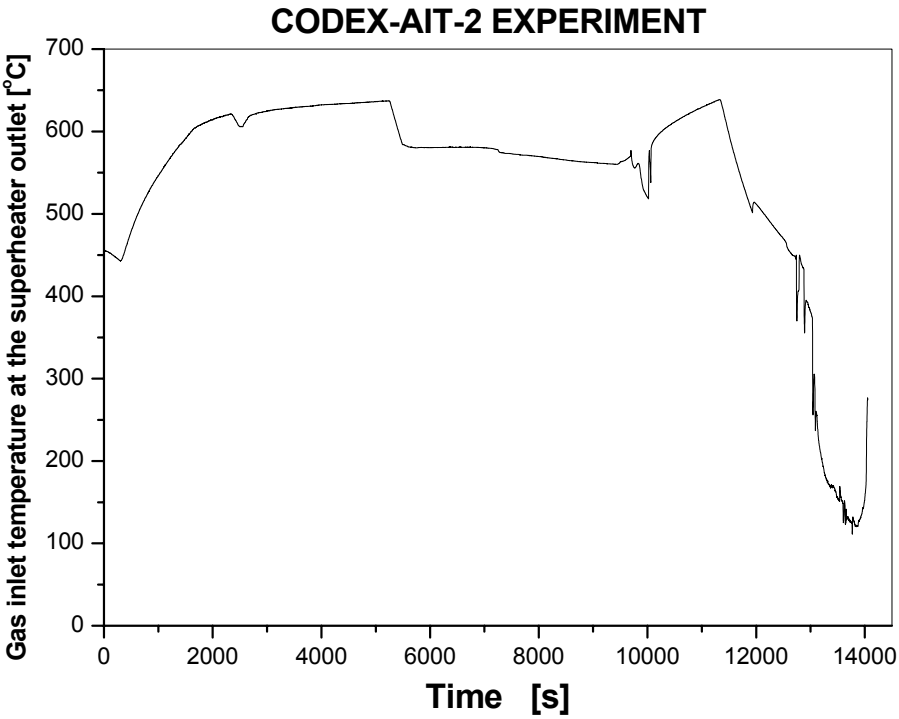

Fig. 43 TIN1: Gas temperature at the superheater outlet

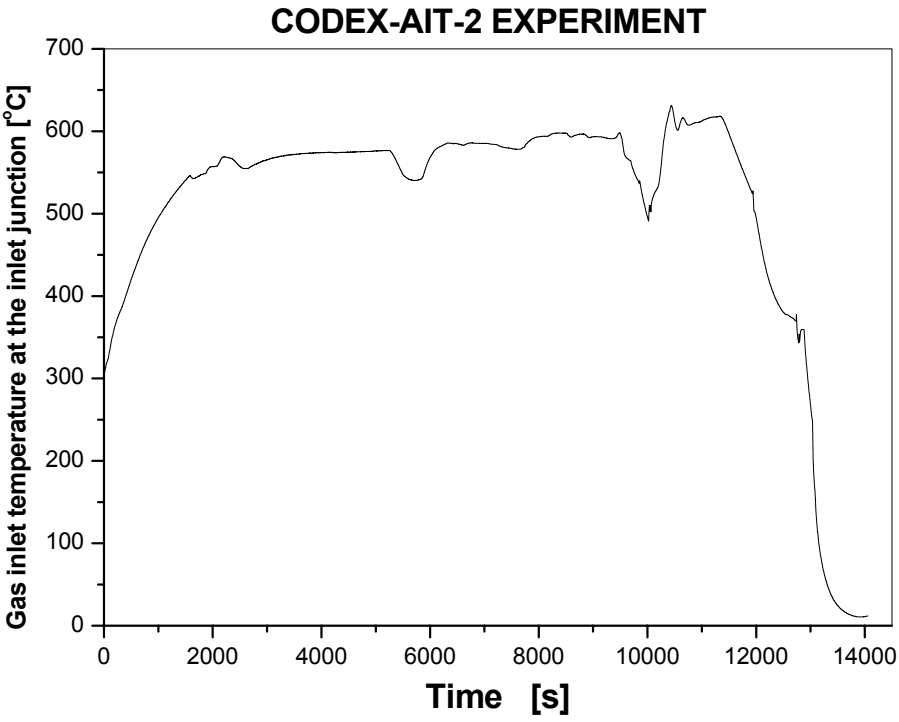

Fig. 44 TIN2: Gas temperature in the inlet junction

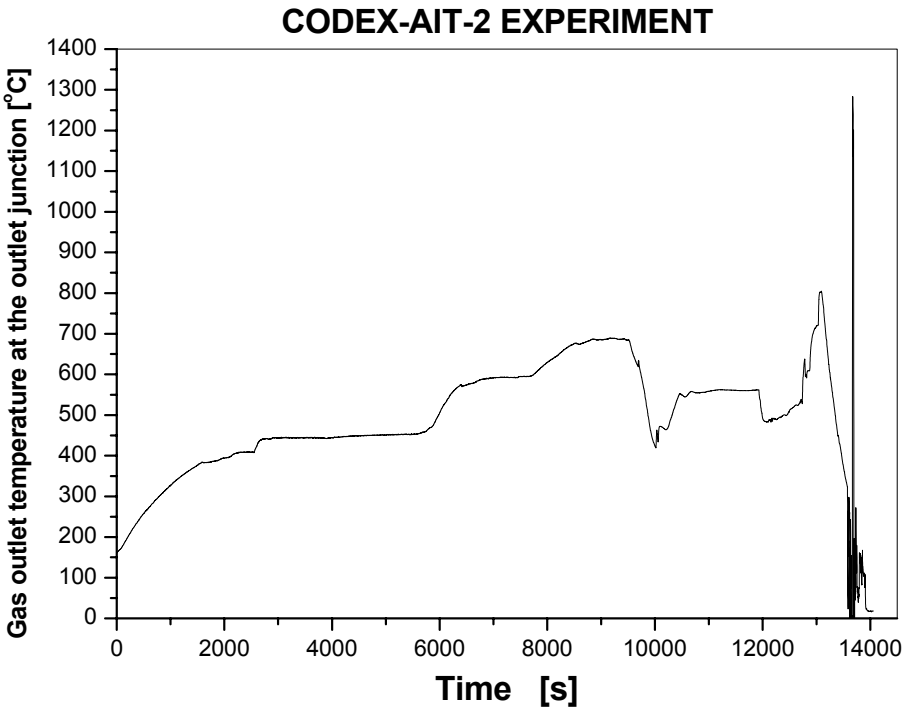

Fig. 45 TCOUT: Gas temperature in the outlet junction

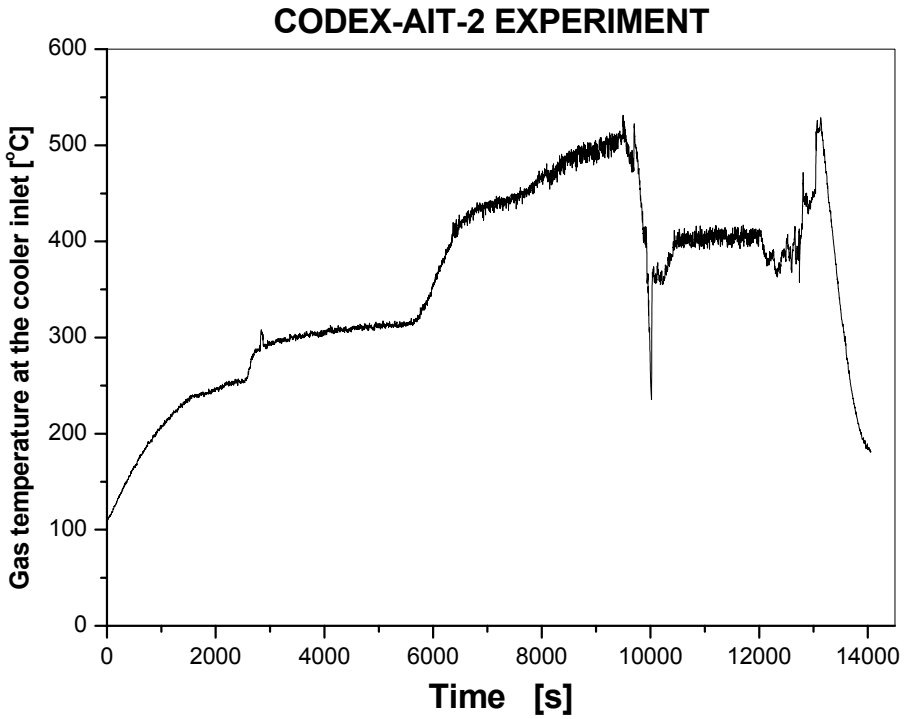

Fig. 46 TCOOL: Gas temperature at the cooler inlet

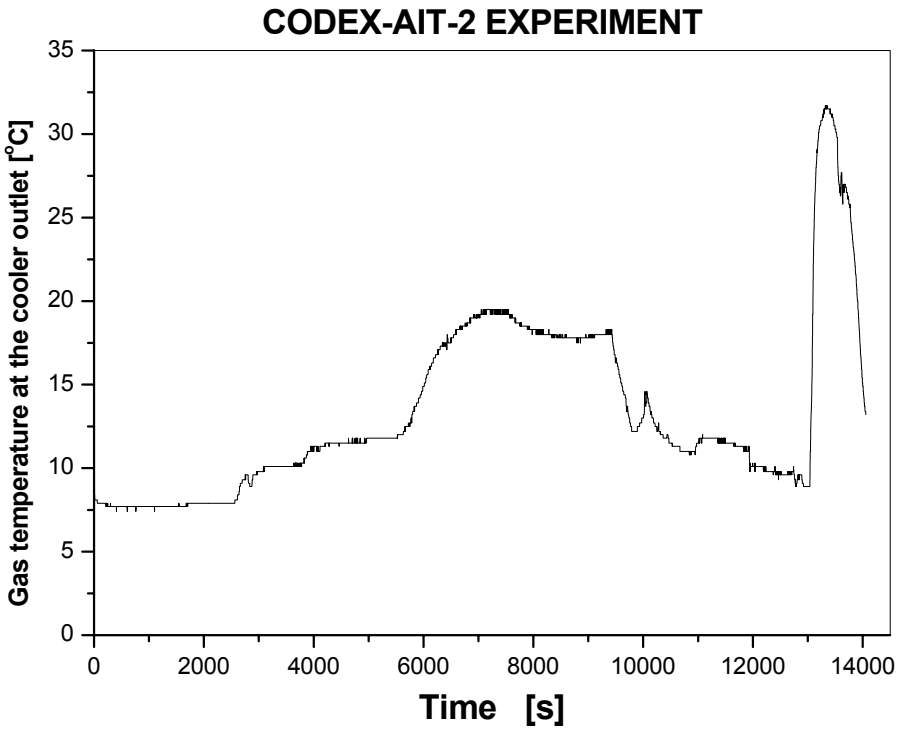

Fig. 47 TOUTC: Gas temperature at the cooler outlet

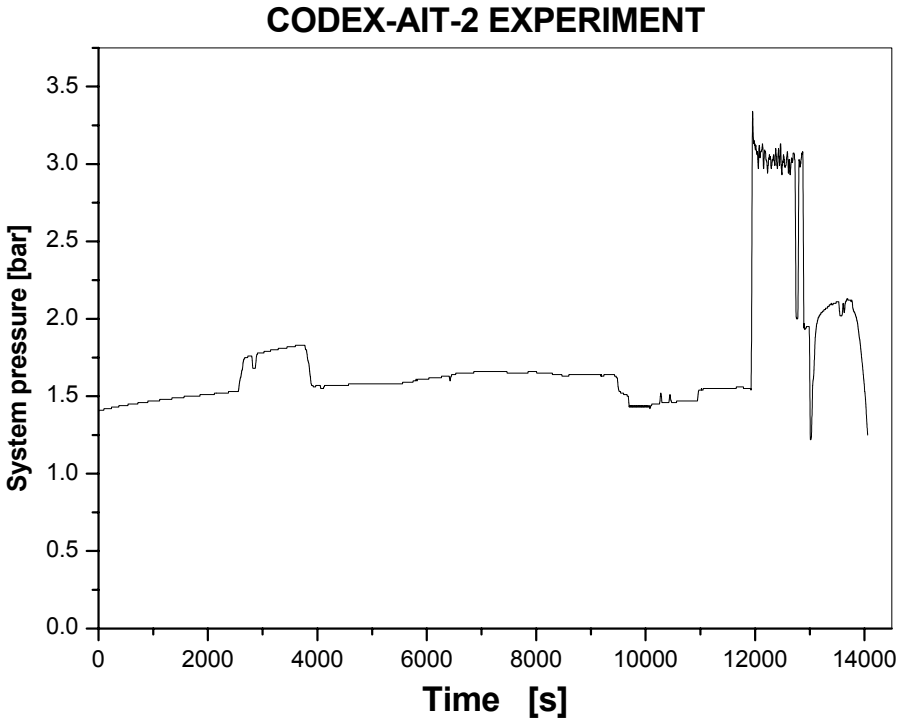

Fig. 48 PSYS: System pressure

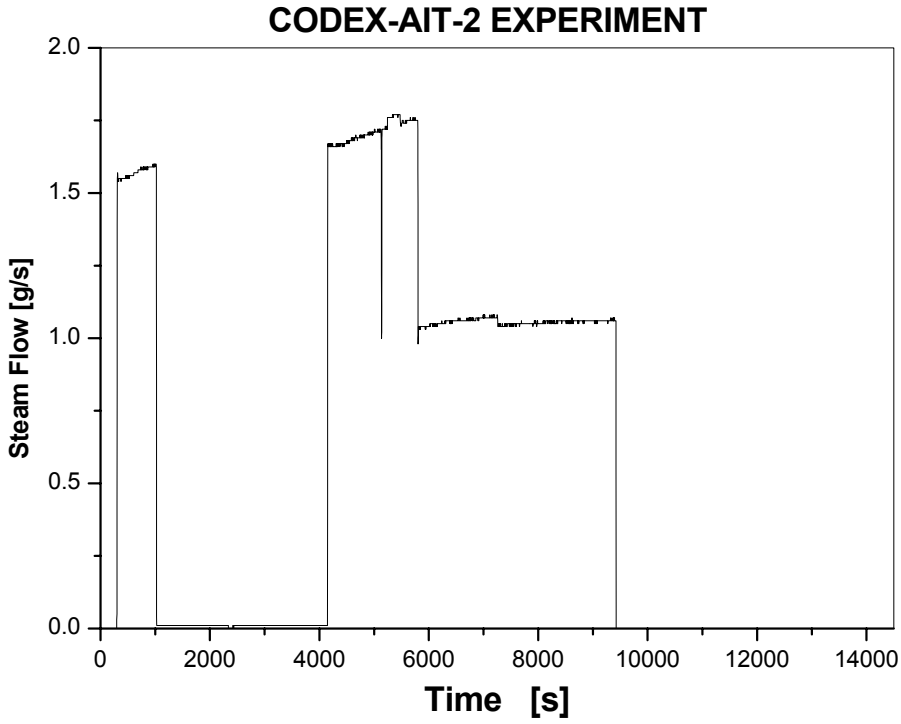

Fig. 49 STEAM: Steam flowrate

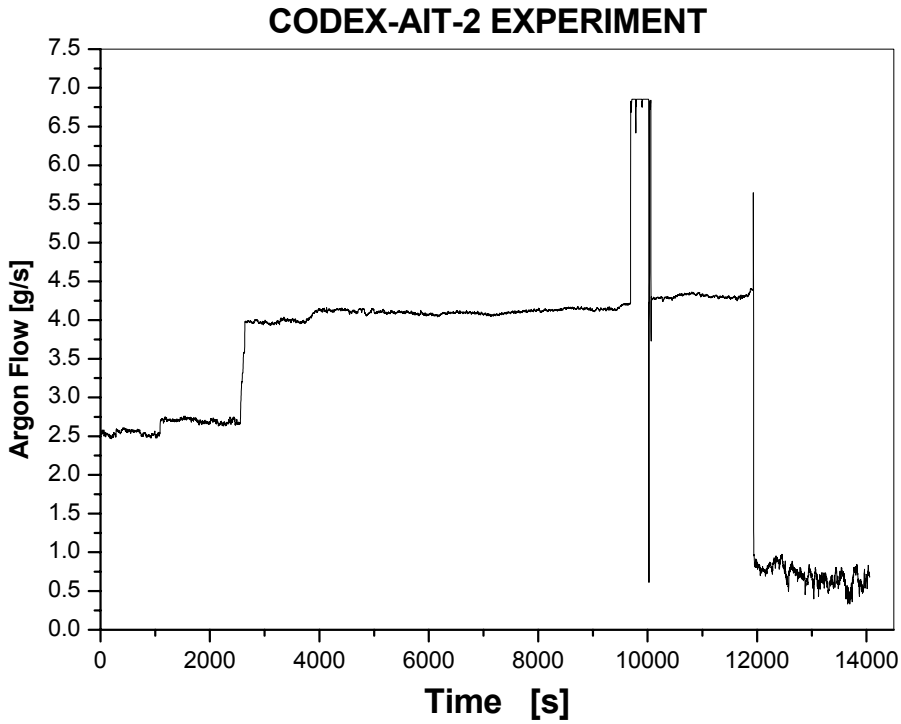

Fig. 50 ARGON: Argon flowrate

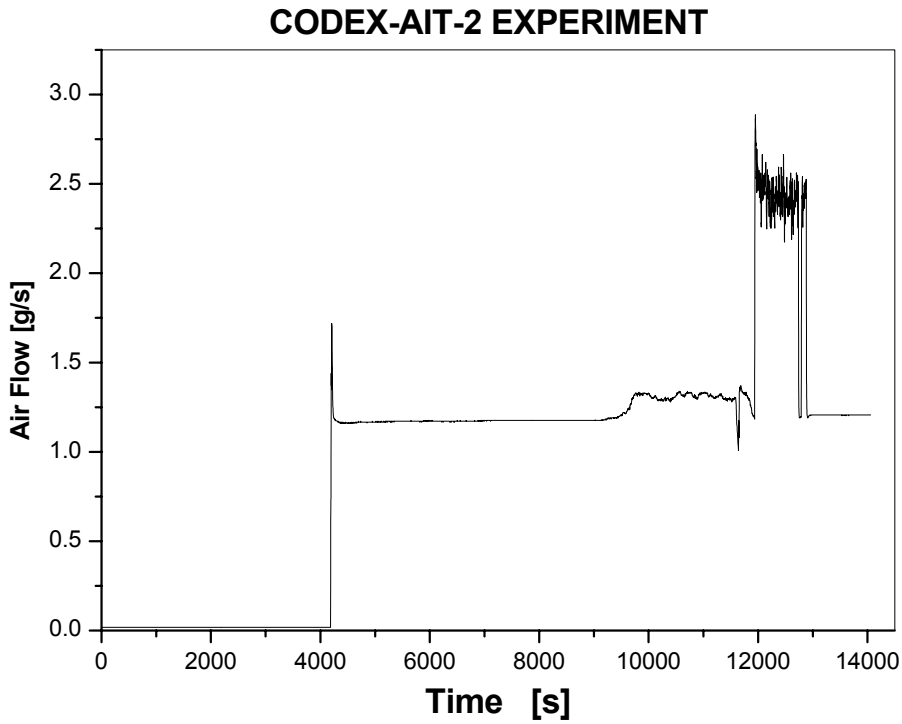

Fig. 51 AIR: Air flowrate

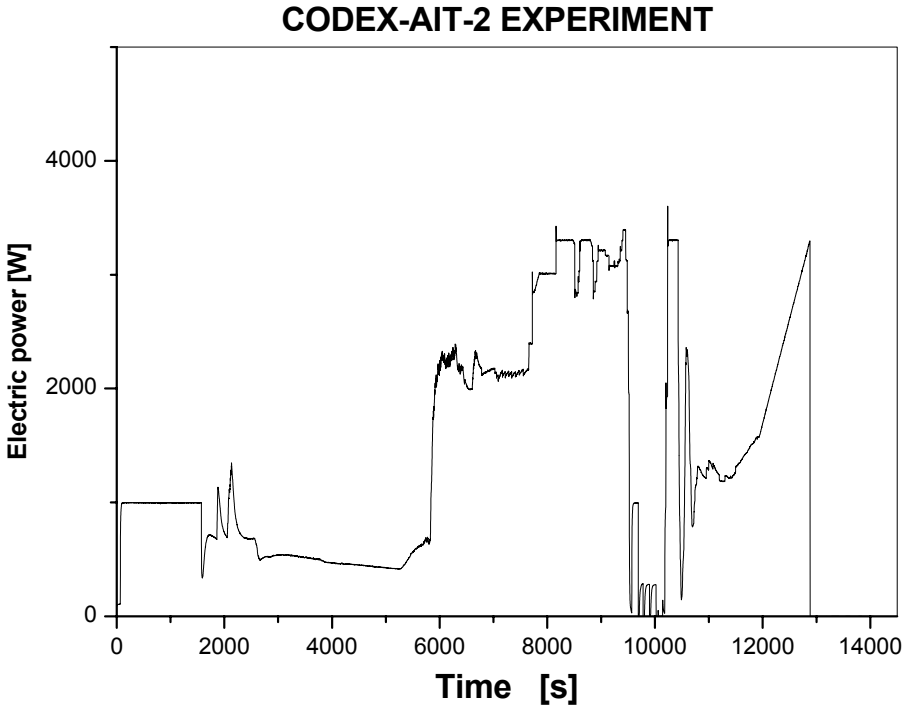

Fig. 52 POWER: Electric power

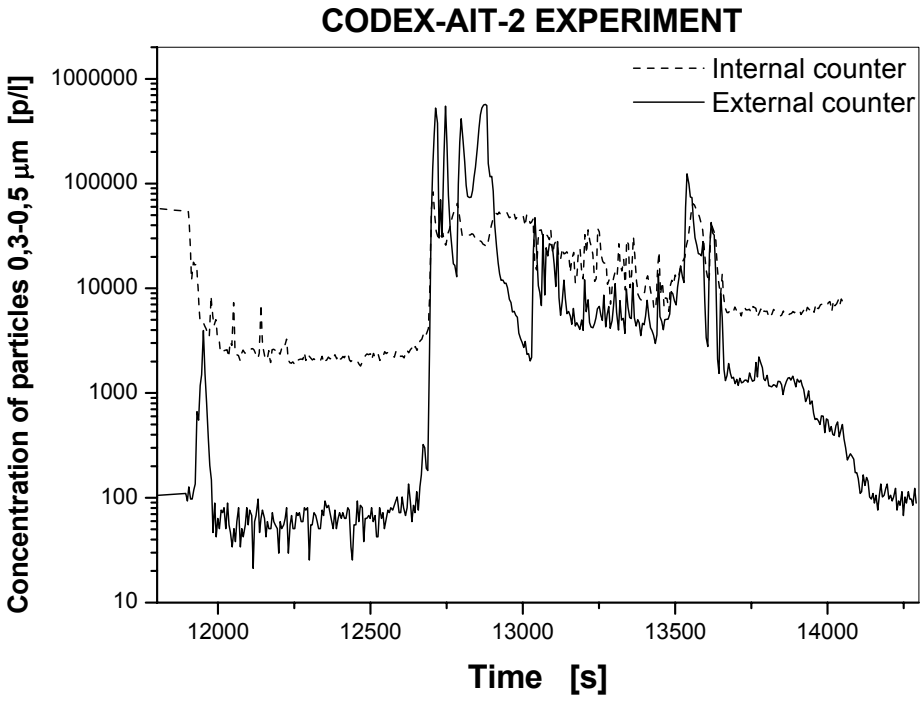

Fig. 53 API1 and APE1: Concentration of 0,3-0,5 µm aerosols

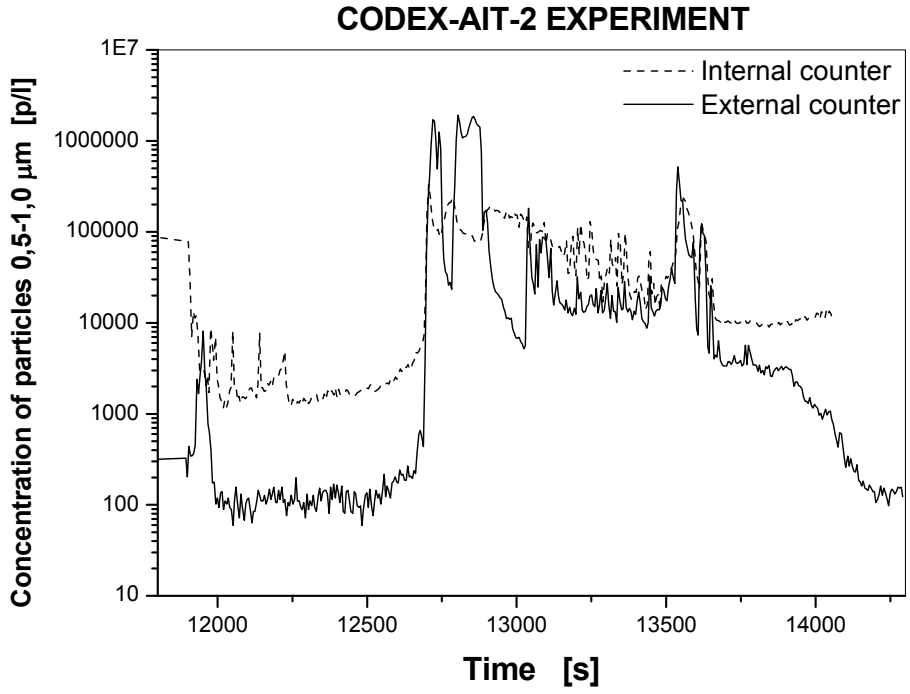

Fig. 54 API2 and APE2: Concentration of 0,5-1,0 µm aerosols

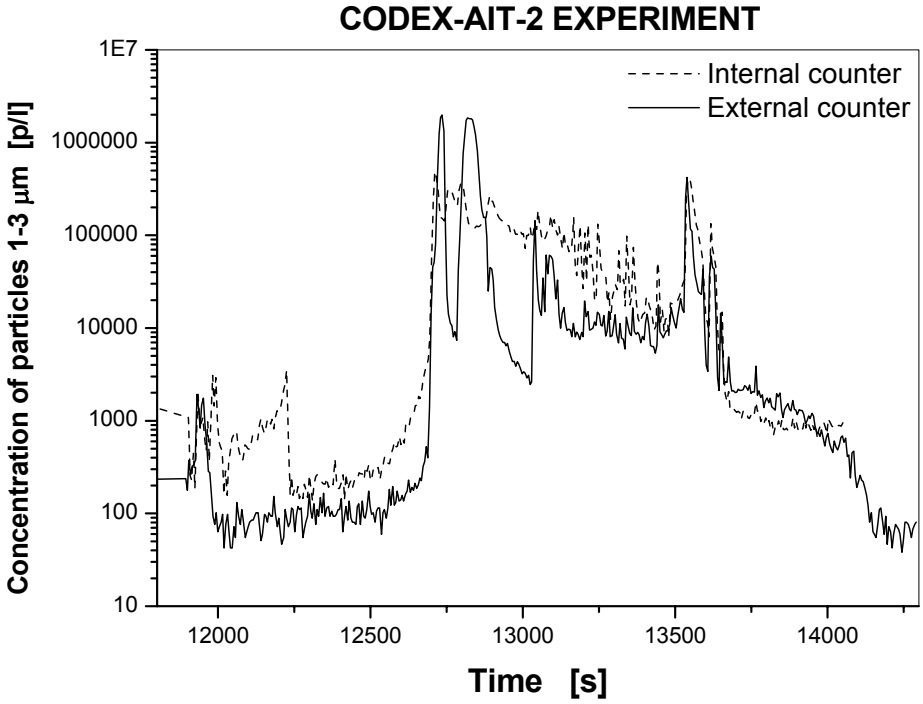

Fig. 55 API3 and APE3: Concentration of 1-3 μm aerosols

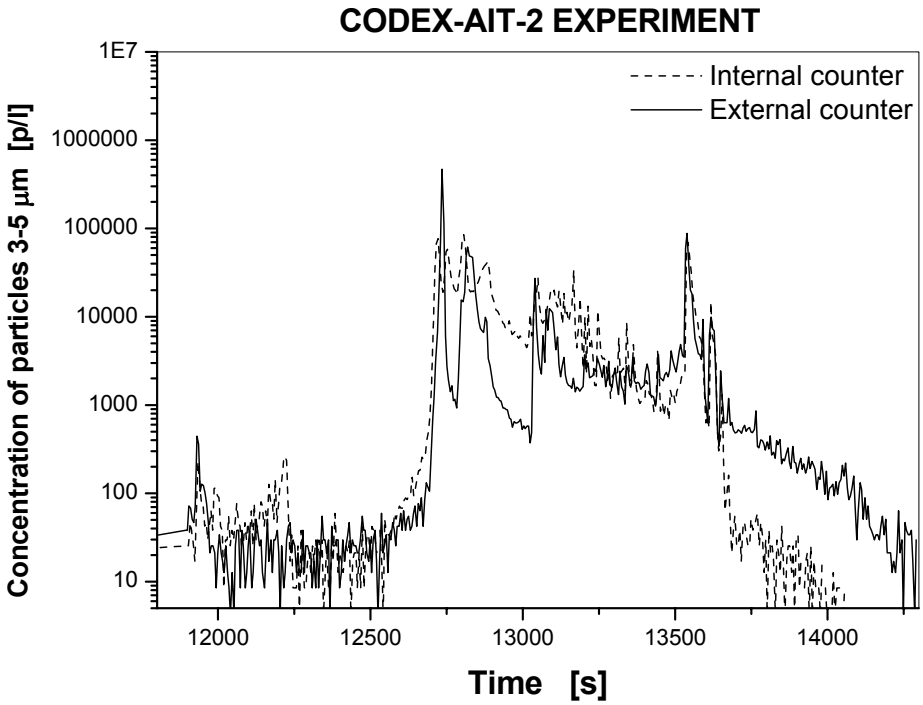

Fig. 56 API4 and APE4: Concentration of 3-5 μm aerosols

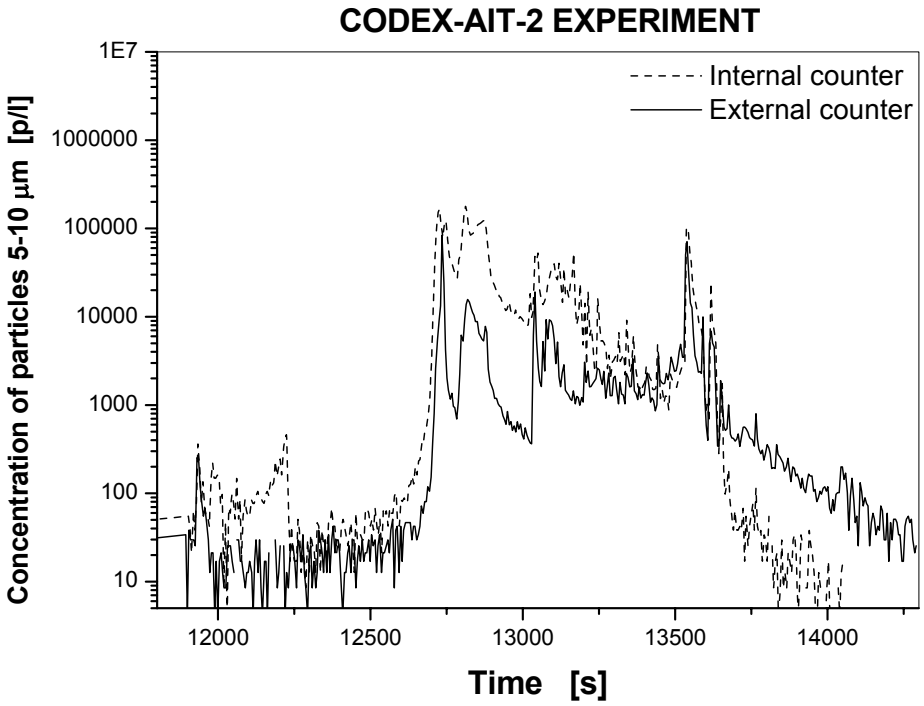

Fig. 57 API5 and APE5: Concentration of 5-10 μm aerosols

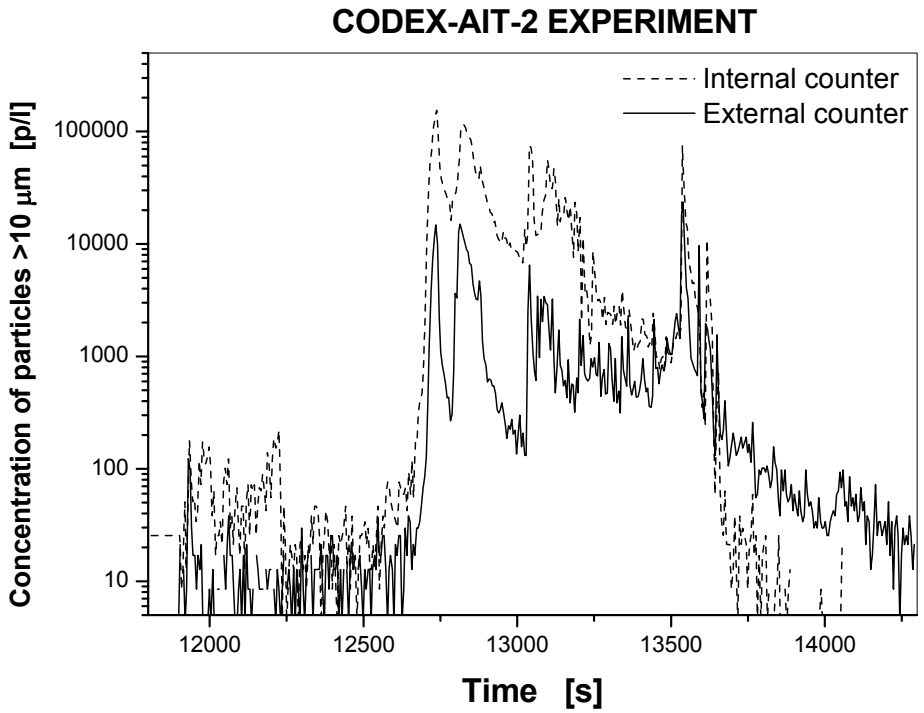

Fig. 58 API6 and APE6: Concentration of >10 μm aerosols

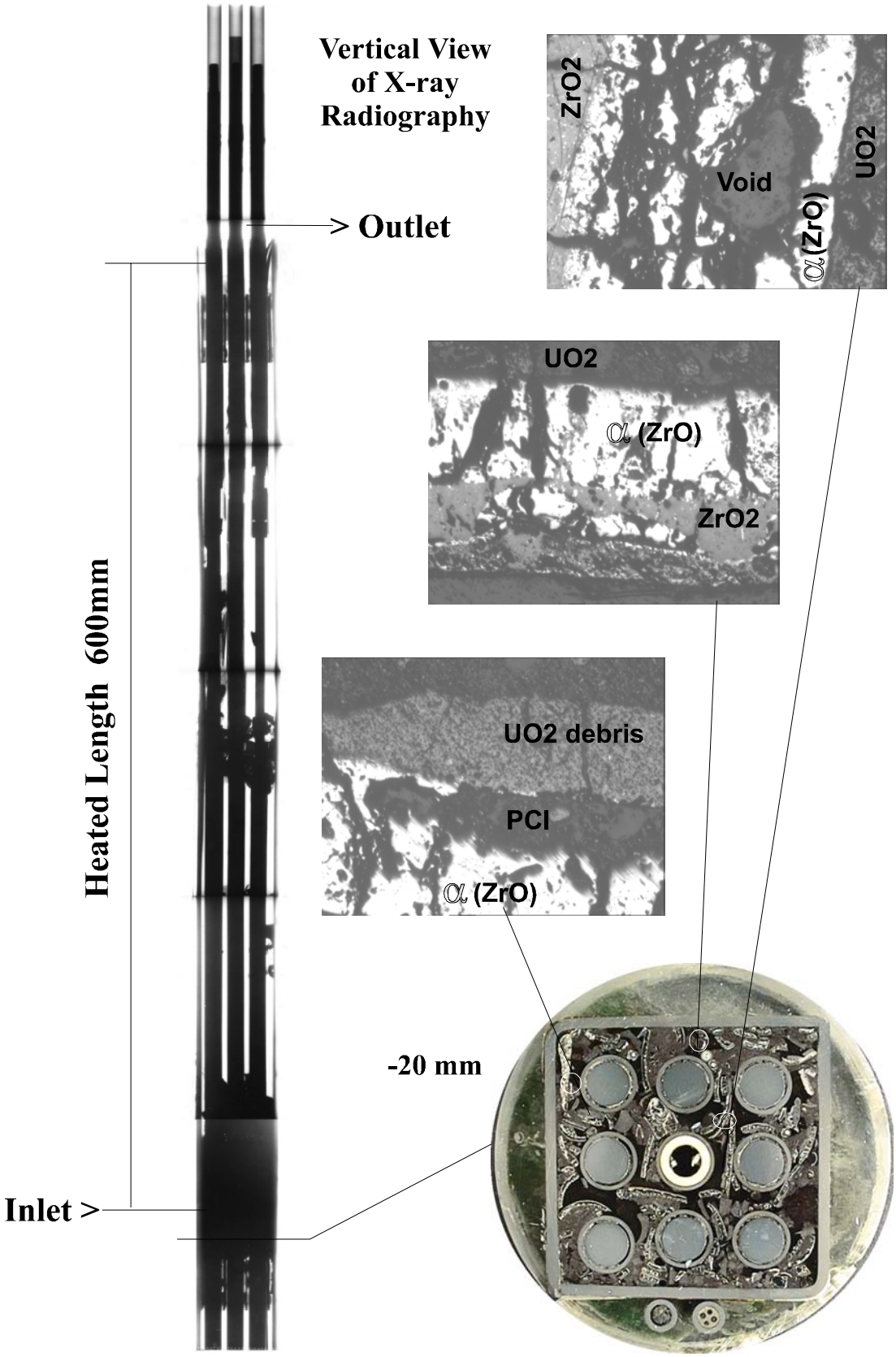

Fig. 59 X-ray radiography of the of CODEX-AIT-2 bundle
and cross section at -20 mm elevation

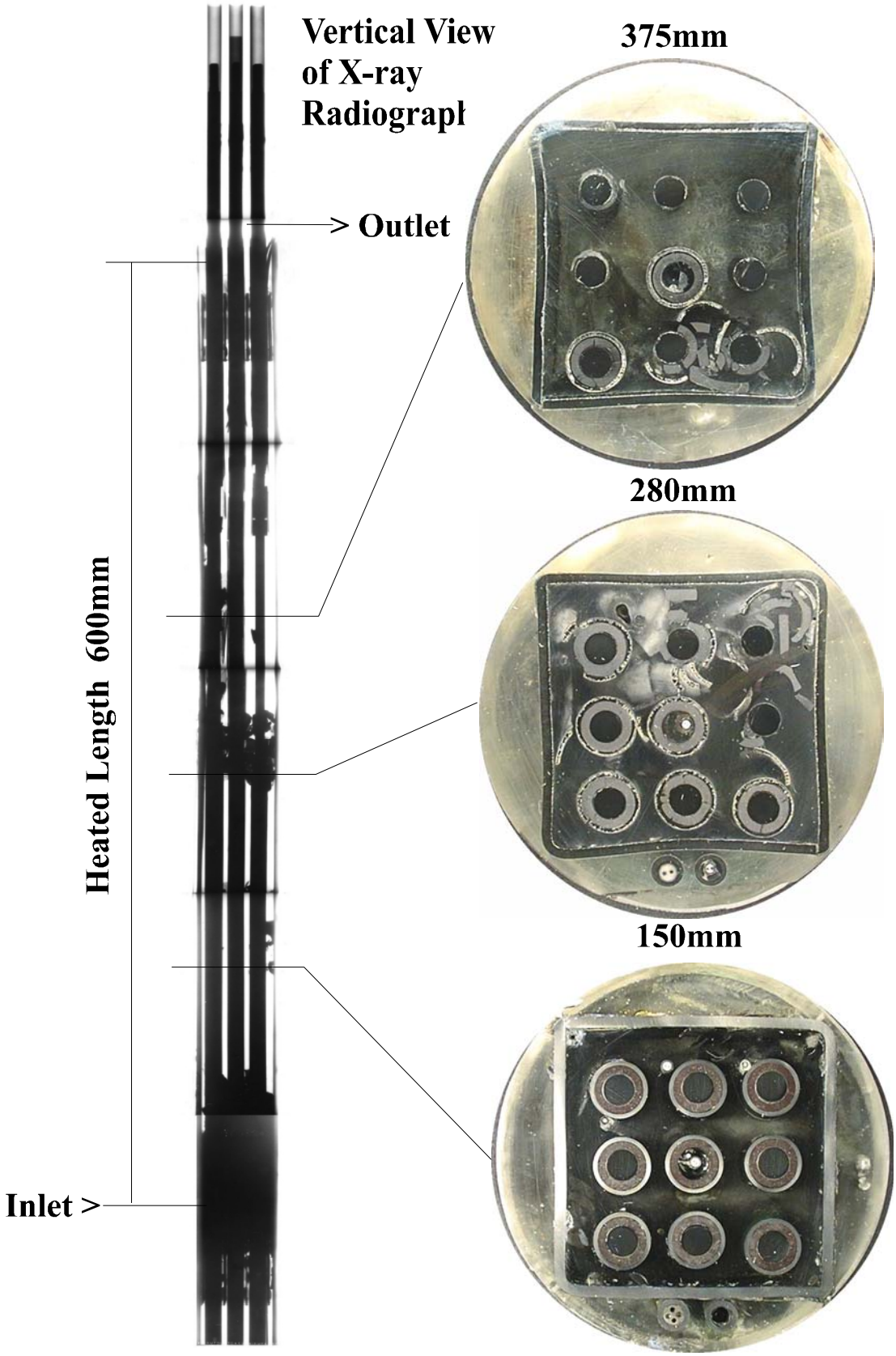

Fig. 60 X-ray radiography of the of CODEX-AIT-2 bundle
and cross sections at 150 mm, 280 mm and 375 mm elevations

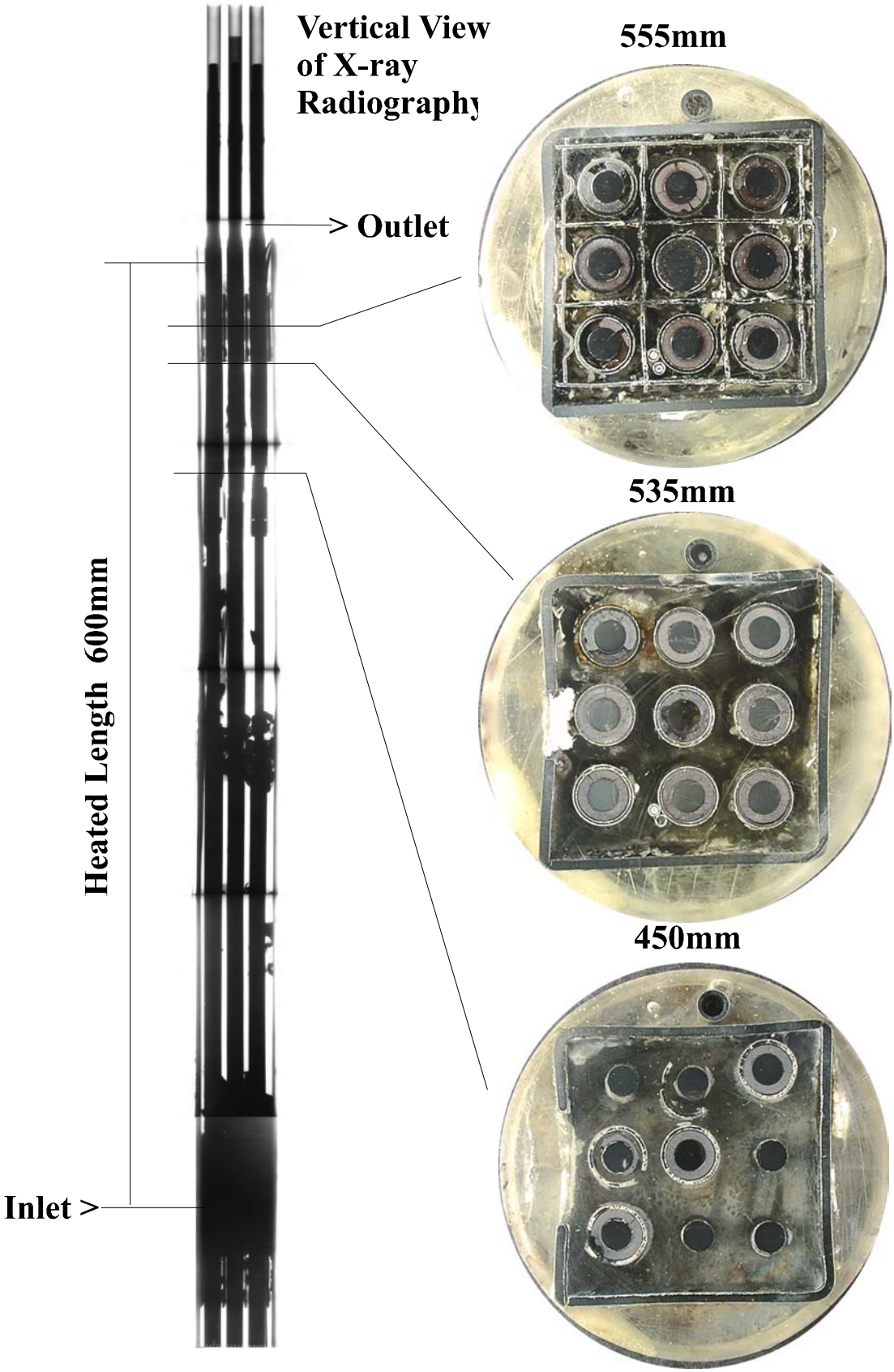

Fig. 61 X-ray radiography of the of CODEX-AIT-2 bundle
and cross sections at 450 mm, 535 mm and 555 mm elevations

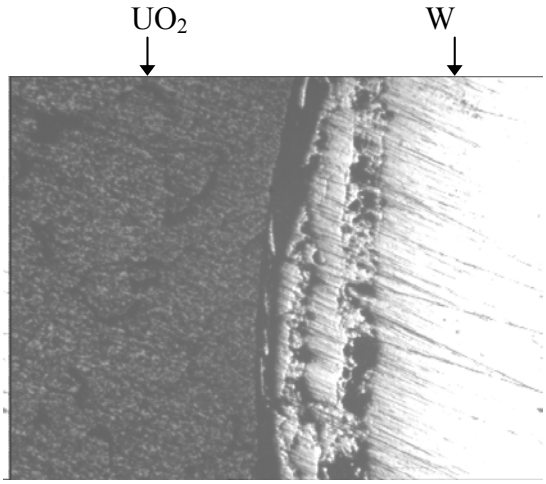

Fig. 62 View of tungsten heater rod damaged at cutting due to the interaction with other metal (rod No. 5 at 150 mm elevation)

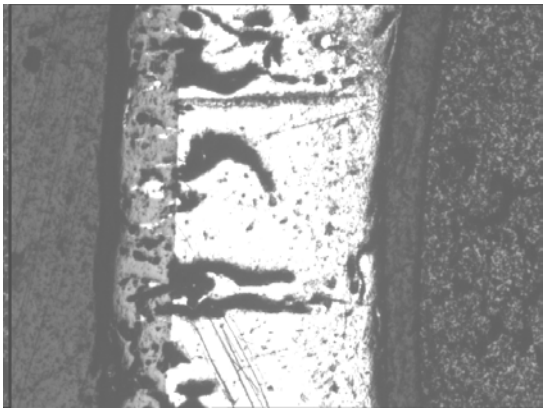

Fig. 63 Cladding and pellet of intact central rod (No. 9) at 280 mm elevation

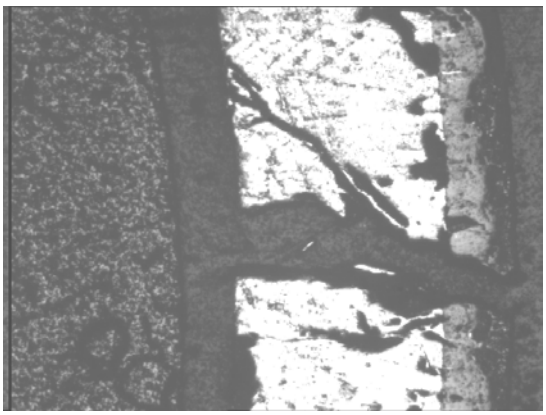

a,

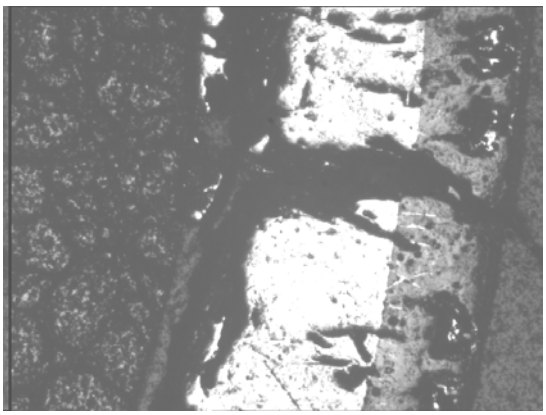

b,

Fig. 64 Broken up cladding at 280 mm elevation
a, rod No.8 non-oxidised pellet
b, rod No. 7 oxidised pellet

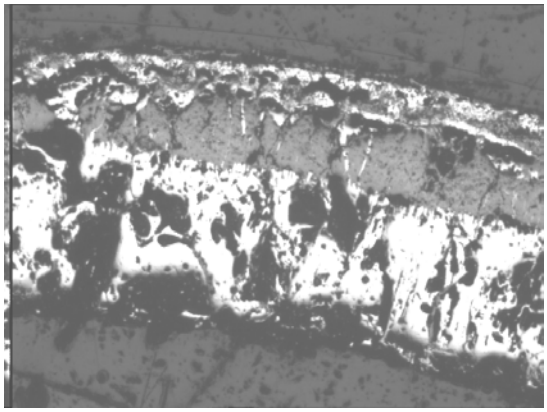

a,

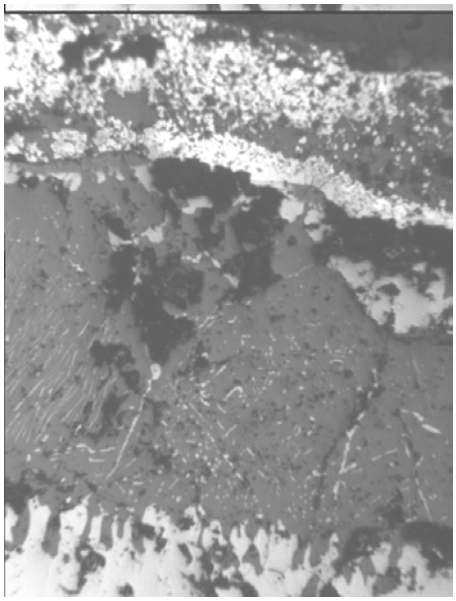

b,

Fig. 65 Oxide and α-phase on rod No.1 at 375 mm elevation

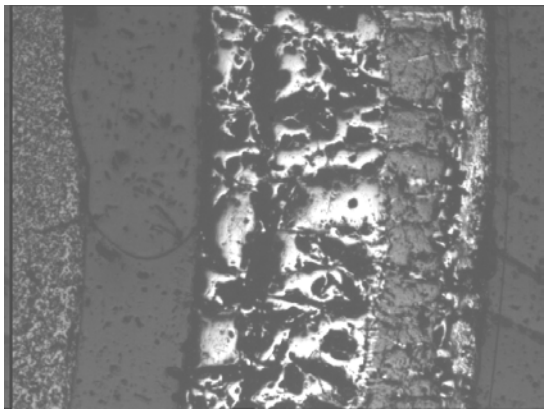

Fig. 66 Cladding of rod No. 9 at 375 mm elevation

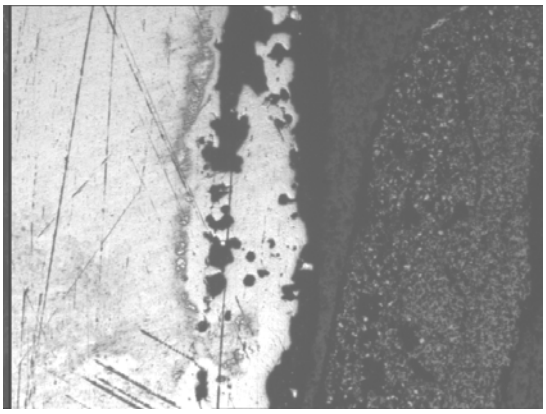

Fig. 67 Tungsten-UO_2 interaction on rod No. 7 at 375 mm elevation

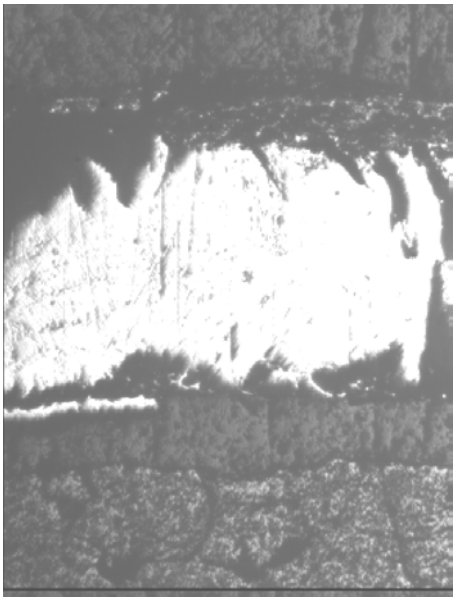

a,

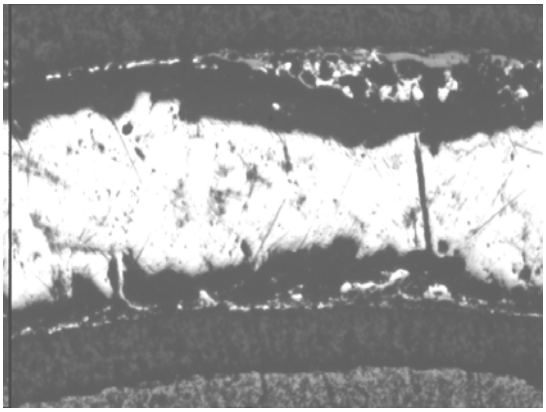

b,

Fig. 68 Intact rods at 450 mm elevation, a) No.1, b) No.9

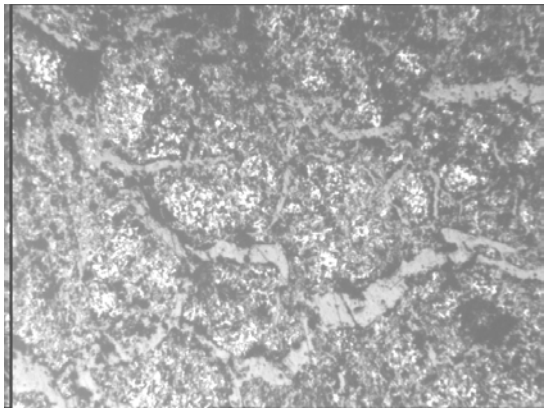

Fig. 69 Oxidised and swelled UO_2 on rod No.5 at 450 mm elevation

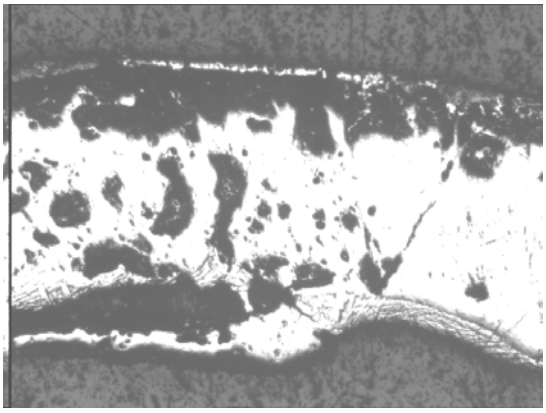

Fig. 70 Peeled off tube near to heater rod of rod No. 8 at 450 mm elevation

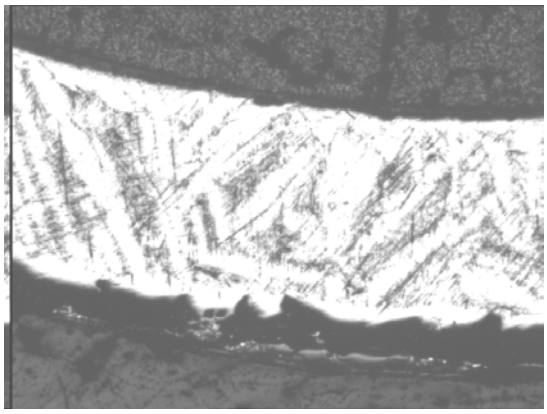

Fig. 71 Cross section of rod No. 1 at 535 mm elevation

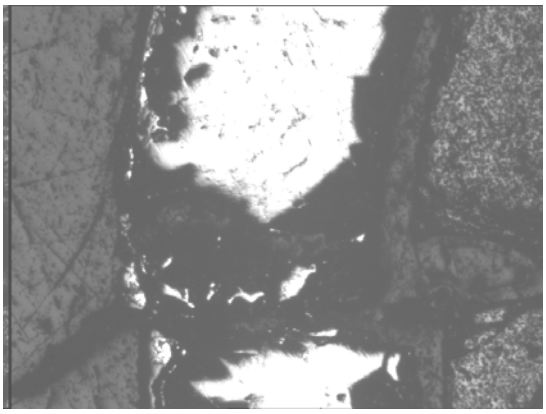

Fig. 72 Break on clad and pellet of rod No. 6 at 535 mm elevation

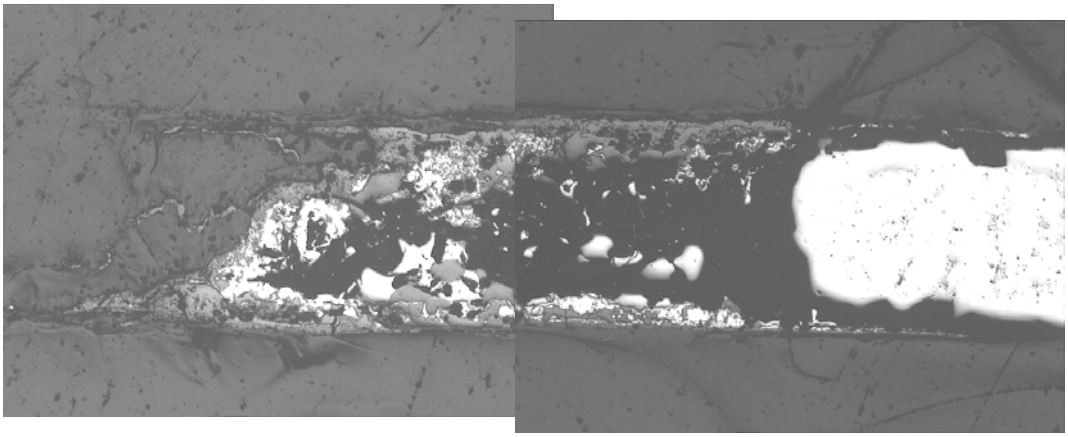

Fig. 73 Spacer at 555 mm elevation

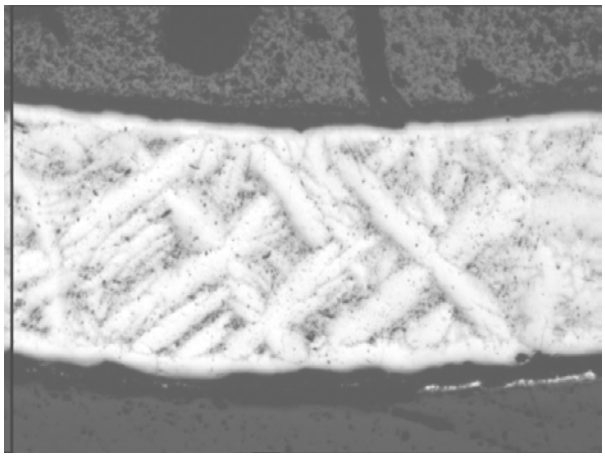

Fig. 74 Earlier β-phase of cladding of rod No. 2 at 555 mm elevation

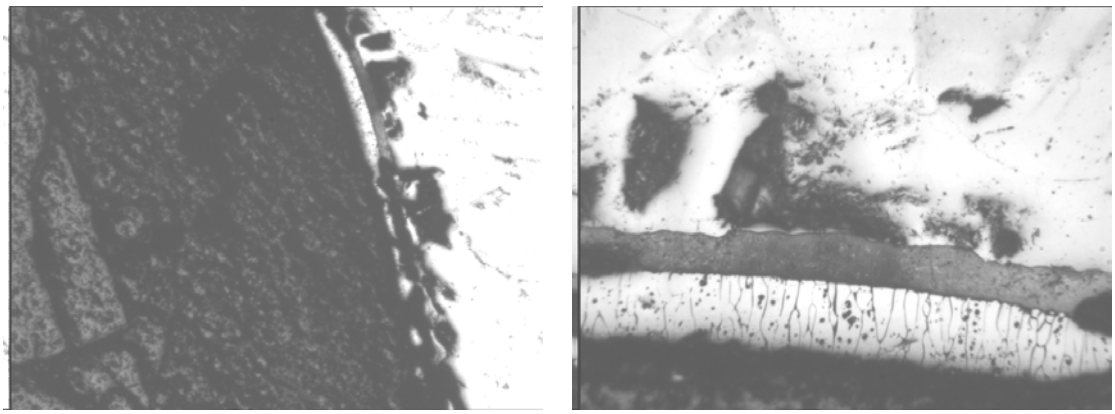

a, b,

Fig. 75 Pellet clad interaction in rod No. 3 at 555 mm elevation
with the hole of escaped U,Zr alloy

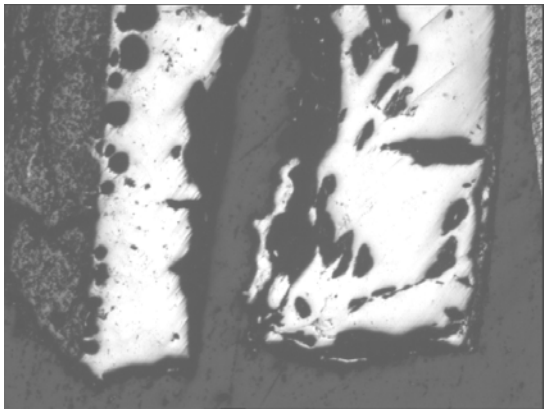

a,

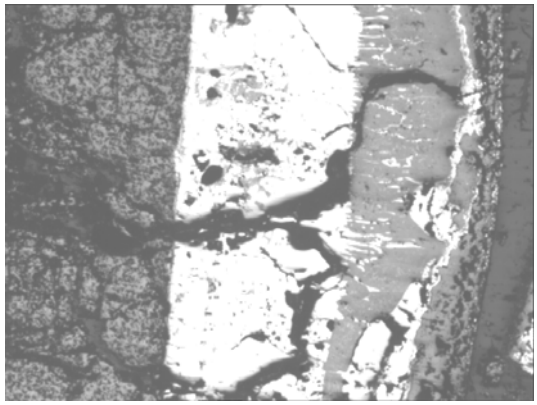

b,

Fig. 76 Details of fragmented particles from the bottom of the bundle (-20 mm)

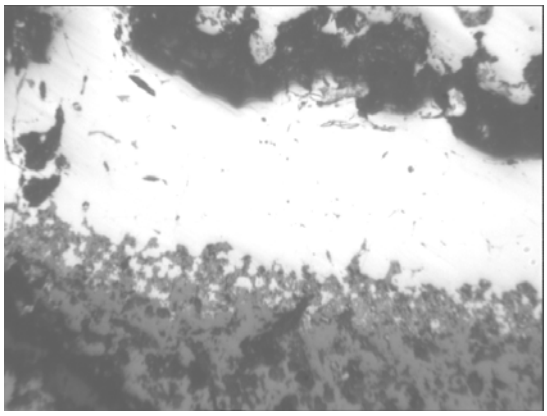

Fig. 77 Diffusion layer on the boundary of UO_2-Zry4 formed through PCI (debris bed particle)

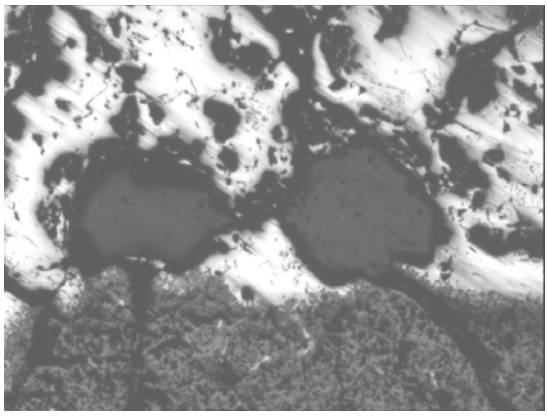

Fig. 78 The site of U,Zr globule, the molten alloy escaped

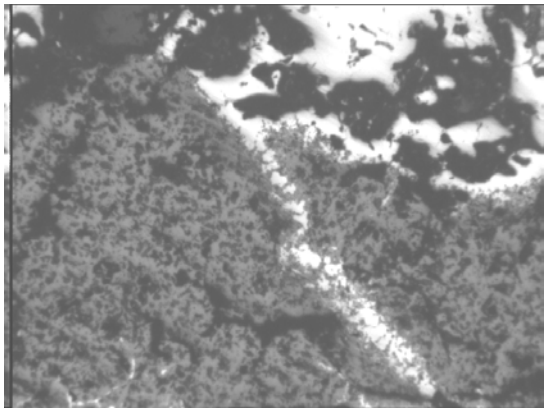

Fig. 79 Advancing of Zr metal α-phase on grain boundary of UO_2

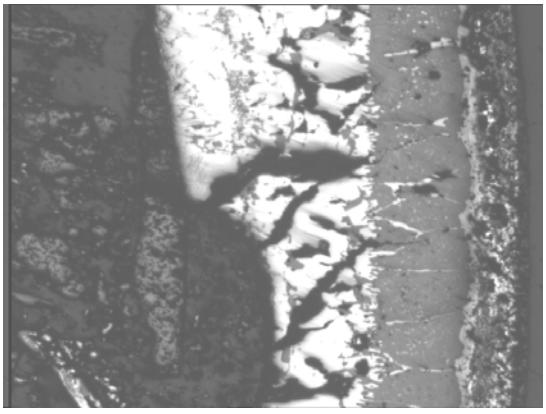

Fig. 80 Characteristic cladding detail of a fallen down fragment

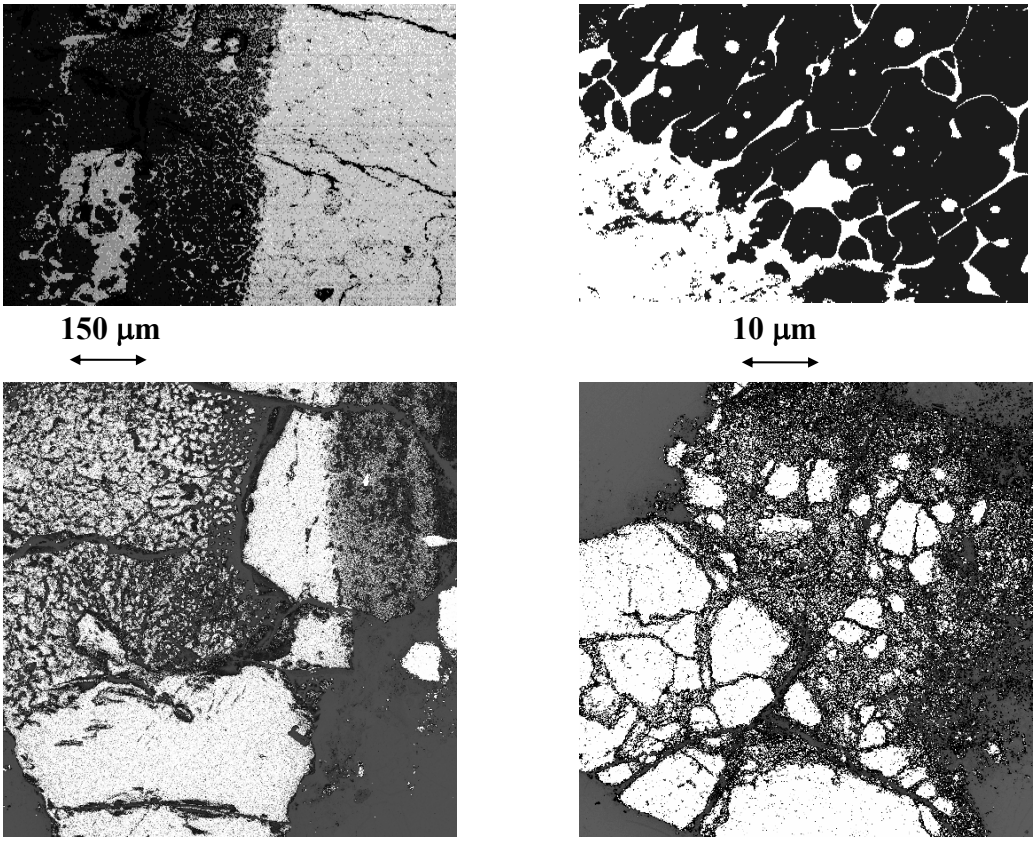

Fig. 81 Selected grains collected from the bottom of the system

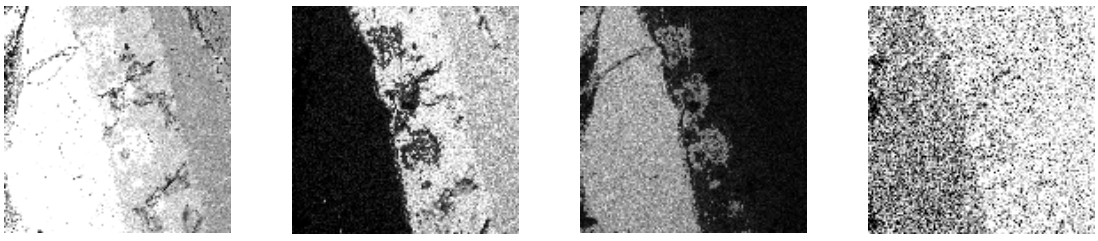

Fig. 82 Digital BEI image and X-ray maps of Zr, U and Si
taken from an interaction zone

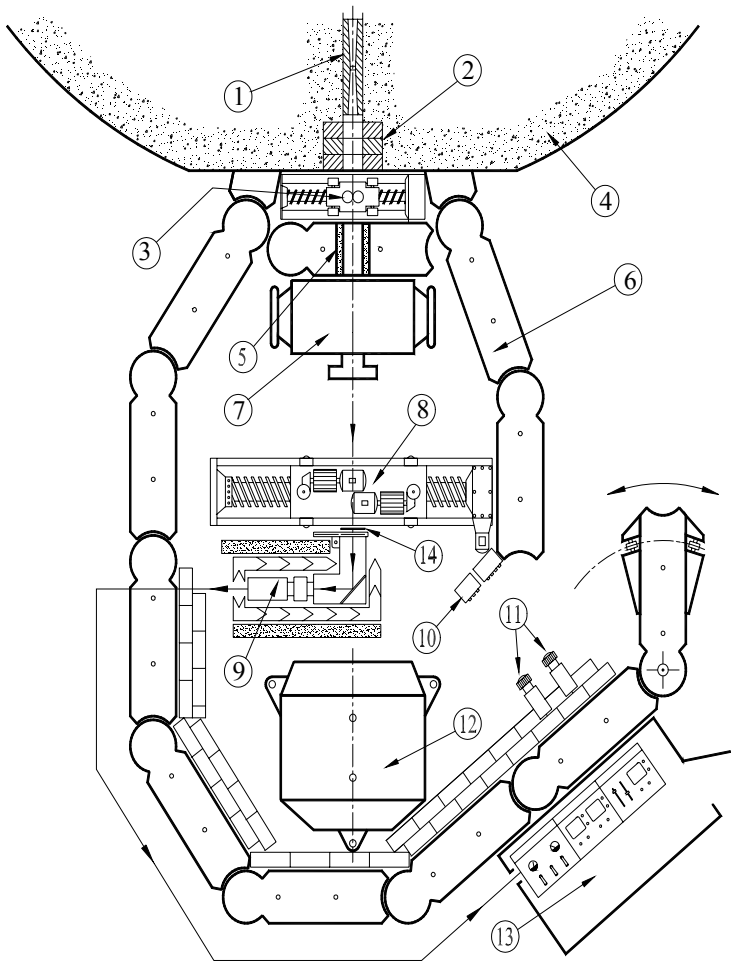

1. Inside collimator
2. Iron shutter system
3. Beam diameter changer and filter unit
4. Reactor shielding
5. Outside collimator
6. Biological shielding
7. X-ray generator
8. Investigated object with remote control mechanism
9. Imaging system with low light level TV camera
10. Working parameter indicators
11. Background TV camera
12. Beam stop
13. Control cabin
14. X-ray film position

Fig. 83 Arrangement of the dynamic radiography station at the Budapest Research Reactor

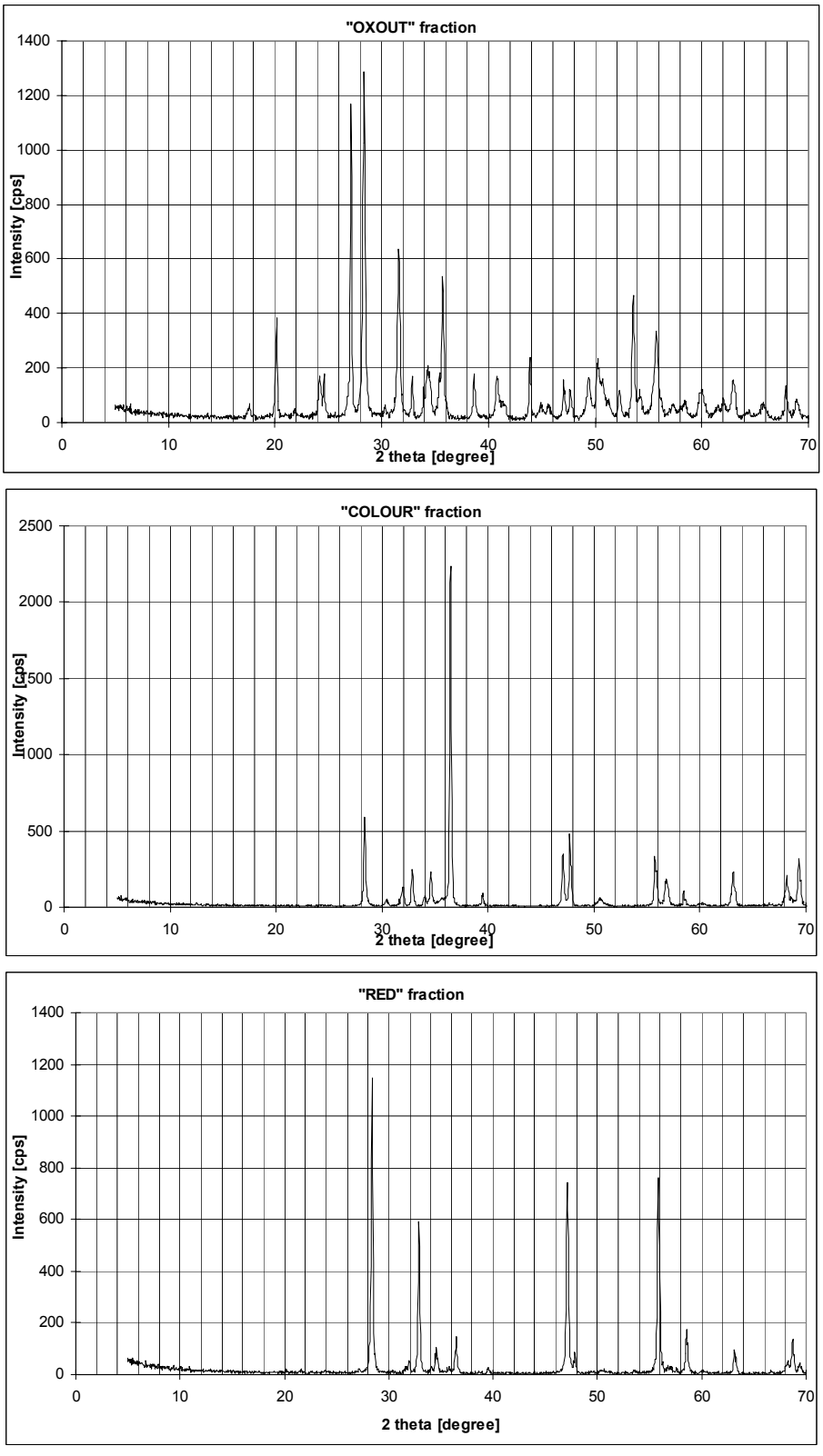

Fig. 84 X-ray diffractograms of different fuel rod samples

Elevation	Rod number								
[mm]	1	2	3	4	5	6	7	8	9
150	679.0	684.3	685.0	687.2	687.4	683.3	681.8	685.3	687.5
280	333.8	336.0					460.0	386.5	322.5
375									
450	400.0					327.7		350.0	320.0
535	500.0	515.0	590.0	365.0	291.0	594.0	565.0	580.7	190.0
555	525.0	620.0	506.0	482.5	610.0	640.0	601.3	599.8	531.0

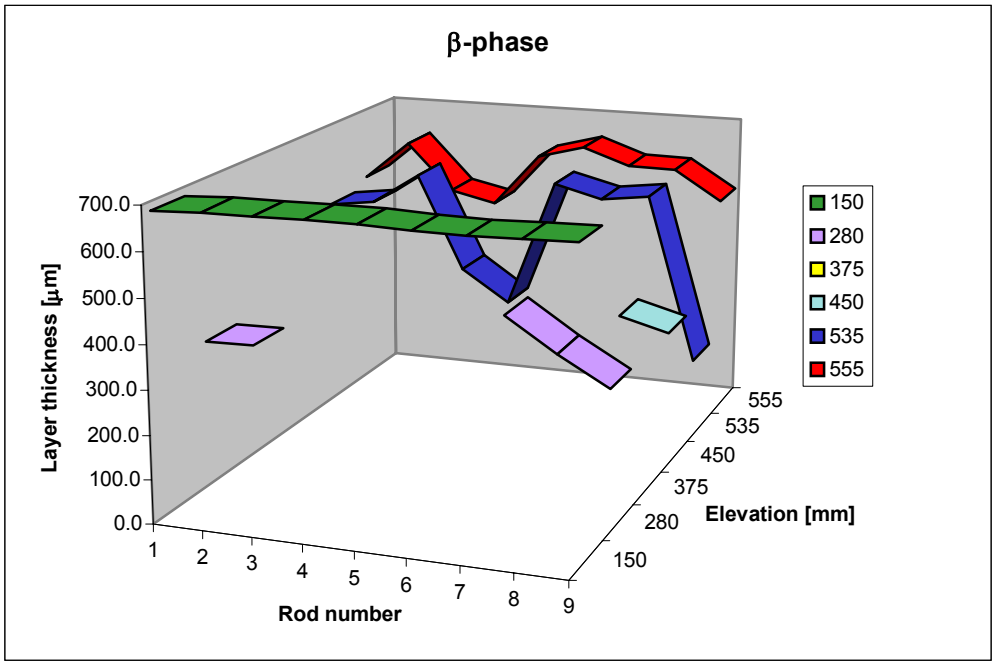

Fig. 85 β-phase thickness on the rods

Elevation	**Rod number**								
[mm]	1	2	3	4	5	6	7	8	9
150	13.3	7.2	10.3	6.8	6.4	4.5	11.2	5.3	6.0
280	257.3	277.0	560.0	510.0			171.3	342.3	406.7
375	438						390	440.0	525
450	252.2				127.3	244.2		505.0	390.0
535	121.4	160.4	97.0	163.8	129.4	100.8	40.4	81.8	355.0
555	68.5	126.4	80.3	86.2	82.7	71.3	78.3	64.5	103.0

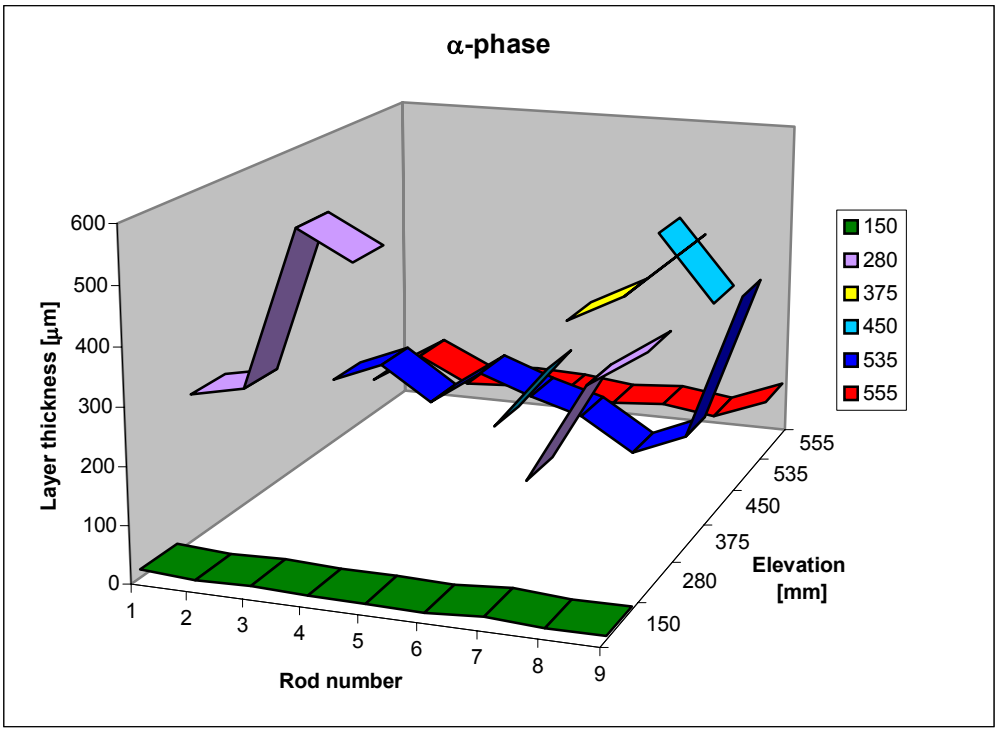

Fig. 86 α-phase thickness on the rods

Elevation	Rod number								
[mm]	1	2	3	4	5	6	7	8	9
150	7.7	8.5	4.8	6.0	6.2	12.2	7.0	9.4	6.5
280	123.1	111.2	85.0	120.2			152.7	80.2	134.0
375	165.7						95.4	111.5	116.1
450	82.0				106.4	127.2		97.2	161.6
535	87.6	80.0	64.6	73.8	75.4	76.7	50.0	35.3	93.5
555	121.2	49.4	60.5	55.8	19.5	53.2	20.3	35.7	65.2

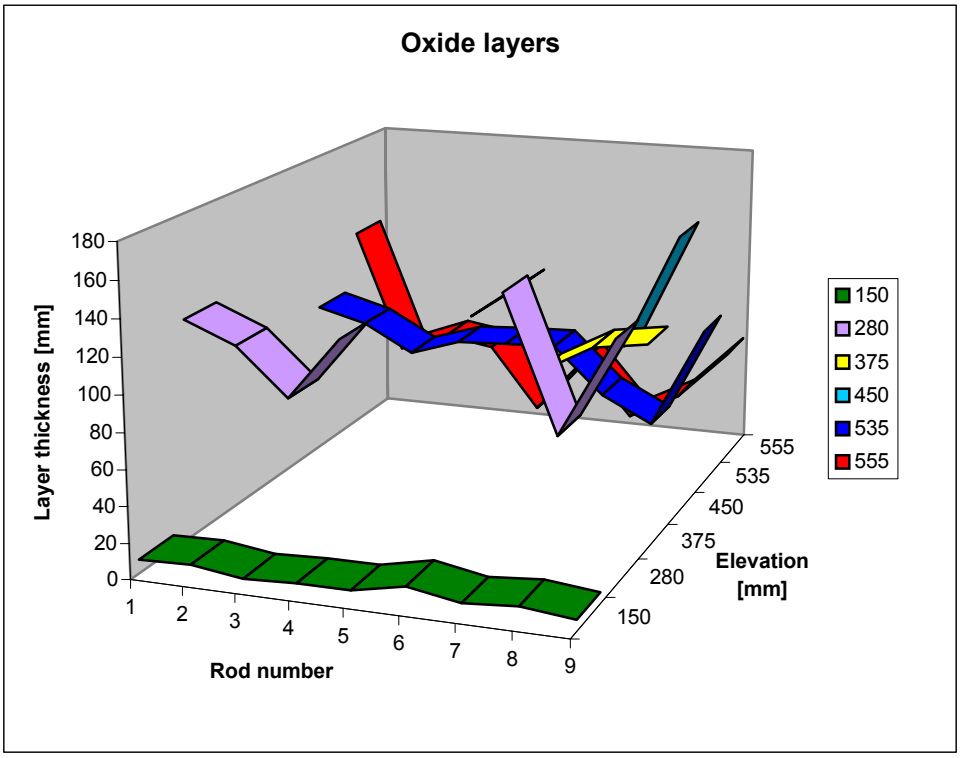

Fig. 87 Oxide layer thickness on the rods

Elevation	Rod number								
[mm]	1	2	3	4	5	6	7	8	9
150									
280			33.6						
375	29								31.5
450					27.2			22.5	
535									
555									

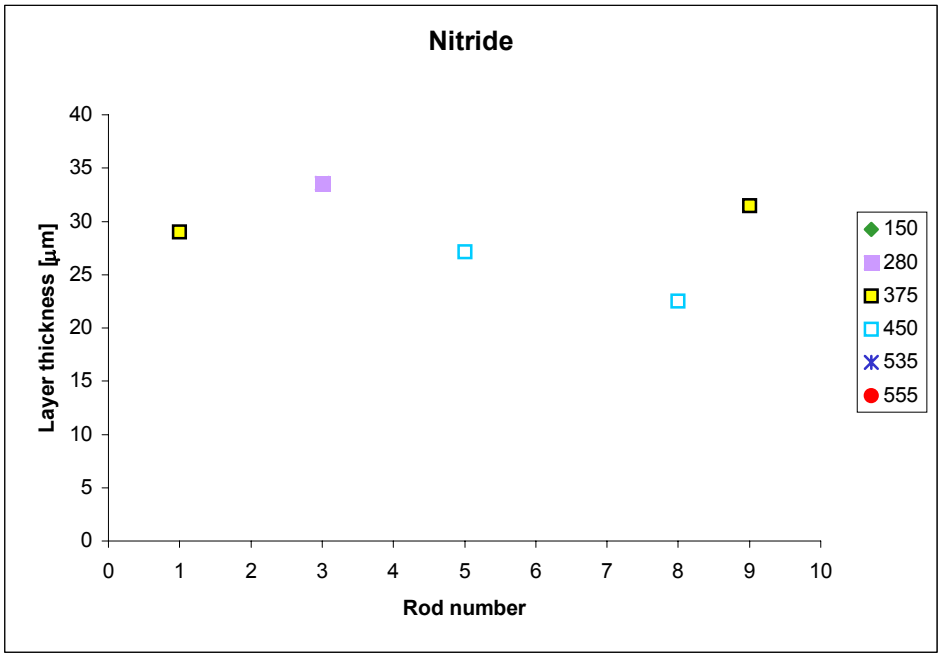

Fig. 88 Nitride layer thickness on the rods

Elevation	Rod number								
[mm]	1	2	3	4	5	6	7	8	9
150									
280	68.3	76.7	76.5				90.3	52.0	76.0
375							70	103.5	75.2
450					120.0				
535				124.3	90.0		34.5		106.5
555			171.0		50.8	181.2			93.2

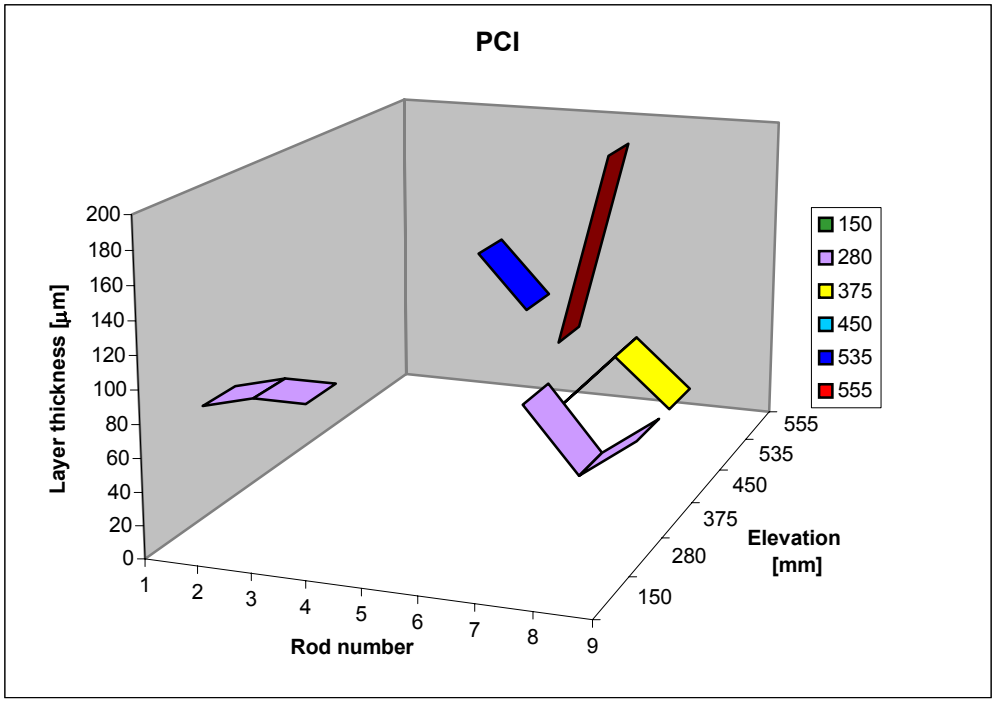

Fig. 89 Pellet-cladding interaction layer thickness on the rods

Elevation	oxide		α-phase	
[mm]	oxide outside	oxide inside	α-phase outside	α-phase inside
150	6.8	5.8	2.3	4.8
280	17	101.5	13.5	180.8
375	14.5	38	27.5	28.3
450	35.2	54.2	29.2	58.0
535	15.8	52.0	29.4	36.5
555	16.5	40.7	16.3	43.8

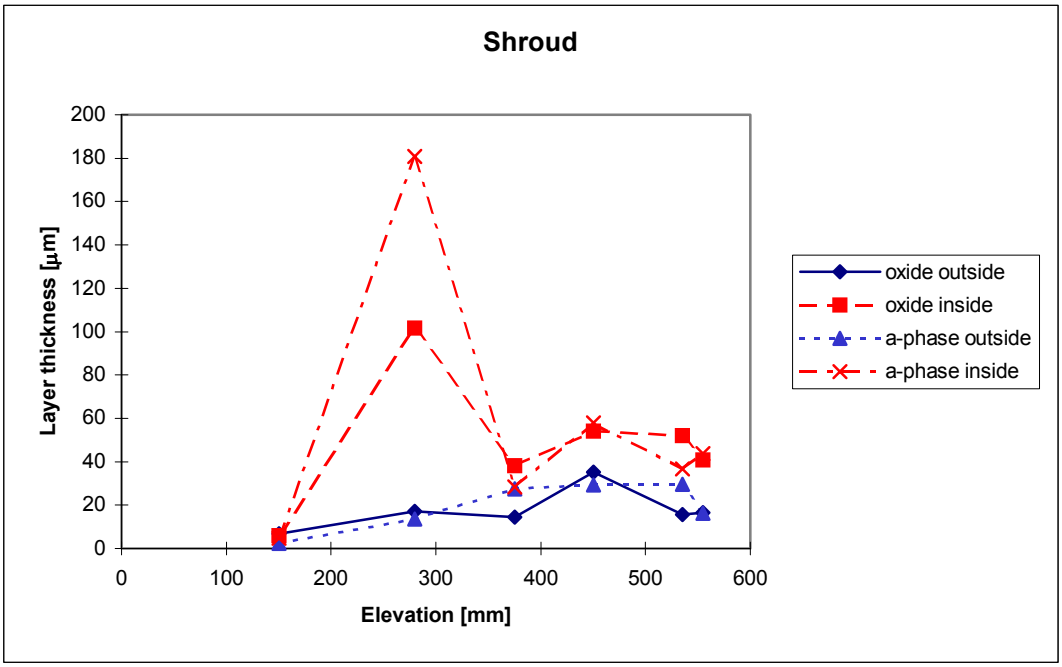

Fig. 90 Oxide and α-phase layer thickness on the shroud

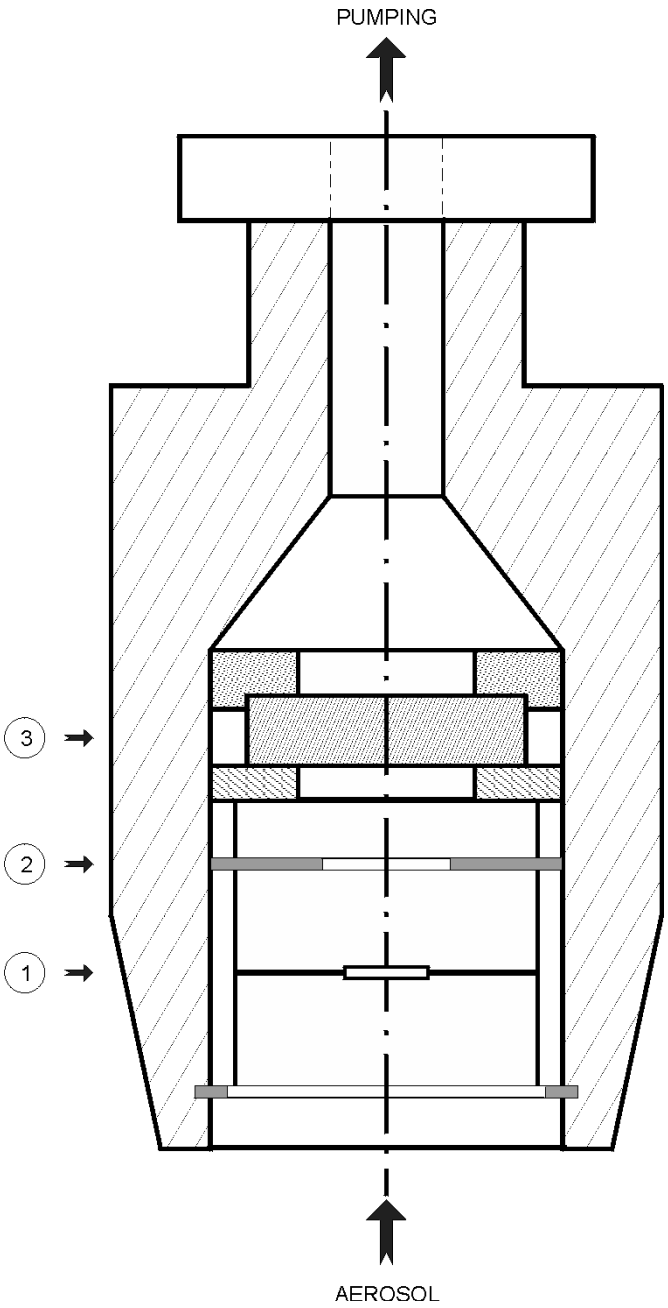

Fig. 91 Scheme of impactor sampler
1. silicon and conductive carbon collector plates
2. stream limiter
3. quartz fibre filter

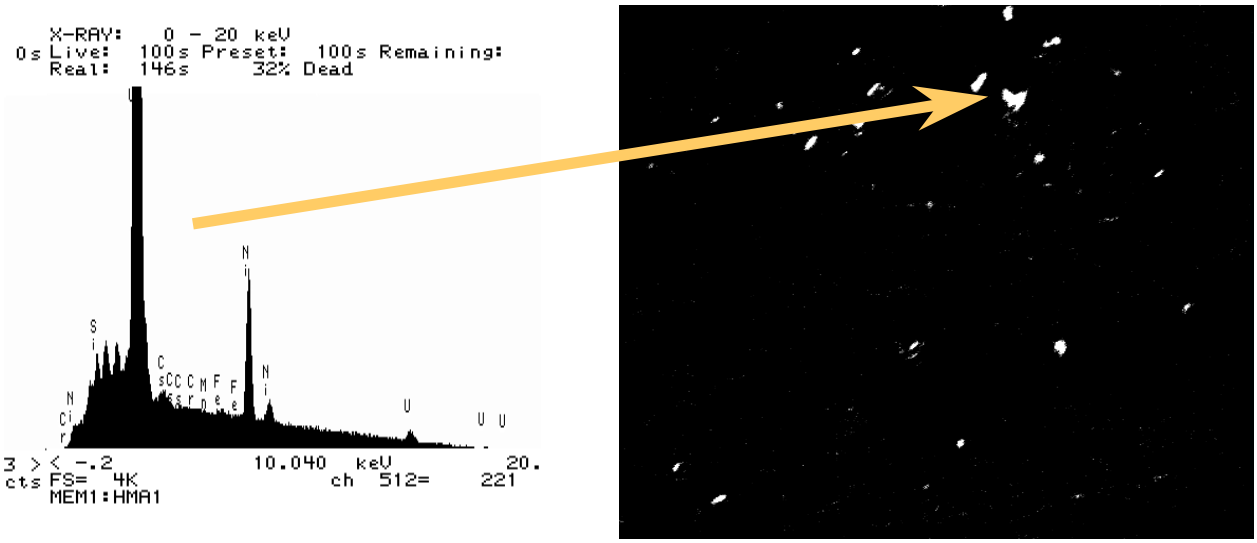

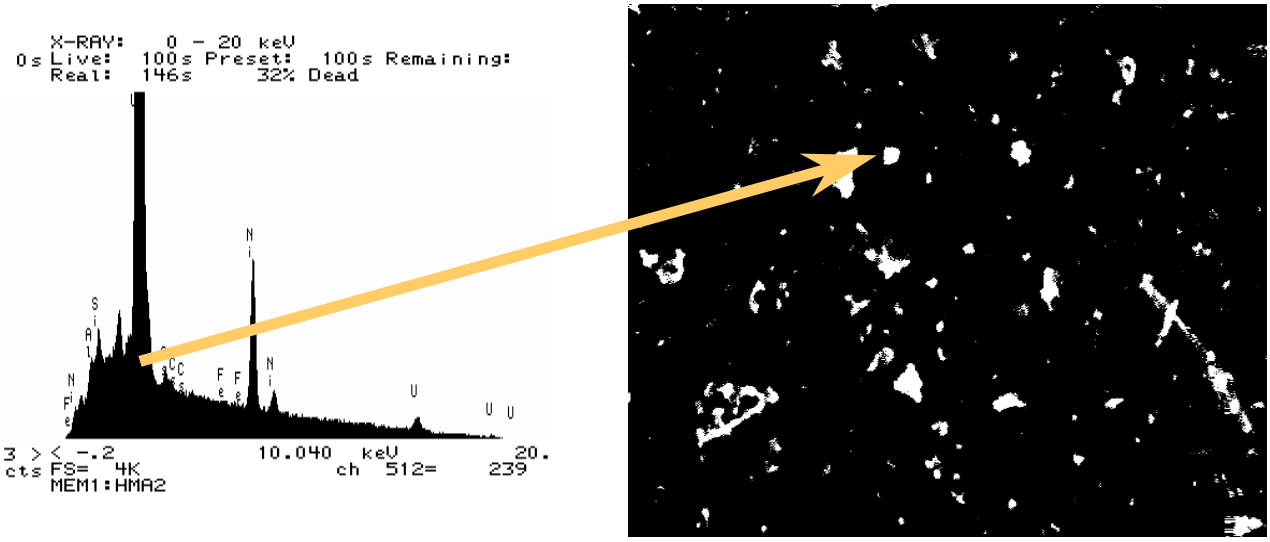

Fig. 92 SEM image and ED spectra of U-rich particles
in the CODEX-AIT-2 test

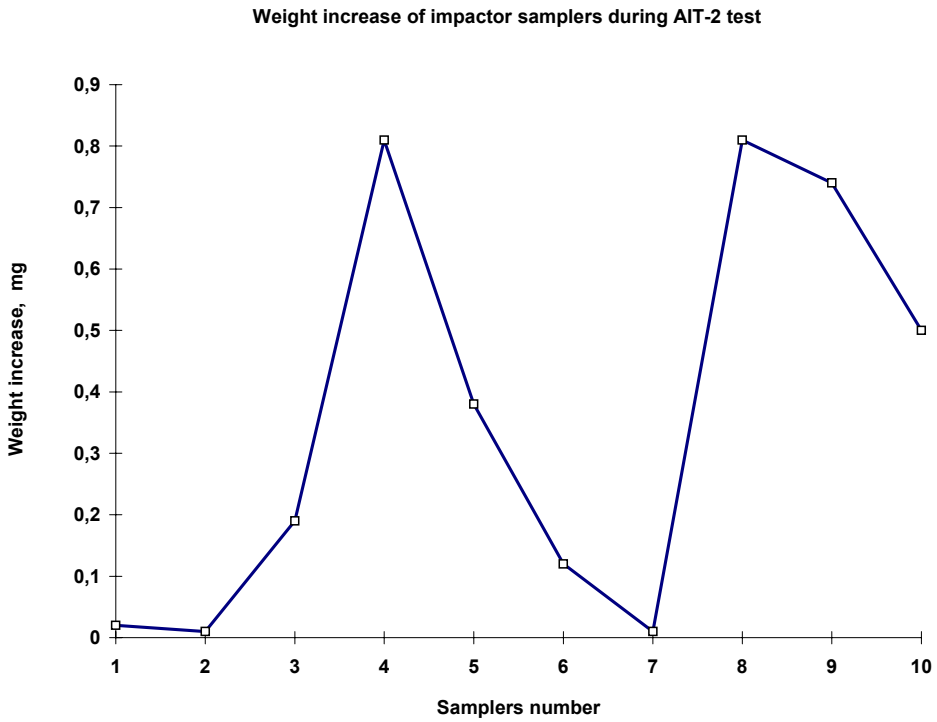

Fig. 93 Weight increase of impactor samples in the AIT-2 test

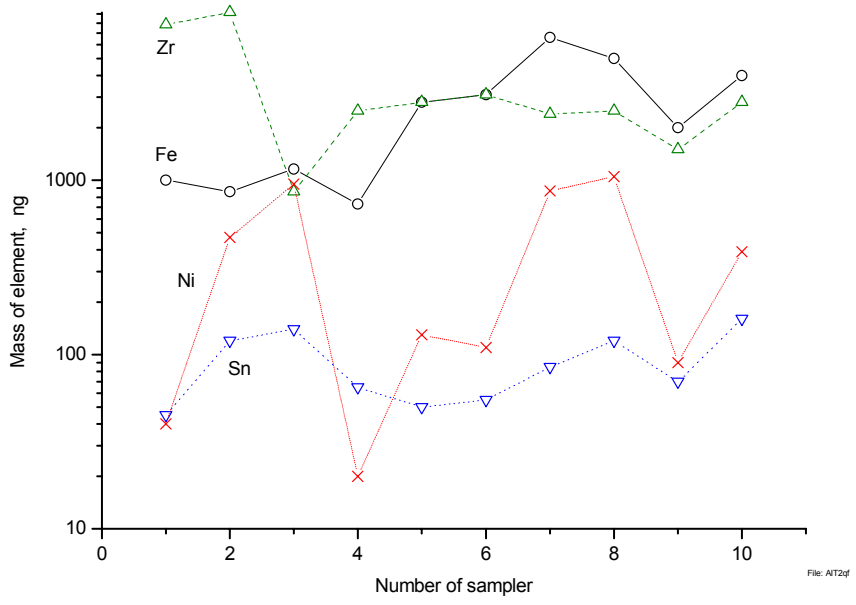

Fig. 94 SSMS results gained on quartz fibre filter